Annex Y – ASAC FINAL REPORT

Note: This Annex appears in its original format.

NORTH ATLANTIC TREATY ORGANIZATION

RESEARCH AND TECHNOLOGY ORGANIZATION

AC/323()

www.STO.nato.int

STO TECHNICAL REPORT

NG-NRMM Simulation Model Development and Analysis of the FED-Alpha Vehicle – Final Project Report

Tamer M. Wasfy and Hatem M. Wasfy

Advanced Science and Automation Corp.

NG-NRMM Simulation Model Development and Analysis of the FED-Alpha Vehicle – Final Project Report

Executive Summary

This report presents a summary of Advanced Science and Automation Corp.'s (ASA) results in the Next Generation NATO Reference Mobility Model (NG-NRMM) Cooperative Demonstration of Technology (CDT) project. The report describes the vehicle model, the soil model, and ASA simulation results for each CDT test event.

Keywords

Off-road and On-road Vehicle Mobility; Multibody Dynamics; Discrete Element Method; Computational Mechanics; Soft Soil; Terramechanics.

Table of Contents

List of Figures and Tables

1. VEHICLE MODEL

The FED-Alpha vehicle model was created using DIS/GroundVehicle. The main sub-tasks included:

- Cleaning up the CAD model for use in visualization of the vehicle.
- Extracting the hard-points of the suspension system, steering system, and drive-line from the CAD model.
- Entering the parameters for the various vehicle systems, such as the vehicle frame, suspension system (Figure 1), steering system, drive-line, and tires in the corresponding DIS/GroundVehicle sheets based on the data provided by Ricardo.

The vehicle model consists of 50 rigid bodies including: frame, suspension control arms, knuckles, wheels, shafts and axles. The bodies are connected using spherical, revolute, prismatic, and CV joints. Rotary actuators are used for the engine, brakes, and steering column. Snapshots of the FED-Alpha vehicle model are shown in Figure 2. The main DIS/GroundVehicle spreadsheets which are used to define the FED-Alpha vehicle model are given in Appendix A.

SuspDWB1	Comment:	Front suspension system			
Parameter Description	**Symbol**	**Value1**	**Value2**	**Value3**	**Units**
Hard points reference frame origin	*origin*	*Axle Center*			
Upper control arm inner front point P_1 (X, Y, Z)	p_1	0.139748	0.29579	0.2872	m
Upper control arm inner rear point P_2 (X, Y, Z)	p_2	-0.176137	0.29579	0.2872	m
Lower control arm inner front point P_3 (X, Y, Z)	p_3	0.279309	0.21821	-0.10418	m
Lower control arm inner rear point P_4 (X, Y, Z)	p_4	-0.305945	0.21821	-0.07315	m
Upper knuckle outer point P_5 (X, Y, Z)	p_5	-0.00922569	0.77536	0.24432	m
Lower knuckle outer point P_6 (X, Y, Z)	p_6	0.00566887	0.8582	-0.16226	m
Lower suspension strut lower point P_7 (X, Y, Z)	p_7	0.118962	0.65018	-0.1002	m
Upper suspension strut upper point P_8 (X, Y, Z)	p_8	0.118963	0.49338	0.57659	m
Lower Suspension Strut P_7 is connected to:	*strutConn*	*Lower control arm*			
Strut Data	*strut*	*Spring1*			
Mass of upper control arm	mU	8.49			kg
Mass of lower control arm	m_L	31.55			kg
Mass of knuckle	m_K	58.44			kg
Mass of strut lower part	m_{SL}	15			kg
Mass of strut upper part	m_{SU}	16			kg
Moment of inertia of upper control arm	i_U	0.3	0.3	0.3	$kg.m^2$
Moment of inertia of lower control arm	i_L	1	1	1	$kg.m^2$
Moment of inertia of knuckle	i_K	1	1	1	$kg.m^2$
Moment of strut lower part	i_{SL}	0.03	0.6	0.6	$kg.m^2$
Moment of strut upper part	i_{SU}	0.03	0.6	0.6	$kg.m^2$
Upper right control arm icon	$file_{UR}$	../VRML/FrontUCAR.wrl			
Upper right control arm icon translation (X, Y, Z)	$trans_{UR}$	0	0	0	m
Upper left control arm icon	$file_{UL}$	../VRML/FrontUCAL.wrl			
Upper left control arm icon translation (X, Y, Z)	$trans_{UL}$	0	0	0	m
Upper control arm icon scale (X, Y, Z)	$scale_U$	1	1	1	
Lower right control arm icon	$file_{LR}$	../VRML/FrontLCAR.wrl			
Lower right control arm icon translation (X, Y, Z)	$trans_{LR}$	0	0	0	m
Lower left control arm icon	$file_{LL}$	../VRML/FrontLCAL.wrl			
Lower left control arm icon translation (X, Y, Z)	$trans_{LL}$	0	0	0	m
Lower control arm icon scale (X, Y, Z)	$scale_L$	1	1	1	

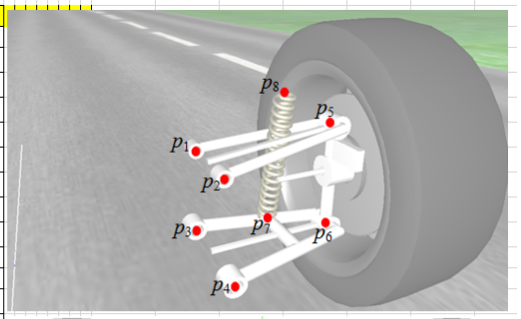

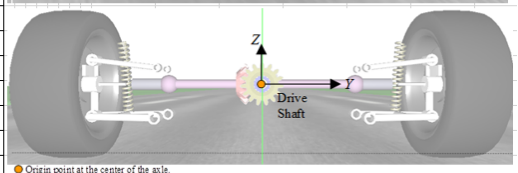

Origin point at the center of the axle.
X-axis is along the length of the vehicle and pointing to the front of the vehicle.

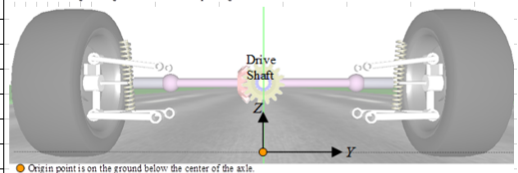

Origin point is on the ground below the center of the axle.
X-axis is along the length of the vehicle and pointing to the front of the vehicle.

Axle1 | Axle2 | TransferCase1 | Brake1 | TireLumped1 | Graph1 | Graph2 | Graph3 | TireDetailed1 | SuspDWB1 | SuspDWB2 | AntiRol ...

Figure 1: FED-Alpha suspension system sheet in DIS/GroundVehicle.

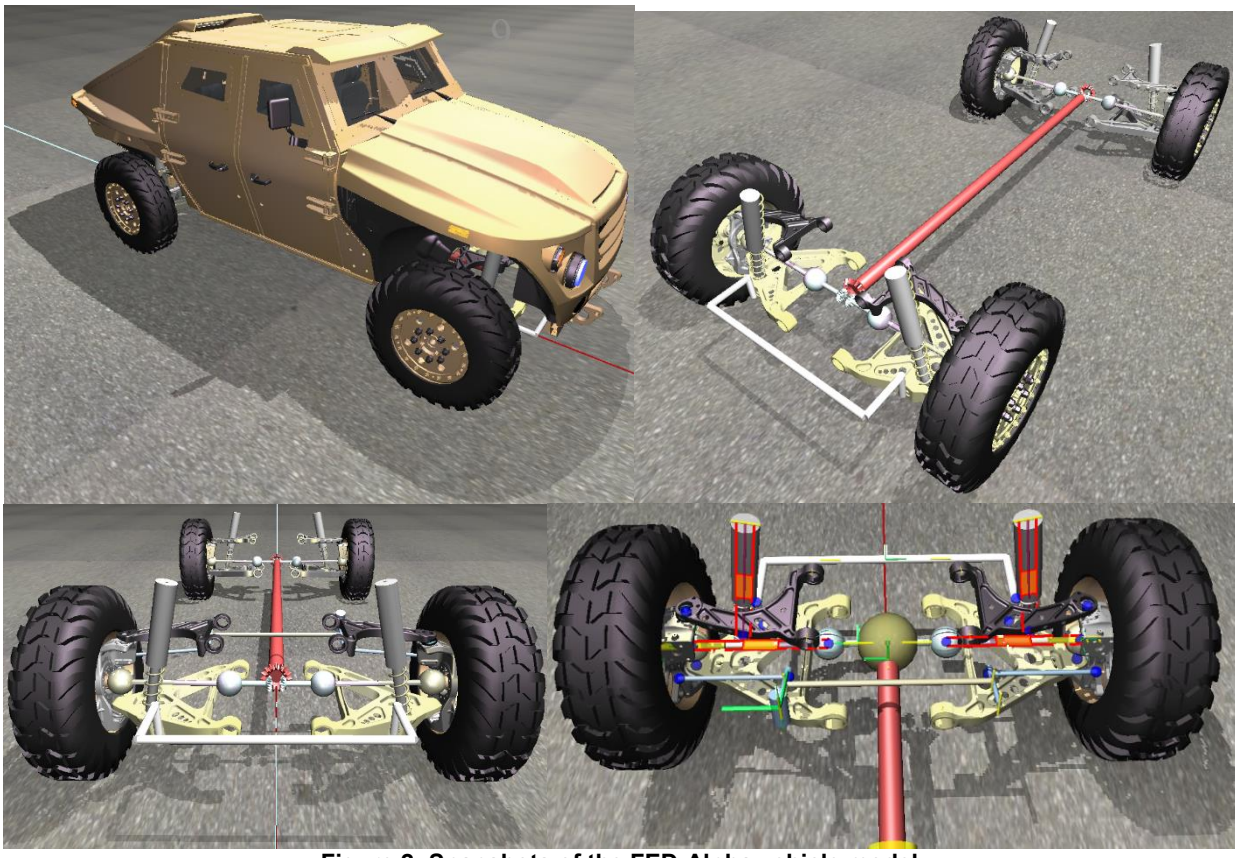

Figure 2; Snapshots of the FED-Alpha vehicle model

1.1. TIRE MODEL AND CALIBRATION

The tire model was calibrated using a test rig for a single tire (Figure 3). The following tire response quantities were calibrated:

- Tire vertical deflection versus normal load for 3 different tire pressures 35, 40 and 60 psi (Figure 4)
- Tire rolling resistance versus speed for a tire normal load of 17,169 N (Figure 5) and tire inflation pressure of 60 psi. At low speeds the tire rolling resistance coefficient is 0.0125 and at 20 m/s (45 mph) the tire rolling resistance coefficient is 0.023.
- Tire lateral force versus slip angle (using the provided Pacjeka 2002 tire data) (Figure 6).
- Tire self-aligning torque versus slip angle (using the provided Pacjeka 2002 tire data) (Figure 7).

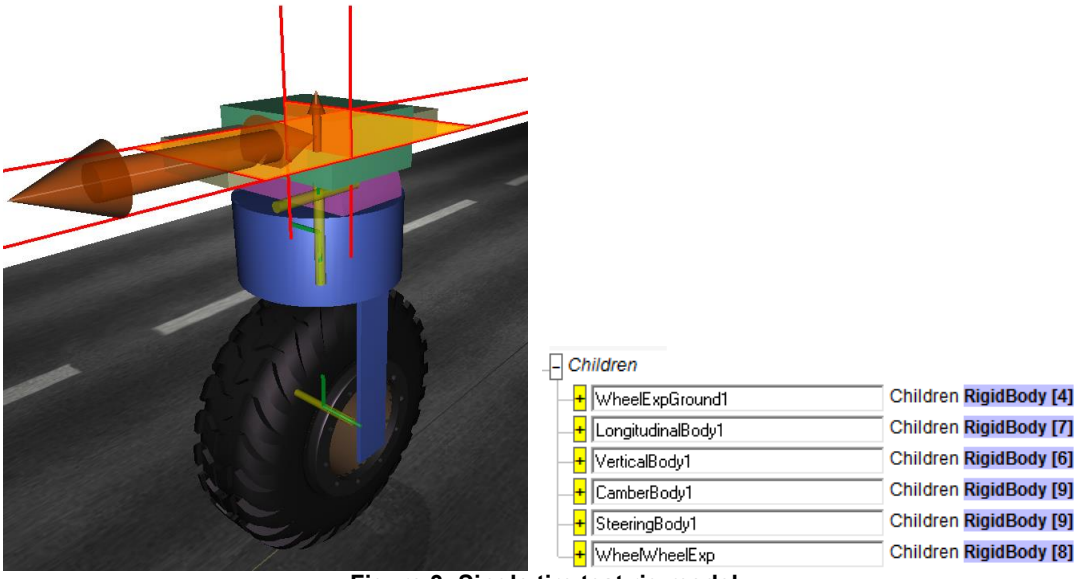

Figure 3: Single tire test rig model.

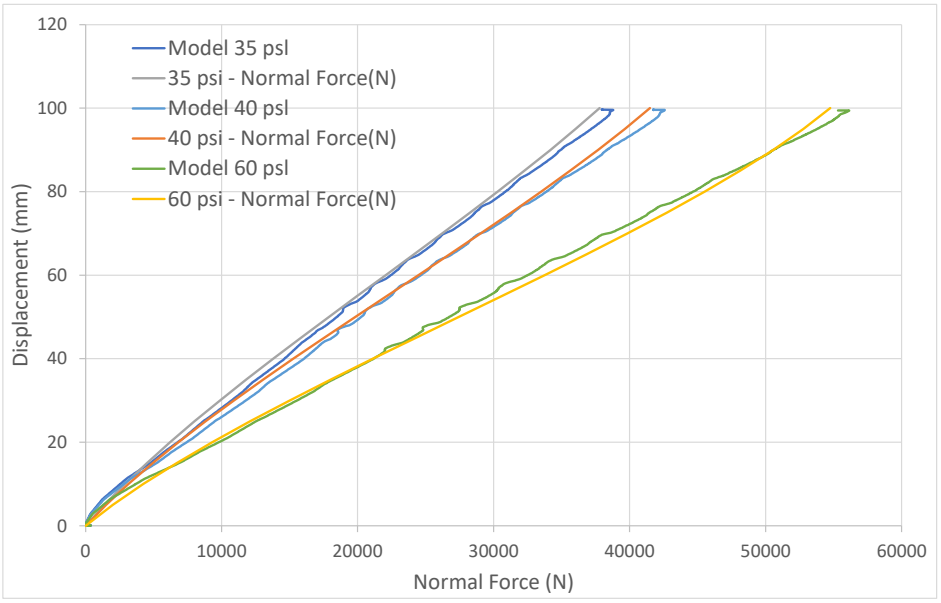

Figure 4: Tire vertical deflection versus normal load - comparison between the tire experiment data provided and the DIS single tire test rig model for 35, 40 and 65 psi.

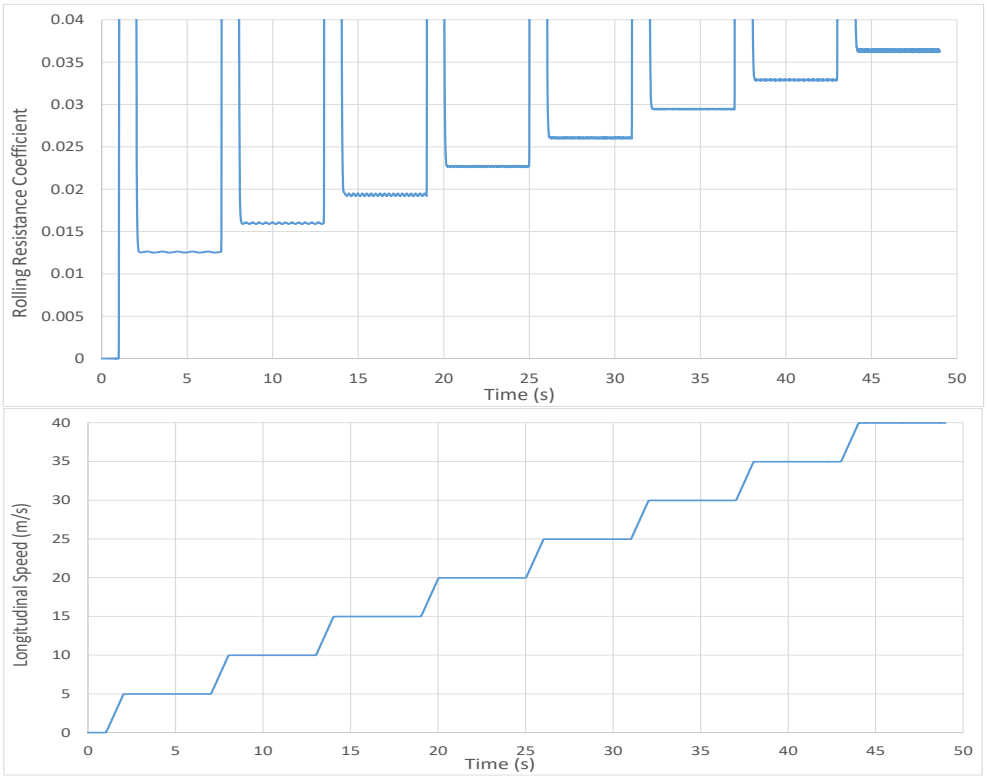

Figure 5: Single tire test rig rolling resistance and longitudinal speed versus time.

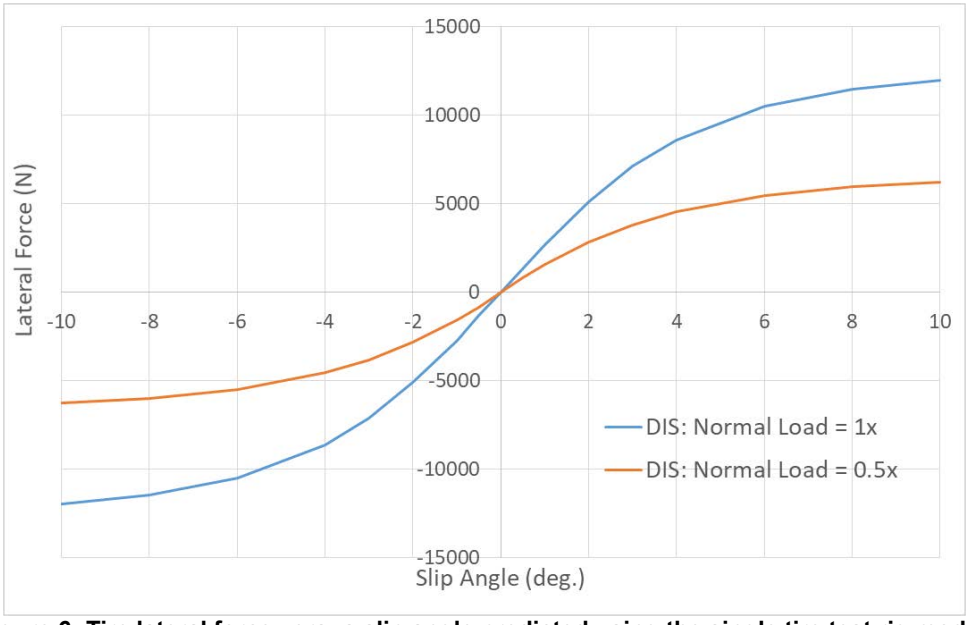

Figure 6: Tire lateral force versus slip angle predicted using the single tire test rig model.

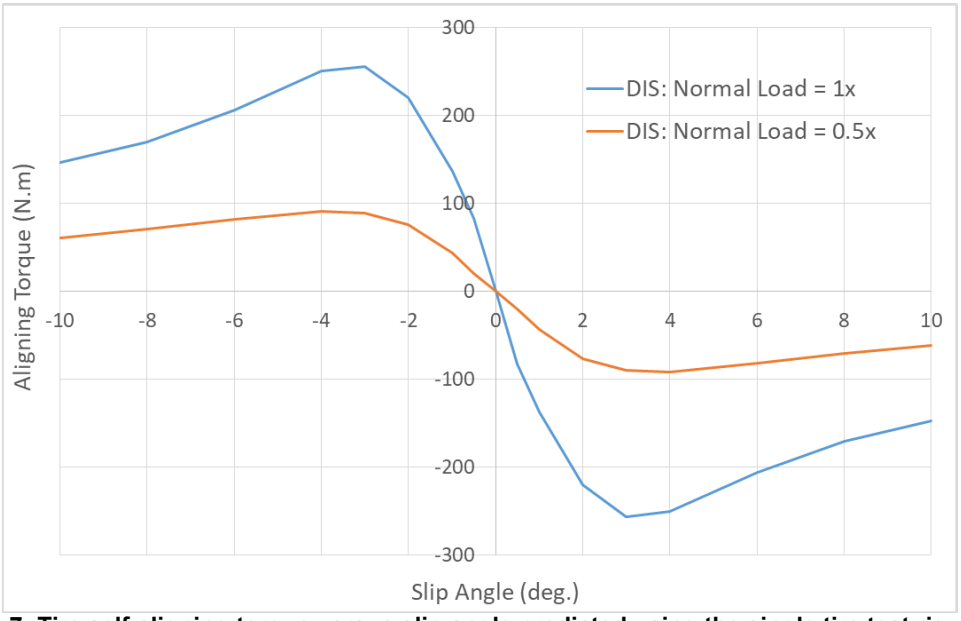

Figure 7: Tire self-aligning torque versus slip angle predicted using the single tire test rig model.

1.2. WEIGHT AND C.G. CALIBRATION

The vehicle is set on ground until it reaches steady-state static equilibrium. Then, the static tire forces and struts lengths are plotted in Figure 9 and Figure 10.

DIS Model

	Left	Right	Total
Front Tire Force (lb)	3136.1	3136.1	**6272.1**
Rear Tire Force (lb)	2918.9	2918.9	**5837.7**
Total	**6054.9**	**6054.9**	12109.9

Test

	Left	Right	Total
Front Tire Force (lb)	3125.0	3135.0	**6260.0**
Rear Tire Force (lb)	2965.0	2860.0	**5825.0**
Total	**6090.0**	**5995.0**	12085.0

Difference (%)

	Left	Right	Total
Front Tire Force	0.4	0.0	0.2
Rear Tire Force	-1.6	2.1	**0.5**
Total	-0.6	1.0	

Figure 8: Comparison between DIS model and test tire static forces.

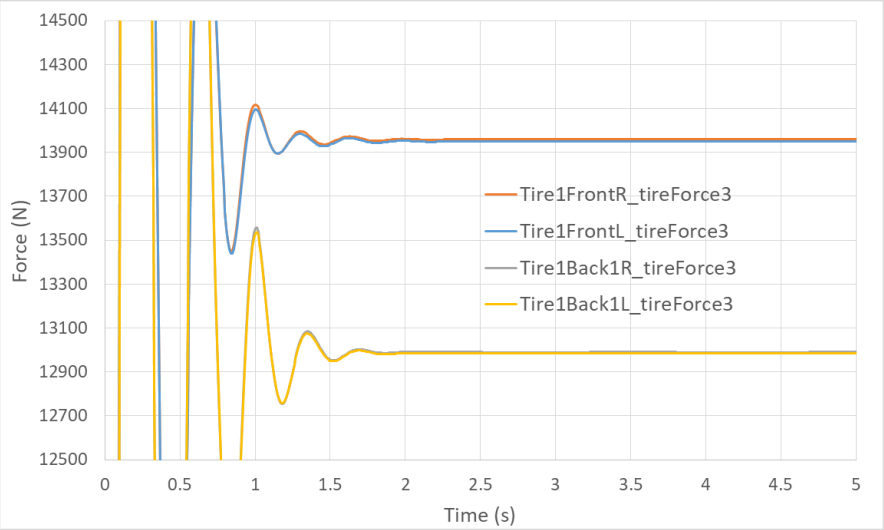

Figure 9: Time-history of DIS model tire forces.

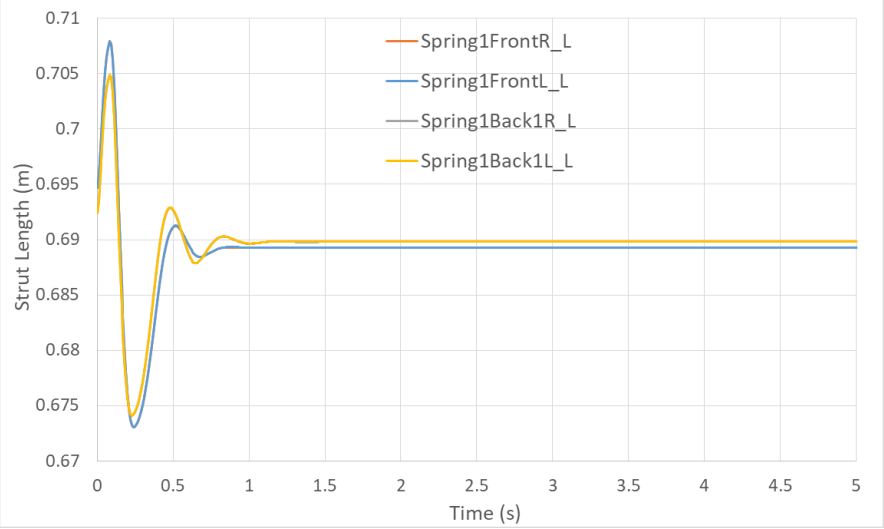

Figure 10: Time-history of DIS model strut length.

2. SOIL MODEL

1. DEM INTER-PARTICLE FORCE MODEL

In this section, the DEM inter-particle force model, presented in in Refs. [1-3], which is used in the DIS software is briefly outlined. The tangential inter-particle force $|F_t|$ is calculated using:

$$|F_t| = F_{viscous} + F_{friction} \tag{2.1}$$

The viscous force $F_{viscous}$ is given by:

$$F_{viscous} = c_t|v_t| \tag{2.2}$$

where:

$$|v_t| = \sqrt{{v_{t1}}^2 + {v_{t2}}^2 + {v_{t3}}^2} \tag{2.3}$$

c_t is the viscosity coefficient and $|v_t|$ is the signed tangential velocity magnitude. The friction force ($F_{friction}$) is calculated using the asperity-based approximate Coulomb friction force model presented in [4]. The normal inter-particle force $|F_n|$ is calculated using:

$$|F_n| = F_{adhesion} + F_{repulsion} + F_{damping} \tag{2.4}$$

$F_{adhesion}$ and $F_{repulsion}$ are both specified as a function of contact point penetration into the contact surface d (Figure 11). Up to a penetration distance d_0 the contact forces are attractive thus joining the two bodies/particles together. A force greater than $F_{adhesion,max}$ is needed in order to separate the two bodies. If the penetration exceeds d_0 then the contact force becomes repulsive thus opposing further penetration. The actual shape of the curve in Figure 11 can be tuned using experimental shear cell and hydrostatic compression data.

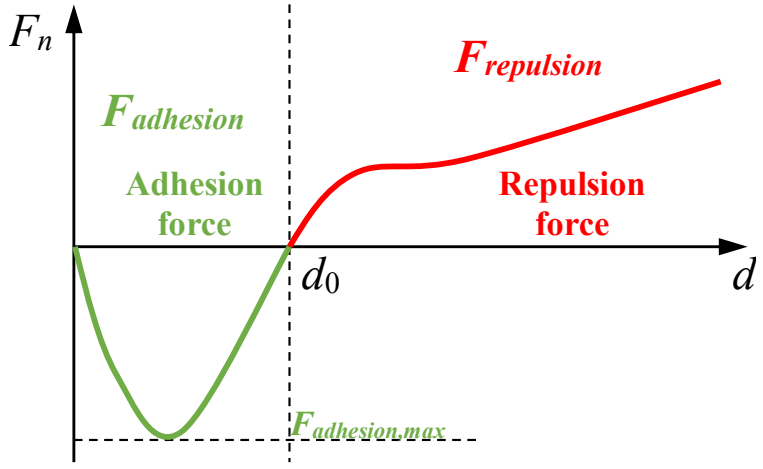

Figure 11: Normal adhesion and repulsion contact forces.

The normal damping force ($F_{damping}$) is given by:

$$F_{damping} = \begin{cases} c_n\dot{d} & \dot{d} \geq 0 \\ s_n c_n \dot{d} & \dot{d} < 0 \end{cases} \tag{2.5}$$

where c_n is the penalty damping coefficient and s_n is a separation damping factor (typically between 0 and 1) which reduces normal damping when the two bodies are moving apart. In order to model the permanent plastic deformation of the soil, plastic deformation ($\delta_{plastic}$) can be specified as a function of repulsion (compression) force ($F_{repulsion}$) (e.g. Figure 12). The plastic deformation is subtracted from the particle radius. The $\delta_{plastic}$ versus $F_{repulsion}$ curve can be tuned to match the bulk density versus consolidating pressure curve for the soil (e.g. Figure 13) obtained using a hydrostatic compression test.

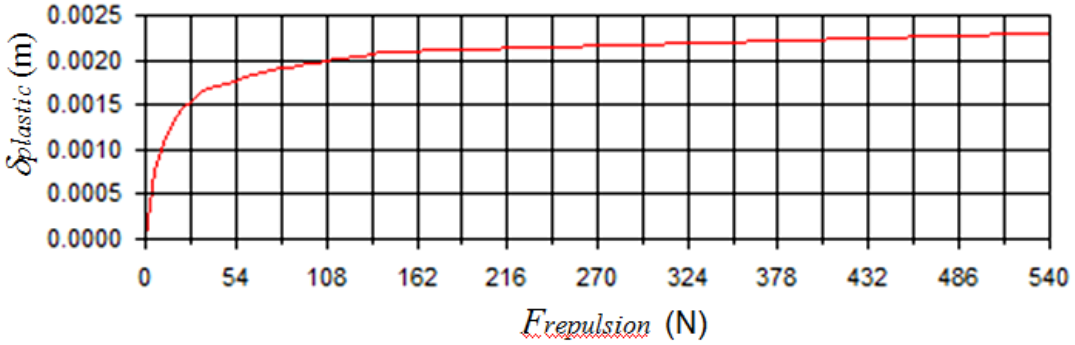

Figure 12: Typical curve of plastic deformation as a function of repulsion force.

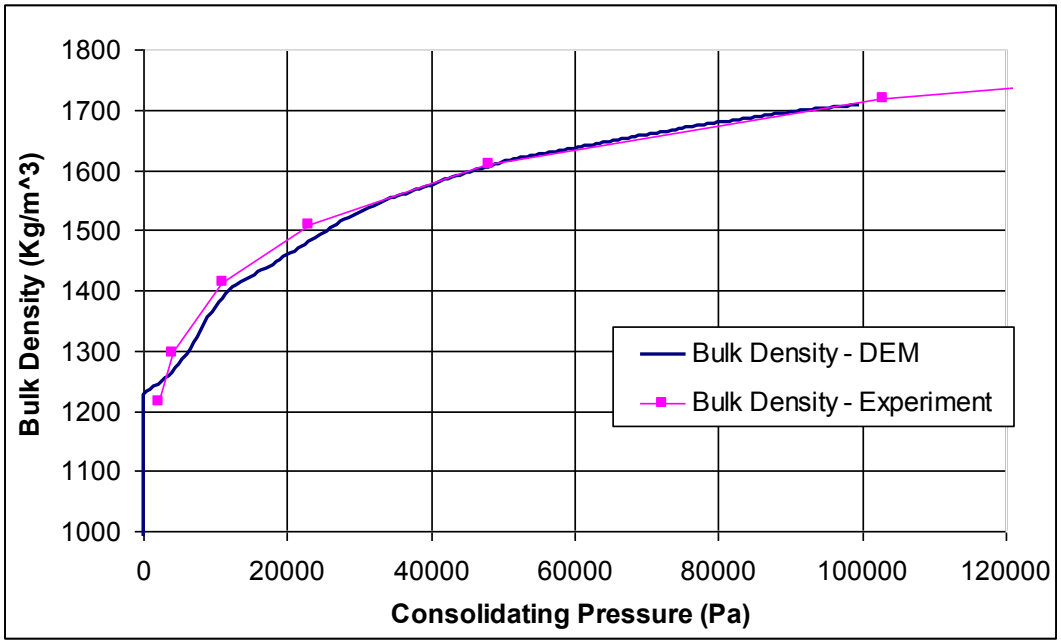

Figure 13: Typical bulk density versus normal pressure curve for a cohesive soft soil - comparison of experiment data obtained using a hydrostatic compression test and the DEM model.

In order to account for the increase in soil cohesive strength after consolidation, the maximum adhesion force ($F_{adhesion,max}$) in Figure 11 can be specified as function of the plastic deformation (e.g. Figure 14). Also, the friction coefficient (μ), viscosity coefficient (c_n) and damping coefficient (c_t) can be specified as a function of

the plastic deformation ($\delta_{plastic}$). The curve in Figure 14 along with the friction coefficient can be tuned to match the shear stress versus normal stress for different pre-shear normal stress values obtained using a shear test or a tri-axial test.

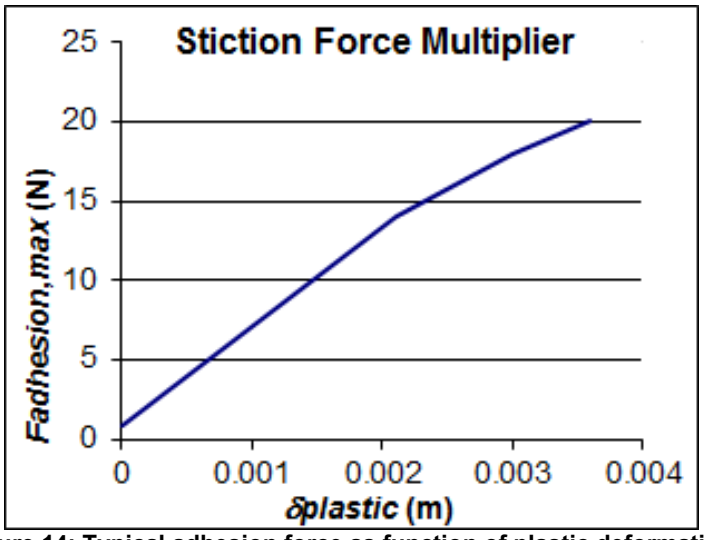

Figure 14: Typical adhesion force as function of plastic deformation.

In order to account for the reduction of soil cohesive strength and soil bulk density due to shear/tension and/or removal of the compression, a time relaxation is applied to the soil plastic deformation each time step such that the plastic deformation of a particle ($\delta_{plastic}$) is given by:

$$\delta_{plastic} = \delta_{plastic} - \begin{cases} 0 & F_{repulsion,max} \geq F_{adhesion,max} \\ V_{relax}\Delta t & F_{repulsion,max} < F_{adhesion,max} \end{cases} \quad (2.6)$$

where V_{relax} is the speed of plastic relaxation (in distance/time) and Δt is the explicit solution time step. If the particle maximum repulsion (compression) force is larger than the maximum adhesion (tension) force then the particle plastic deformation is left unchanged. If the particle maximum repulsion force is smaller than the maximum adhesion force then the particle plastic deformation is reduced at a speed of V_{relax}. The plastic deformation smallest allowable value is zero. The value of V_{relax} must be experimentally tuned.

In summary, the DEM force model used in DIS (Figure 15) includes the following soil mechanics effects:

- Change in bulk density/plastic strain as a function of normal stress.
- Change in cohesion as a function of bulk density/ plastic strain.
- Internal soil friction.
- Internal soil viscosity.
- Soil damping.
- Soil dilatency (increase in bulk density/plastic strain after shear type loading).
- Elasticity (normal elastic strain versus normal stress).
- DEM particle shape including spherical, cubical, and polyhedral.
- Adhesive stress between vehicle surface and soil as a function of bulk density/ plastic strain.
- Friction coefficient

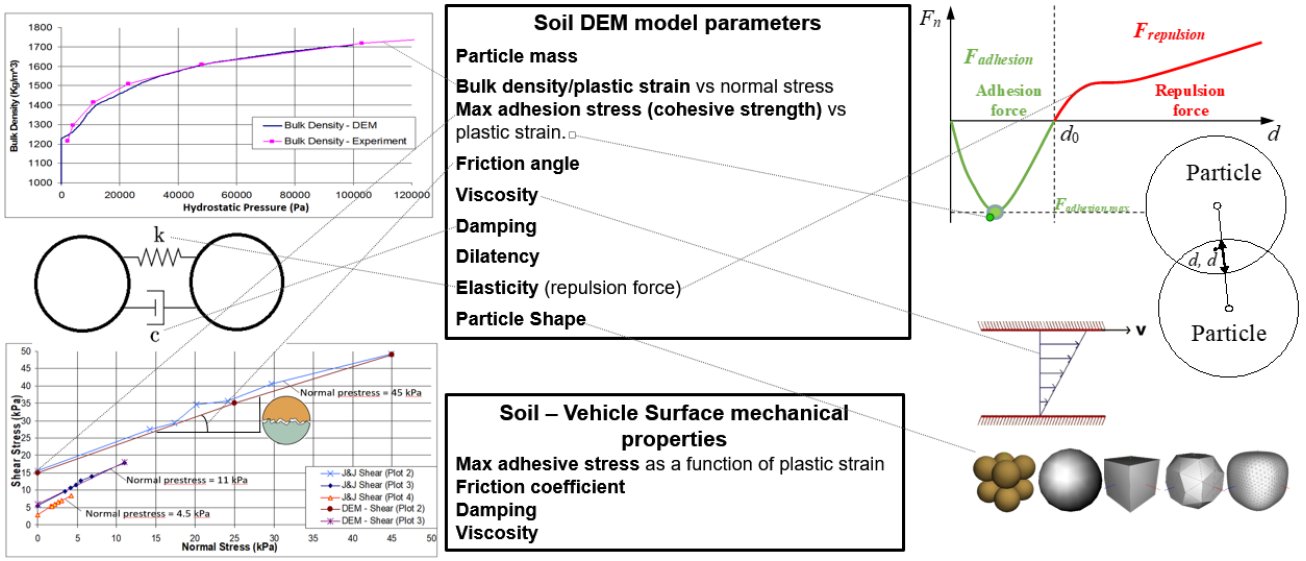

Figure 15: Overview of the DEM force model using in DIS.

2. SOIL MODEL CALIBRATION

The DEM model can be calibrated using terramechanics tests such as: hydrostatic compression, shear cell, tri-axial cell, bevameter, penetroplate, and cone penetrometer. For the CDT, the following 3 step procedure (Figure 16) was used to calibrate the DEM soil model.

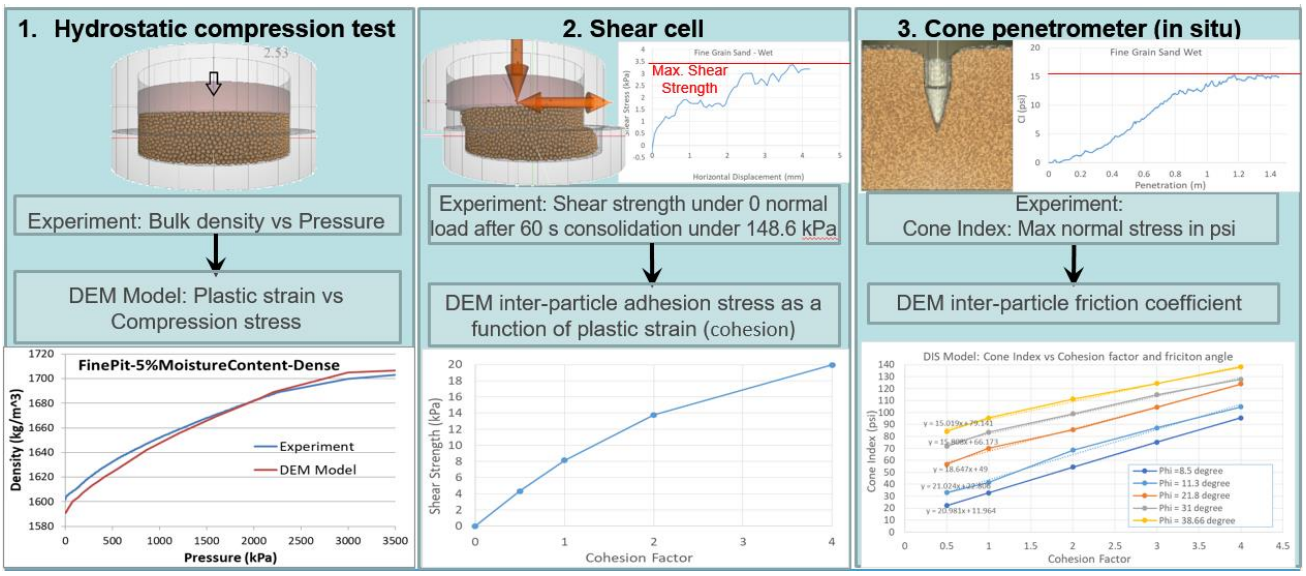

Figure 16: Overview of the DEM soil model calibration procedure used in the CDT.

2.2.1. Hydrostatic compression

The hydrostatic uniaxial compression test is used to measure the soil bulk density versus hydrostatic pressure. This data is then used to tune the DEM particles plastic strain versus compression stress.

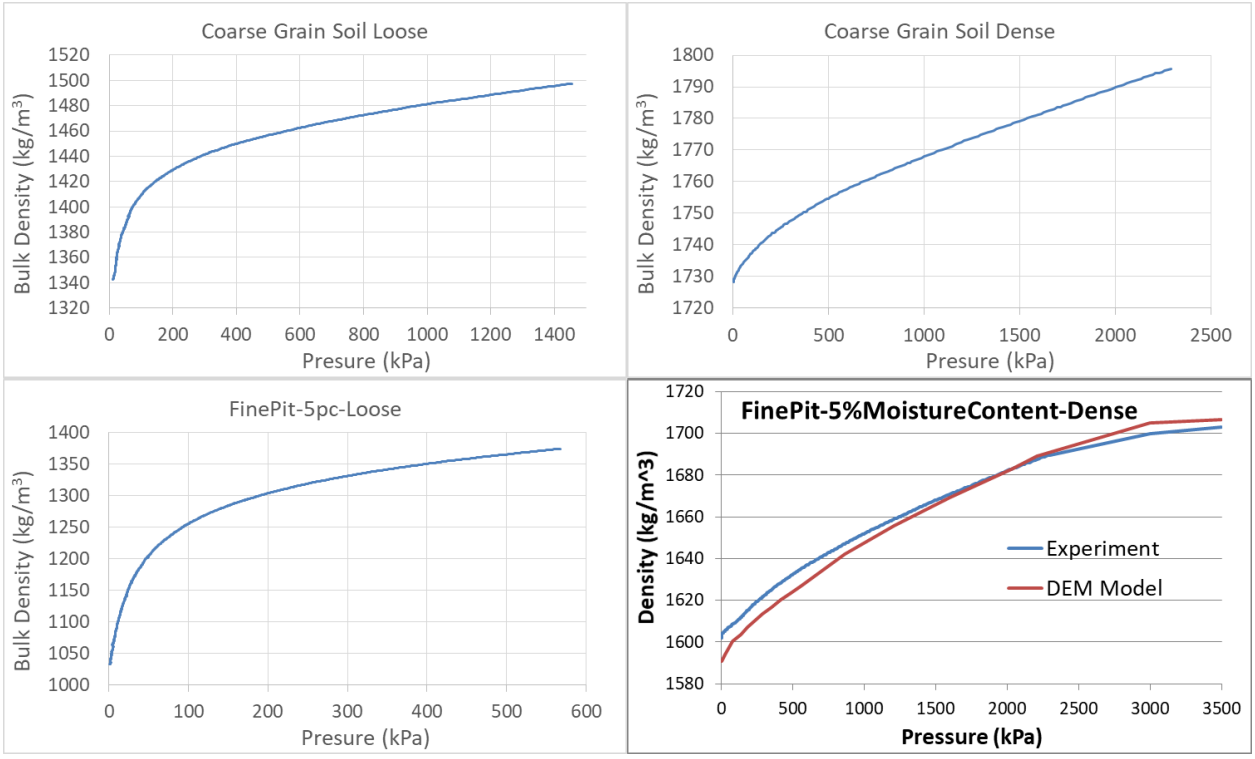

Figure 17: Uniaxial compression test results for Coarse and fine grain soil: Bulk density versus hydrostatic pressure.

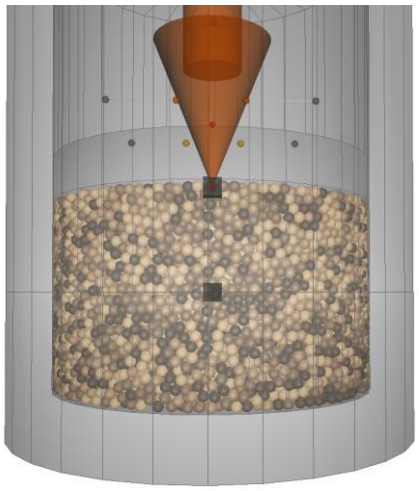

Figure 18: Uniaxial compression cell.

2.2.2. Shear cell

The shear strength of soil under zero normal load is the cohesive shear strength of the soil. The shear cell is used to measure the cohesive shear strength of a pre-consolidated soil sample. First, the soil sample is consolidated with a normal stress of 150 kPa for 60 sec. Note that this normal stress is close to the normal stress of the tire on the soil. The total vehicle weight per tire is 13,500 N. The tire contact patch area is about 0.0625 m^2 (0.25 m × 0.25 m). Accordingly, the average tire ground pressure is 216 kPa. The normal stress on the soil sample is then removed. Next the soil sample is sheared under zero normal load and we plot the shear stress versus the shear displacement (Figure 19). The maximum shear stress during the soil sample shearing process is then extracted from the graph (see Table 1). This maximum shear stress is a measure of the cohesive strength of the soil.

The shear cell is modeled using the DIS software. The shear cell test and model dimensions are given in Table 2. Note that the virtual shear cell dimensions are about 16 times larger the physical shear cell. This is due to the fact that the DEM particle diameter is 0.03 m. Thus, if the physical cell dimensions are used then the cell will only contain 4 particles. Since the soil strength characteristics are in terms of stress, we can scale up the cell as long as the same normal and shear stress values are used.

Similar to the experiment, in the virtual DIS shear cell, the soil sample is first consolidated using a normal load of 150 kPa. Then, the normal load is removed, then the soil sample is sheared under zero normal load. Figure 21 shows a typical shear stress versus horizontal displacement curve from the virtual shear cell. The maximum shear stress value is extracted from the curve. This value represents the cohesive strength of the DEM soil. In Figure 22 the DEM soil strength is plotted versus the DEM soil cohesion factor (C). From the curve in Figure 22, we can calculate the cohesion factor for the 5 soil types in Table 2.

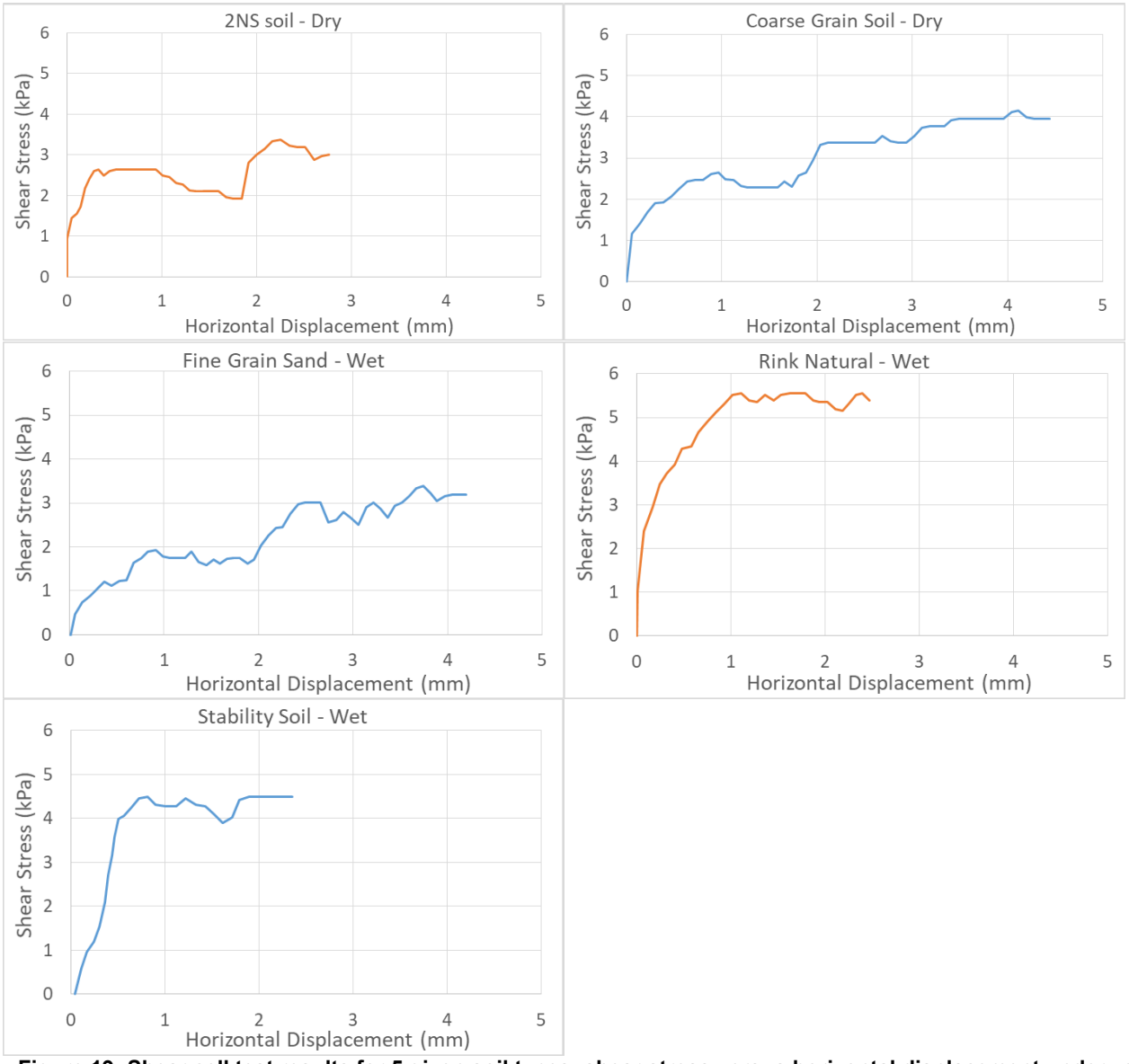

Figure 19: Shear cell test results for 5 given soil types: shear stress versus horizontal displacement under zero normal load after the soil sample being consolidated with a 148 kPa normal load for 60 sec in the shear cell.

Table 1: Shear cell test results for 5 given soil types: Maximum shear soil strength for the shear cell results in Figure 19.

Soil Type	Shear Strength (kPa)
2NS - Dry (1.2% mc)	3.38
Coarse Grain Soil – Dry (3.4% mc)	4.15
Fine Grain Soil – Wet (16.9% mc)	3.38
Rink Natural – Wet (15.4% mc)	5.56
Stability – Wet (18.6% mc)	4.49

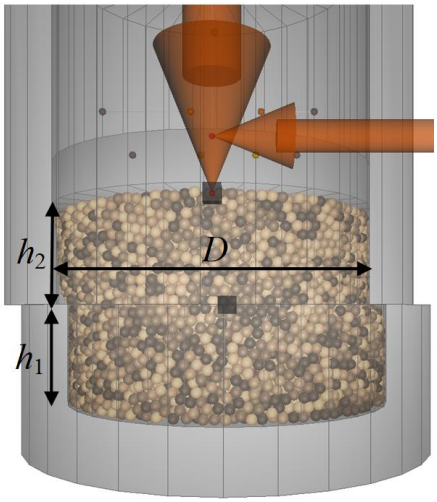

Figure 20: Shear cell model.

Table 2: Dimensions of the physical shear cell and the virtual shear cell in Figure 20.

	Physical Cell	Virtual Cell
Diameter (D)	0.0635 m	1.0 m
Bottom height (h_1)	0.0127 m	0.3 m
Top height (h_2)	~ 0.0127 m	0.3 m

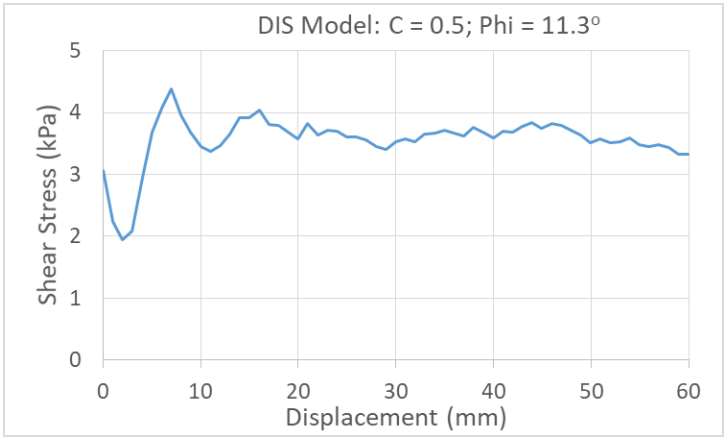

Figure 21: Shear cell DIS model simulation results: shear stress versus horizontal displacement under zero normal load after the soil sample being consolidated with a 150 kPa normal load in the virtual shear cell. The DEM soil parameters are C = 0.5 and internal friction angle of 11.3°

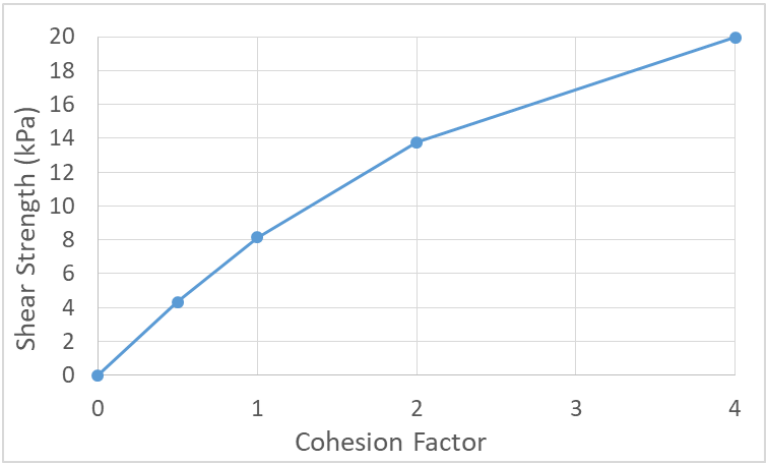

Figure 22: Shear cell DIS model results: Soil shear strength versus the cohesion factor.

Table 3: Shear cell test results for 5 given soil types: Maximum shear soil strength for the shear cell results in Figure 19.

Soil Type	Shear Strength (kPa)	DEM Cohesion factor (*C*)
2NS - Dry (1.2% mc)	3.38	0.388
Coarse Grain Soil – Dry (3.4% mc)	4.15	0.484
Fine Grain Soil – Wet (16.9% mc)	3.38	0.388
Rink Natural – Wet (15.4% mc)	5.56	0.666
Stability – Wet (18.6% mc)	4.49	0.529

2.2.3. Cone penetrometer

The Cone Index (CI) combines friction and cohesion. Since we know cohesion from the shear cell test in Section 2.2.2, we can use CI to get friction. Thus, after tuning the cohesive strength of the DEM soil using the shear cell, the cone penetrometer test is used to tune the friction angle of the DEM soil. Snapshots of the cone

penetrometer model and simulation are shown in Figure 23. The parameters of the cone penetrometer model are shown in Table 4.

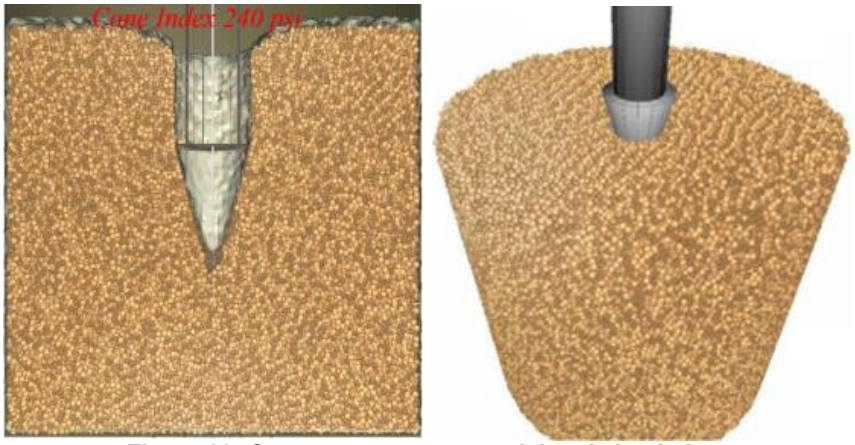

Figure 23: Cone penetrometer model and simulation.

Table 4: Parameters of the cone penetrometer model.

Cylindrical container diameter	1.3 m
Consolidating lid pressure	600 kPa
Cone penetrometer base diameter	0.375 m
Cone penetrometer length	0.7 m
Cone penetrometer cone angle	30^{o}
Penetrometer speed	0.07 m/s

Table 5 shows the cone index for the six types of KRC soils tested at 2", 4" and 6" depths. An average cone index across the height is calculated and shown in the table. The average is weighed towards the 2" depth values from strong soils (CI > 60) since the tire penetration is expected to be small for those soils. While for weak soils (CI < 60) the average cone index is weighed towards the 6" depth values since the tire is expected to penetrate deeper in the soil.

Table 5: Average insitu cone index for the given 6 soil types at 2", 4" and 6" depths along with the weighted average cone index through the effective depth of the soil for the vehicle.

Soil Type	Average Cone Index (2")	Average Cone Index (4")	Average Cone Index (6")	**Weighted Averaged Cone Index**
2NS – Dry	29.0	69.7	116.3	**50.3 psi**
Coarse Grain Soil – Dry	26.1	73.6	125.3	**50.1 psi**
Fine Grain Soil – Dry	56.3	145	284.3	**85.0 psi**
Fine Grain Soil – Wet	5.5	5.5	32.0	**21.4 psi**
Rink Natural – Wet	152.3	261.3	261.3	**165.8 psi**
Stability – Wet	139.4	249.4	249.4	**150.1 psi**

Figure 24 shows the results of the cone penetrometer simulations of the cone index versus the DEM model inter-particle cohesion factor and internal friction angle.

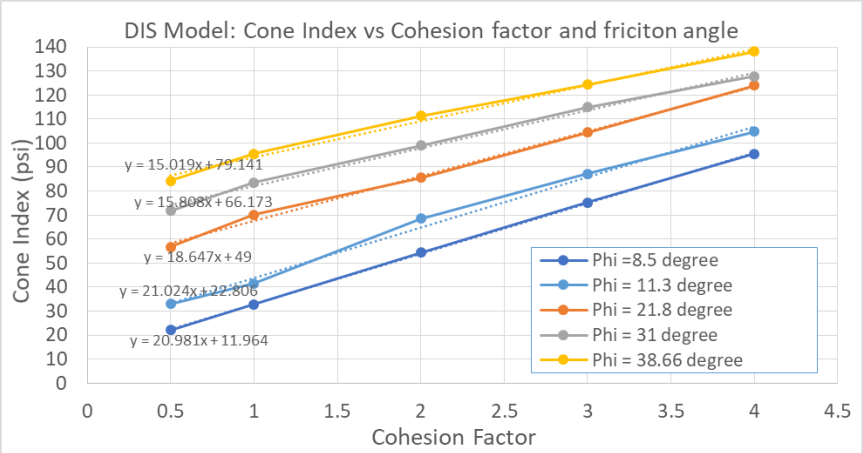

Figure 24: Cone penetrometer DIS model results: Cone index versus the DEM model cohesion factor and internal friction angle.

The cohesion factor in Table 3 along with the cone index test average values in Table 5 and the cone index versus DEM cohesion factor and friction angle in Figure 24 are used to tune the DEM friction angle for the 4 types of soils that will be used in the drawbar pull and sand slope tests. The final DEM tuned values for those soils are shown in Table 6.

Table 6: DEM cone index and corresponding cohesion factor (Table 3) and friction angle (Figure 24).

Soil Type	Cone Index	DEM Cohesion Factor	DEM Friction angle
2NS – Dry	50.3 psi	0.388	21.8º
Coarse Grain Soil – Dry	50.1 psi	0.484	21.7º
Fine Grain Soil – Dry	85.0 psi	0.388 (estimated)	38º
Fine Grain Soil – Wet	21.4 psi	0.388	11.3º

Notes:

The shear cell, tri-axial, and bevameter tests with the soil under a normal load result in soil internal friction angle which is much higher than the soil friction angle predicted using the cone penetrometer or the drawbar pull tests. Possible reasons why the friction angle from the lab shear and tri-axial, and insitu bevameter tests are higher than the friction angle from the cone index are:

- The confined soil response (inside a shear or tri-axial cell) or semi-confined response in a Bevameter is different than the unconfined response with a cone or a tire.
- The insitu soil is loose, so it's internal friction/cone index is low and lab soil gets compacted so its internal friction is high. So this means that the soil friction coefficient maybe a function of the compaction (plastic deformation of the soil).
- Under dynamic unconfined loading of a tire or cone some soils is more flowable so that the effective friction is low.

This issue needs further investigation.

3. PHASE II SIMULATION EVENTS: MODEL COMPARISON TO LIVE TEST

In Phase I all most of the simulations performed in Phase II (with the exception of the mobility traverse simulations) were performed using the model based on the supplied vehicle parameters in addition to assumptions that we made for missing data (which mainly included tire normal damping, tire rolling resistance, and driveline losses for each driveline component). In Phase II the missing data values were tuned based on the straight-line acceleration, 10" half-round results, and 4" symmetric RMS results which were supplied by TARDEC in order to tune the vehicle model. In this Chapter we present the Phase II results of the final tuned vehicle/soil models.

1. EVENT 1: STRAIGHT-LINE ACCELERATION ON PAVEMENT

The FED vehicle is accelerated from time 5 s to time 60 s at the maximum possible acceleration on level pavement terrain. The results of the comparison between the test and the DIS model are shown in Figure 25 to Figure 28.

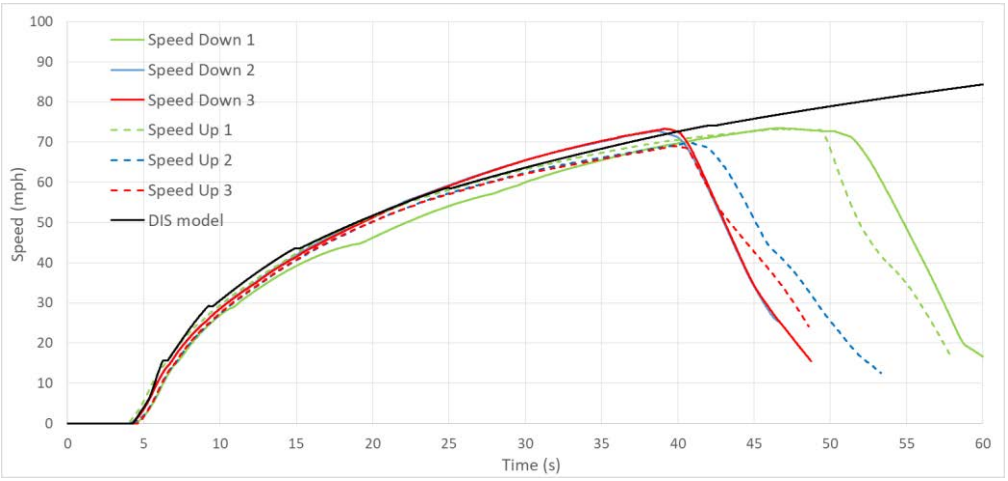

Figure 25: Comparison of DIS model and test: Straight-line acceleration on pavement: vehicle speed versus time.

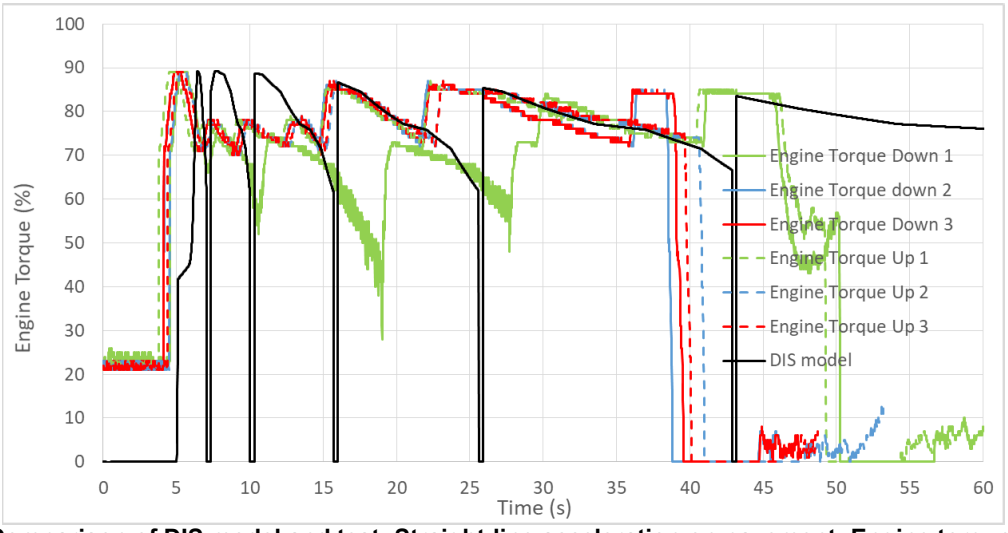

Figure 26: Comparison of DIS model and test: Straight-line acceleration on pavement: Engine torque (% of max) versus time.

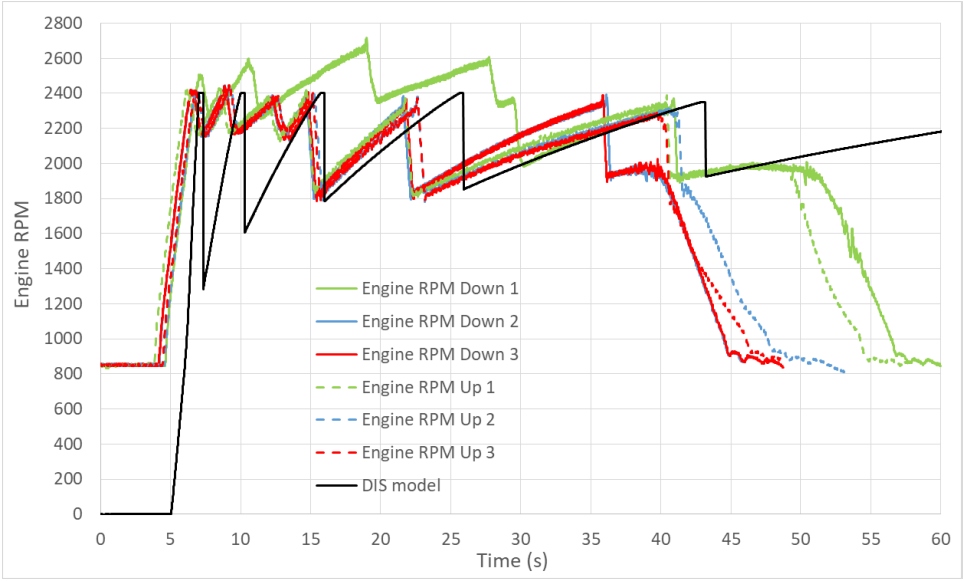

Figure 27: Comparison of DIS model and test: Straight-line acceleration on pavement: Engine RPM versus time.

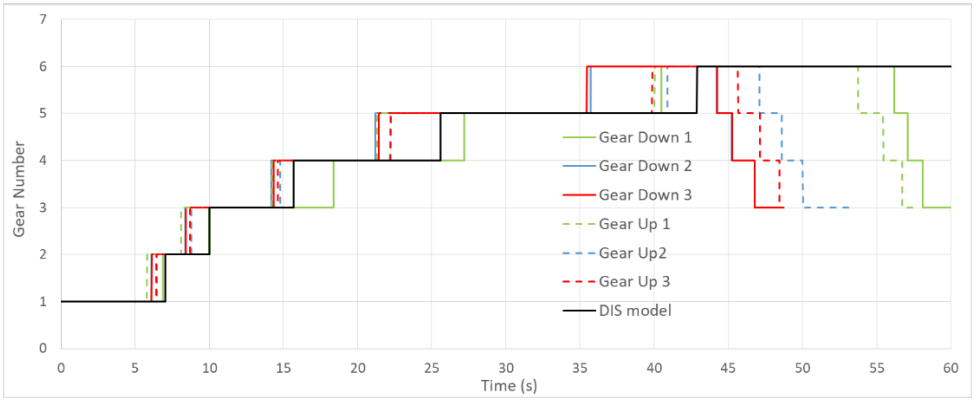

Figure 28: Comparison of DIS model and test: Straight-line acceleration on pavement: Gear number versus time.

2. EVENT 2: WALL-TO-WALL TURN RADIUS

The vehicle pitman arm is moved to the maximum CW steering angle. Then the vehicle is linearly accelerated until a constant speed of 2 m/s is reached. The simulation is repeated in the CCW direction. The results are shown below:

- Test
  - CW radius = 51.1 ft, Pitman Arm Angle = 27.9º
  - CCW radius = 50.8 ft
- DIS model
  - CW radius = **50.41 ft** (Difference from test =1.35%), Pitman Arm angle = **28.0º** (Difference from test = 0.36%)
  - CCW radius = **50.42 ft** (Difference from test =0.76%), Pitman Arm angle = **-28.0º** (Difference from test = -0.36%)

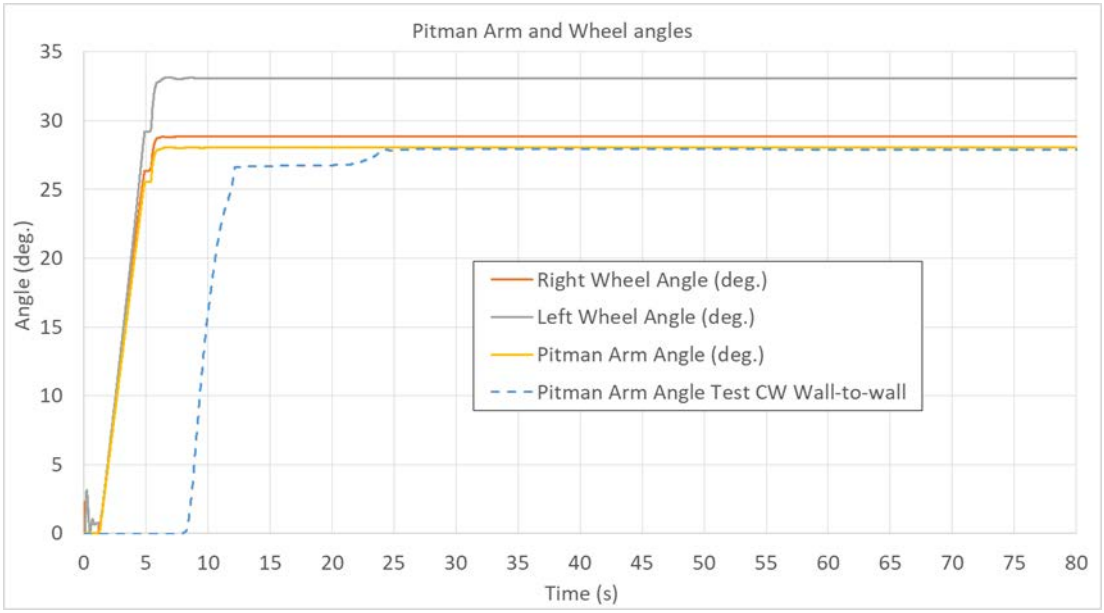

Figure 29: Wall-to-wall turn radius simulation time-histories of pitman arm, inner (left) wheel, and outer (right) wheel angles. The test pitman arm angle is also shown for comparison.

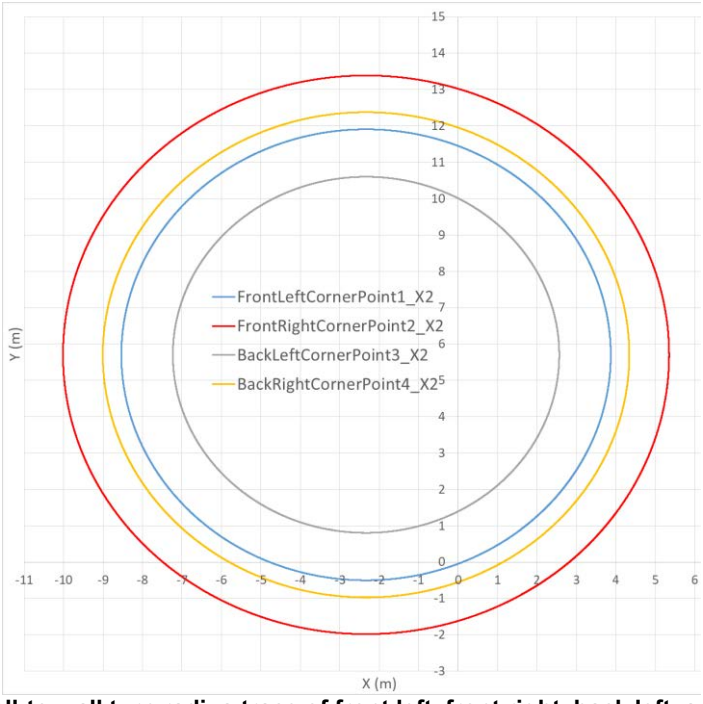

Figure 30: Wall-to-wall turn radius trace of front left, front right, back left, and back right.

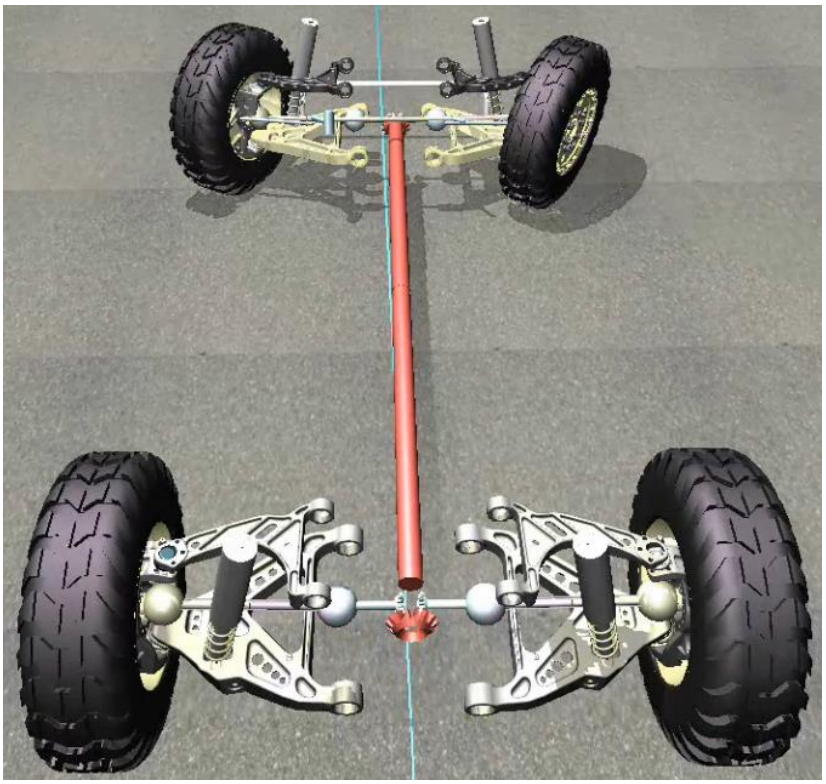

Figure 31: Snapshot of the wall-to-wall simulation.

3. EVENT 3: STEADY-STATE CORNERING

The vehicle is accelerated until a speed of 25 mph is reached while going on a 30 m radius circle on pavement (COF = 0.8). The DIS model and test results are compared in Figure 33

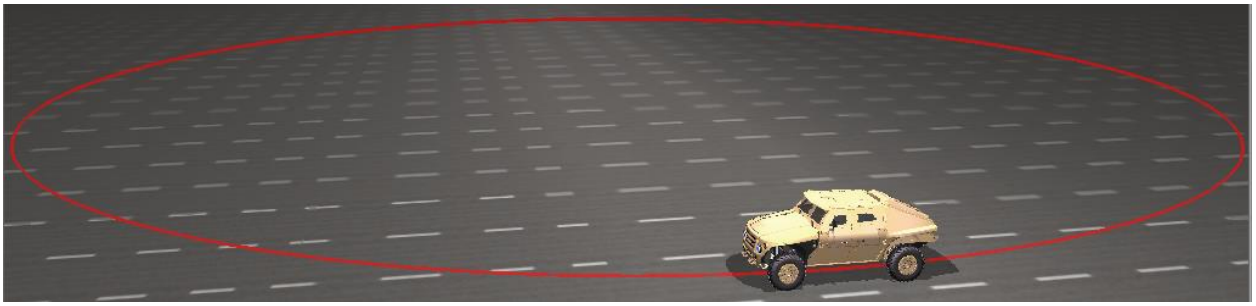

Figure 32: Snapshot of the 30 m cornering simulation.

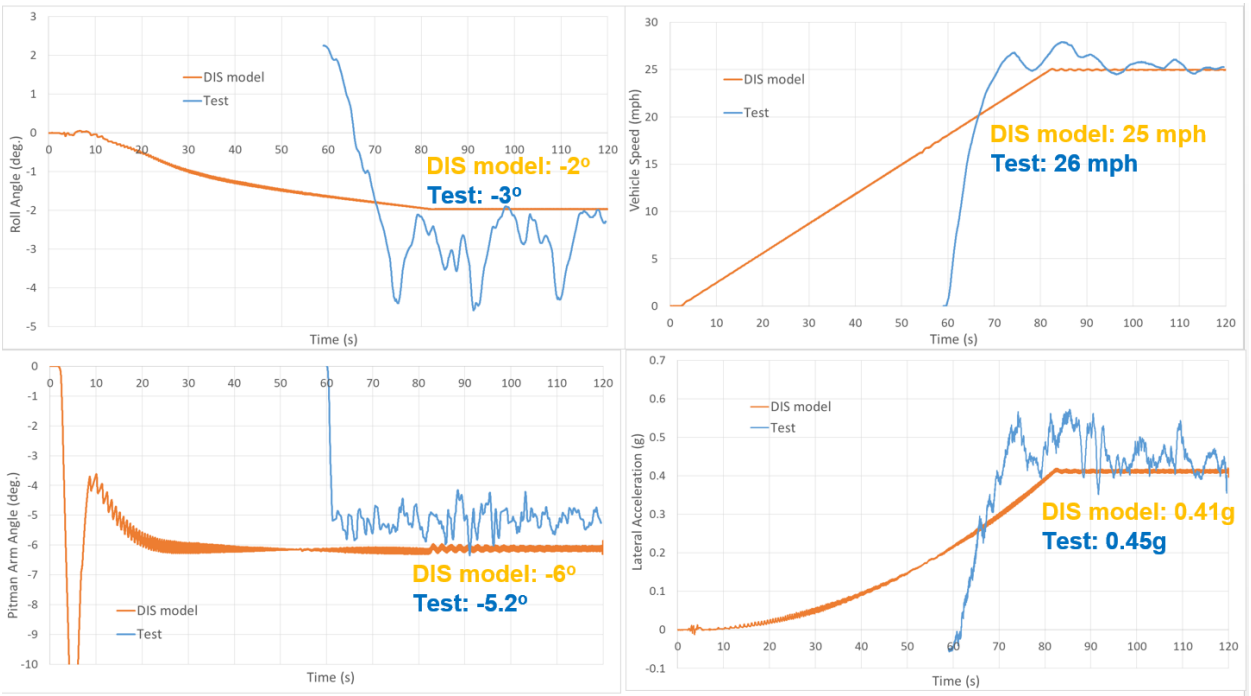

Figure 33: Comparison between test and simulation: 30 m cornering: Time-histories of roll angle, vehicle speed, Pitman arm angle and lateral acceleration.

4. EVENT 4: DOUBLE-LANE CHANGE ON PAVEMENT

The vehicle is accelerated to the constant final speed of 30 mph on pavement (COF = 0.8). Then the vehicle performs the NATO AVTP03-160W double-lane change maneuver. A comparison between the DIS model and the test is shown in Figure 34.

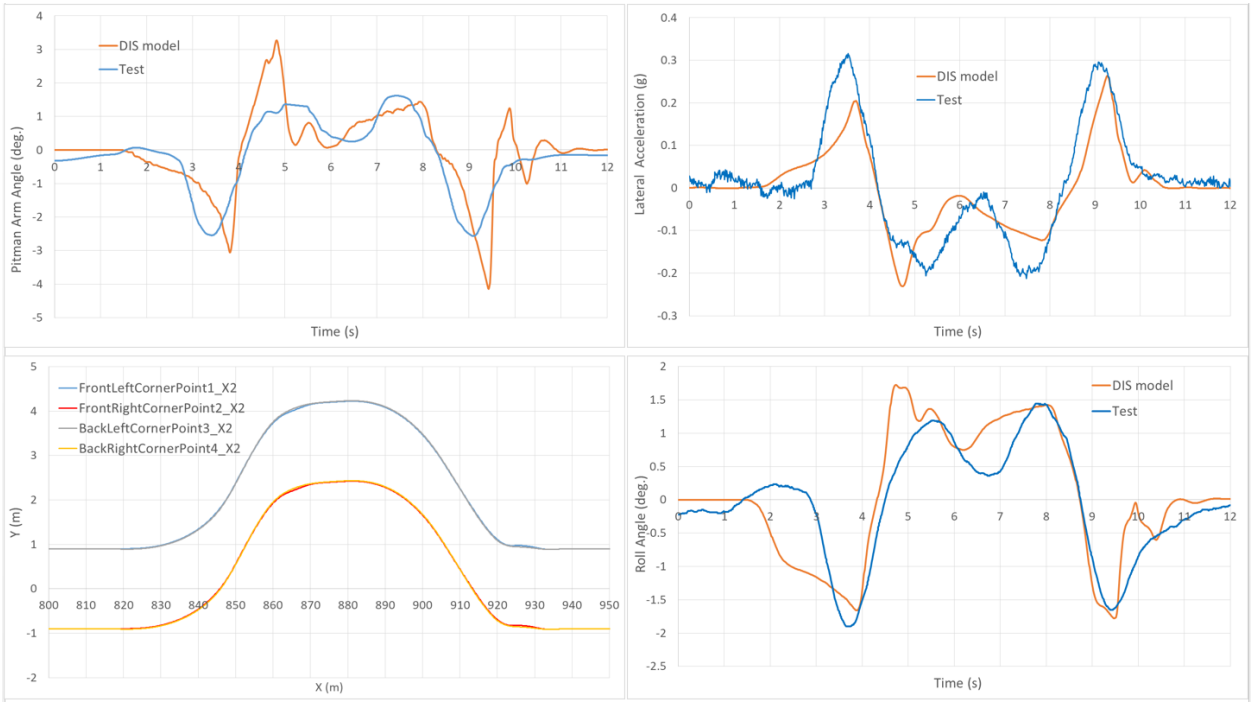

Figure 34: Comparison between test and simulation: double-lane change at 30 mph: Time-histories of pitman arm angle, lateral acceleration, and roll angle. Also, the positions of the vehicle 4 corners are plotted.

DIS simulations were then run for the NATO AVTP03-160W double-lane change maneuver on pavement (COF = 0.8) with vehicle speeds in the range from 20 to 53 mph. At 50 mph, the vehicle goes outside the NATO AVTP03-160W double-lane change limits. Thus **the maximum double-lane change vehicle speed on pavement is 49 mph**. Snapshots from the double-lane change simulation at 49 mph are shown in Figure 35. The following simulation data of the vehicle in the NATO format was uploaded to the CDT ftp site:

- Paved, double-lane change at 20 mph Left turn first: PavedLaneChange_20mphLTF.csv
- Paved, double-lane change at 30 mph Left turn first: PavedLaneChange_30mphLTF.csv
- Paved, double-lane change at 40 mph Left turn first: PavedLaneChange_40mphLTF.csv
- Paved, double-lane change at 46 mph Left turn first: PavedLaneChange_46mphLTF.csv
- Paved, double-lane change at 49 mph Left turn first: PavedLaneChange_49mphLTF.csv
- Paved, double-lane change at 50 mph Left turn first: PavedLaneChange_50mphLTF.csv
- Paved, double-lane change at 51 mph Left turn first: PavedLaneChange_51mphLTF.csv
- Paved, double-lane change at 52 mph Left turn first: PavedLaneChange_52mphLTF.csv
- Paved, double-lane change at 53 mph Left turn first: PavedLaneChange_53mphLTF.csv
- Paved, double-lane change at 49 mph Right turn first: PavedLaneChange_49mphRTF.csv

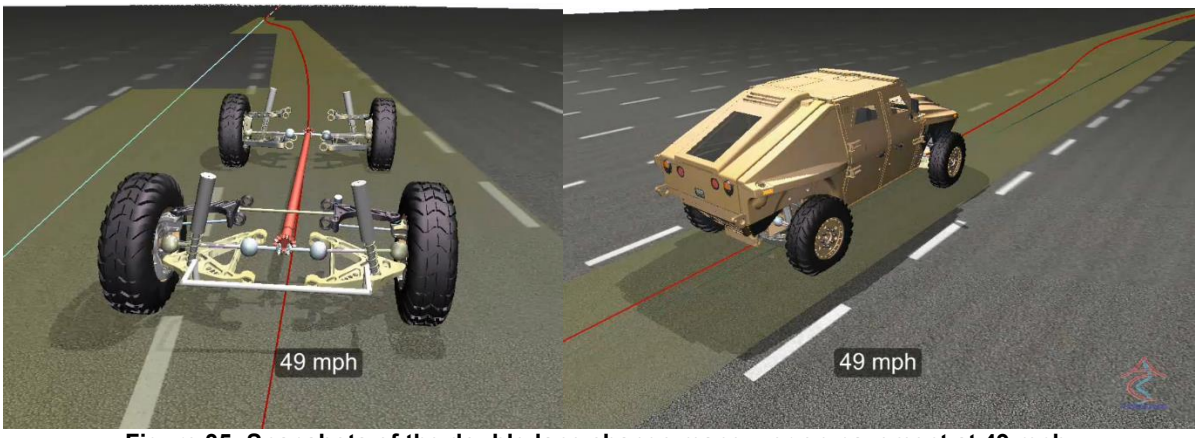

Figure 35: Snapshots of the double-lane change maneuver on pavement at 49 mph.

5. EVENT 5: DOUBLE-LANE CHANGE ON GRAVEL

DIS simulations were run for the NATO AVTP03-160W double-lane change maneuver on gravel (COF = 0.5) with vehicle speeds from 20 to 44 mph (Figure 36). At 44 mph, the vehicle goes outside the NATO AVTP03-160W double-lane change limits. Thus **the maximum double-lane change vehicle speed on gravel is 43 mph**. The following simulation data in the NATO format was uploaded to the CDT ftp site:

- Gravel, double-lane change at 20 mph Left turn first: GravelLaneChange_20mphLTF.csv
- Gravel, double-lane change at 30 mph Left turn first: GravelLaneChange_30mphLTF.csv
- Gravel, double-lane change at 40 mph Left turn first: GravelLaneChange_40mphLTF.csv
- Gravel, double-lane change at 42 mph Left turn first: GravelLaneChange_42mphLTF.csv
- Gravel, double-lane change at 43 mph Left turn first: GravelLaneChange_43mphLTF.csv
- Gravel, double-lane change at 44 mph Left turn first: GravelLaneChange_44mphLTF.csv
- Gravel, double-lane change at 43 mph Right turn first: GravelLaneChange_43mphRTF.csv

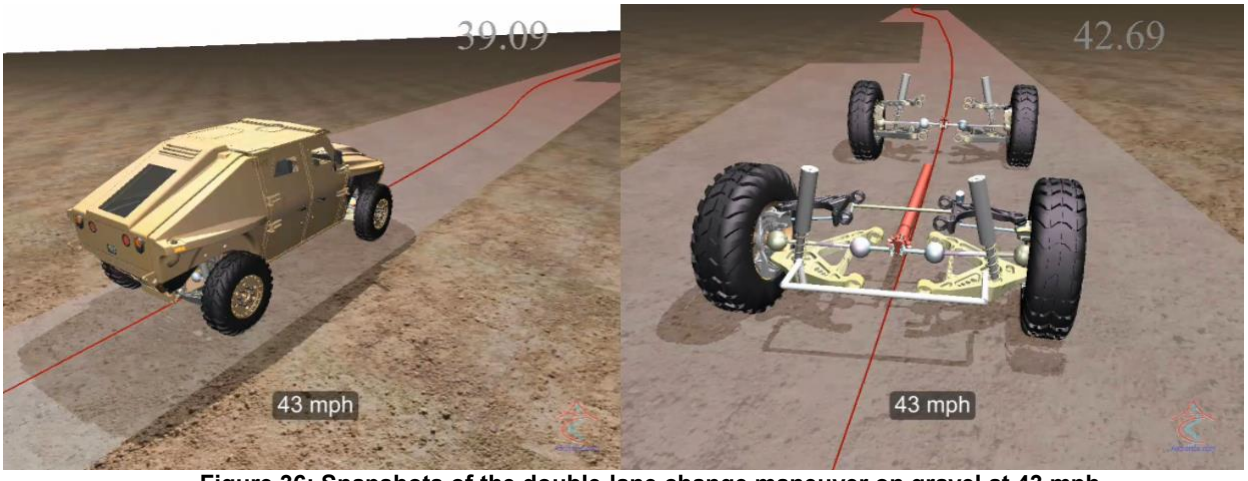

Figure 36: Snapshots of the double-lane change maneuver on gravel at 43 mph.

6. EVENT 6: SIDE-SLOPE WITH SINUSOIDAL STEER

Simulations are carried out on a gravel (COF = 0.5) 30% side slope. The vehicle is accelerated until a constant desired speed (5, 6, 7, 8, and 9 mph) is reached. The X versus Y coordinate of the center of the vehicle is plotted. The vehicle is required to maneuver around a 3 m obstacle in less than 30 m. Since the width of the vehicle is 2.288 m. Therefore, the Y coordinate of the center of the vehicle must maneuver around a virtual obstacle hat has a width given by:

$$(3 + 2.288/2)\cos(16.7^{o}) = 3.97 \text{ m}$$

Note that in order for the corners of the vehicles to maneuver around the obstacle, the maximum value of the Y coordinate of the of the center of the vehicle must be reach around 4.4 m at the corner of the turn.

Figure 37 shows the X-Y path of the vehicle's center for the vehicle in low gear setting mode with the axles and center differentials locked. The figure shows that the maximum speed that the vehicle can maneuver around the obstacle is 6 mph. At 7 mph the vehicle cannot return to a parallel path with the original vehicle path within 30 m. Figure 38 shows snapshots from the vehicle simulation at 6 mph.

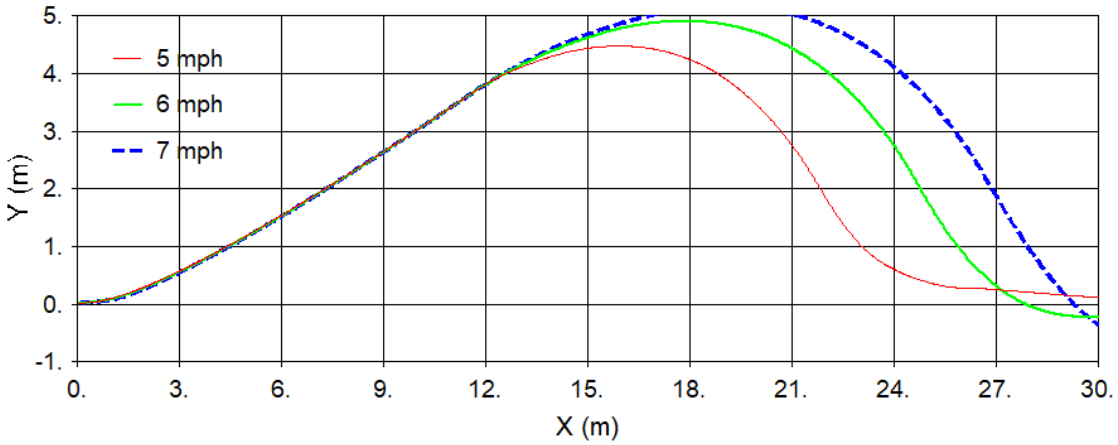

Figure 37: X-Y path of the vehicle's center for the vehicle in low gear setting mode with the axles and center differentials locked while performing the side slope obstacle avoidance maneuver.

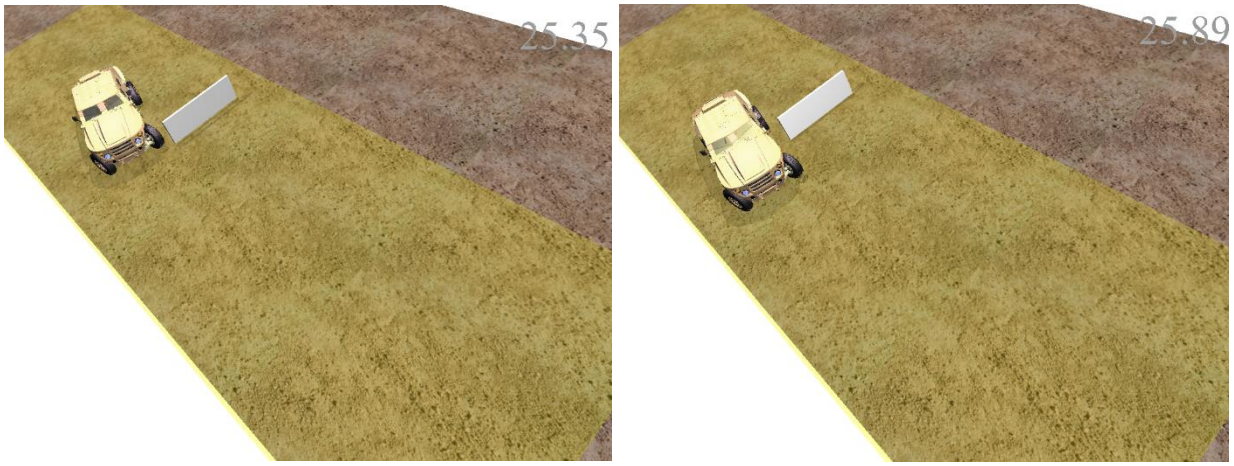

Figure 38: Snapshots of the vehicle simulation at 6 mph in low gear setting with the axles and center differentials locked while performing the side slope obstacle avoidance maneuver.

Figure 39 shows the X-Y path of the vehicle's center for the vehicle in high gear setting mode with the axles and center differentials open. The figure shows that the maximum speed that the vehicle can maneuver around the obstacle is 7 mph. At 8 mph the vehicle cannot return to a parallel path with the original vehicle path within 30 m. Figure 40 shows snapshots from the vehicle simulation at 7 mph.

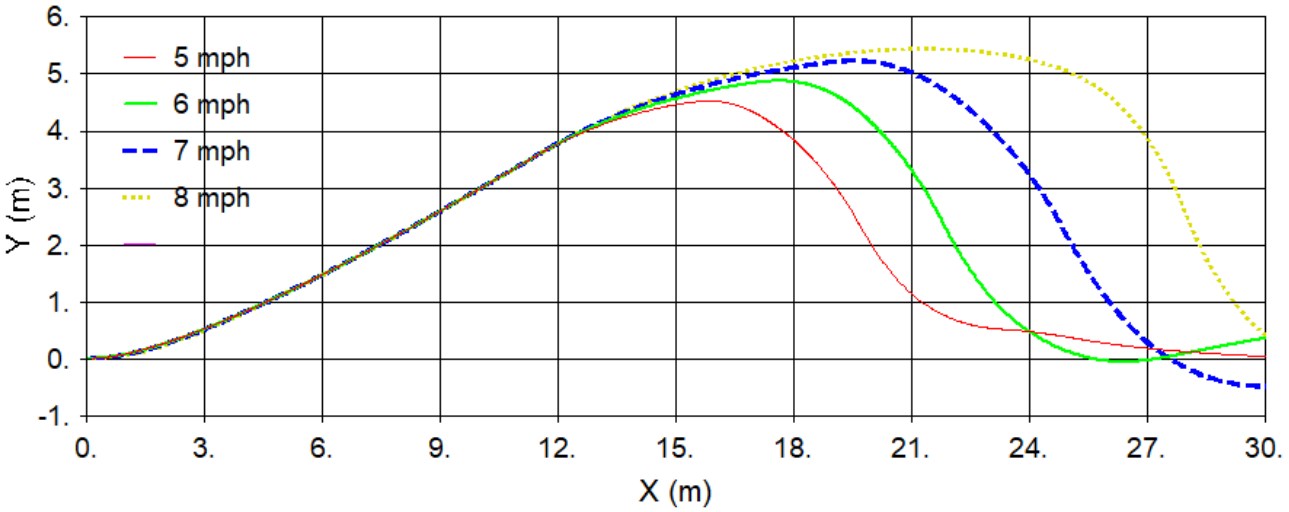

Figure 39: X-Y path of the vehicle's center for the vehicle in high gear setting mode with the axles and center differentials open while performing the side slope obstacle avoidance maneuver.

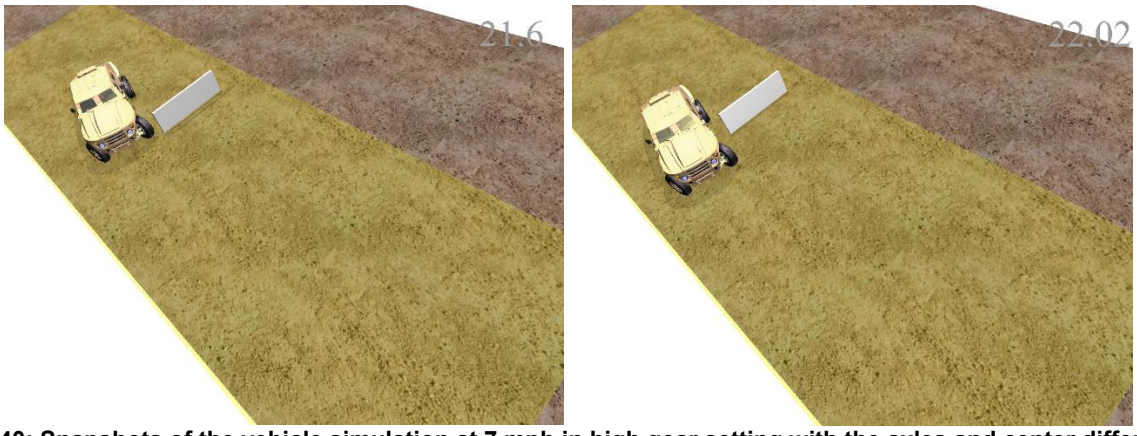

Figure 40: Snapshots of the vehicle simulation at 7 mph in high gear setting with the axles and center differentials open while performing the side slope obstacle avoidance maneuver.

In summary the simulations give the following the values for the maximum 30% side slope 3 m obstacle avoidance maneuver vehicle speed:

- **Low gear, Locked axles and center differentials. Max. Speed = 6 mph**
- **High gear, Open axles and center differentials. Max. Speed = 7 mph**

7. EVENT 7: MAXIMUM LONGITUDINAL GRADE ON PAVEMENT

Simulations are carried out on paved (COF = 0.8) grades from 0 to 85%. The vehicle is accelerated at the maximum possible acceleration until the maximum speed is reached. The maximum speed is them plotted as a function of grade % with the transfer case set to low and high ranges. The following data as uploaded to the NATO ftp site:

- HighGearRange_00grade.csv; HighGearRange_05grade.csv; HighGearRange_10grade.csv; HighGearRange_15grade.csv;
  HighGearRange_20grade.csv; HighGearRange_25grade.csv;
  HighGearRange_30grade.csv; HighGearRange_35grade.csv;
  HighGearRange_40grade.csv; HighGearRange_45grade.csv; HighGearRange_50grade.csv;
  HighGearRange_55grade.csv; HighGearRange_60grade.csv; HighGearRange_65grade.csv.

- LowGearRange_00grade.csv; LowGearRange_05grade.csv; LowGearRange_10grade.csv;
  LowGearRange_15grade.csv; LowGearRange_20grade.csv; LowGearRange_25grade.csv;
  LowGearRange_30grade.csv; LowGearRange_35grade.csv; LowGearRange_40grade.csv;
  LowGearRange_45grade.csv; LowGearRange_50grade.csv; LowGearRange_55grade.csv;
  LowGearRange_60grade.csv; LowGearRange_65grade.csv; LowGearRange_70grade.csv;
  LowGearRange_75grade.csv; LowGearRange_80grade.csv; LowGearRange_85grade.csv.

Figure 41 shows the maximum vehicle speed versus grade on pavement in the high and low transfer case gear ranges.

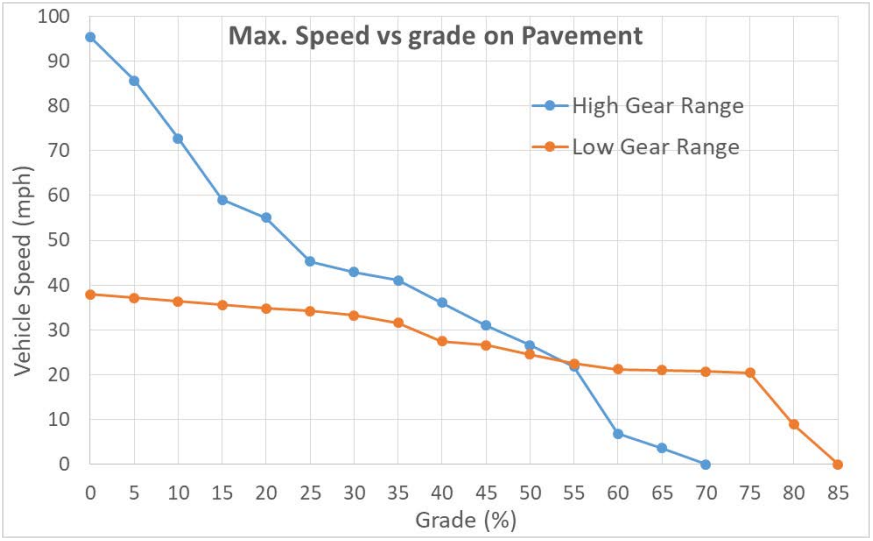

Figure 41: Maximum vehicle speed versus grade on pavement in the high and low transfer case gear ranges.

8. EVENT 8: MAXIMUM LONGITUDINAL GRADE ON SAND

The vehicle is simulated on the KRC variable sand grade in which the grade varies from 0 to 30% with an increment of 5%. The sand type is 2NS sand. Based on the shear cell noLoad.xlsx results the cohesion of the 2NS sand is set to 1 kPa. Based on the KRC cone index experiments for the 2NS sand the sand cone index range is 50 to 70 psi. Using the cone penetrometer simulations and based on the cone index and the cohesion, the internal friction angle of the 2NS sand range is 22^{o} to 25^{o}.

Based on the simulations of the vehicle on the variable sand slope, **the maximum slope that the vehicle can climb is in the range of 15% to 23%**.

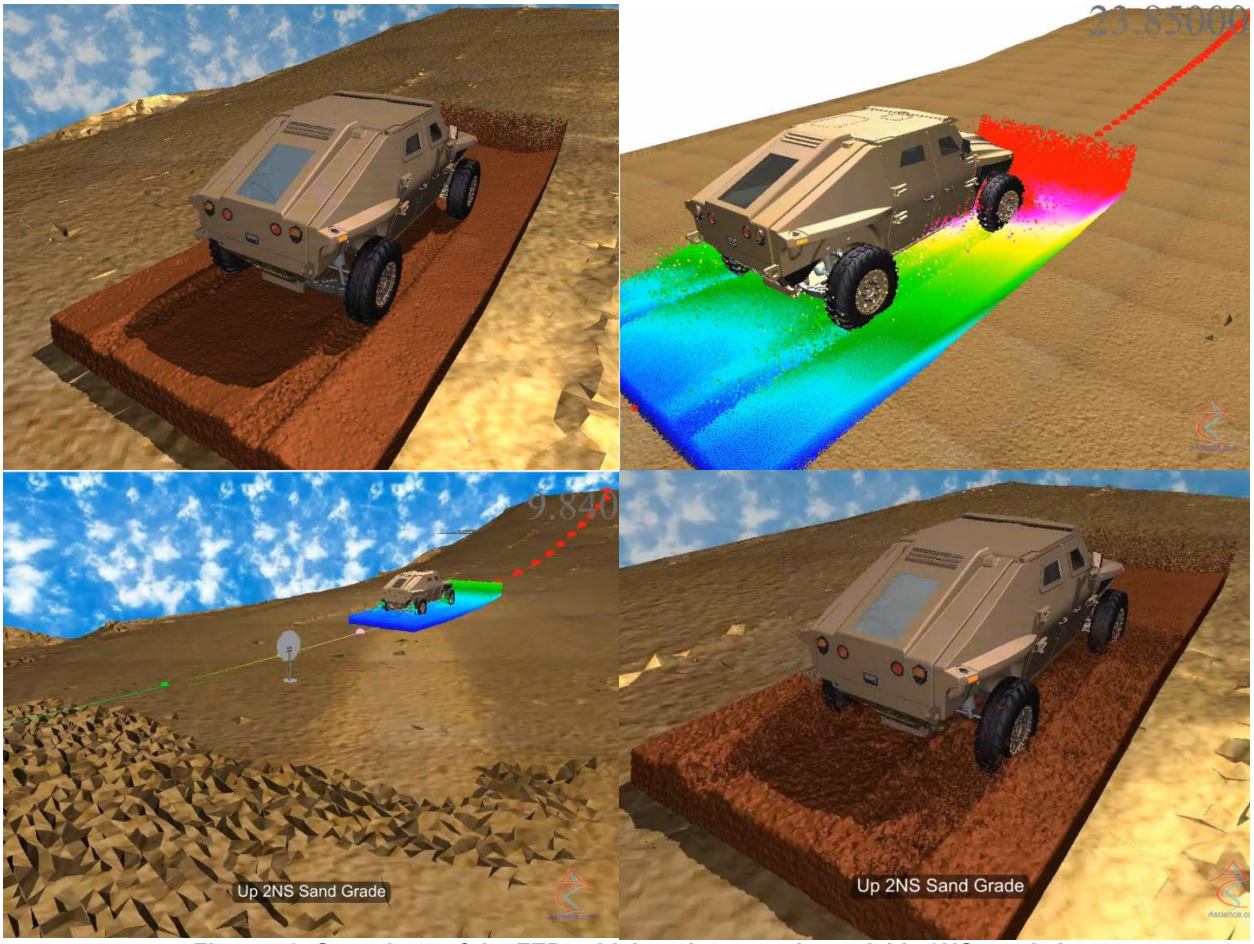

Figure 42: Snapshots of the FED vehicle going over the variable 2NS sand slope.

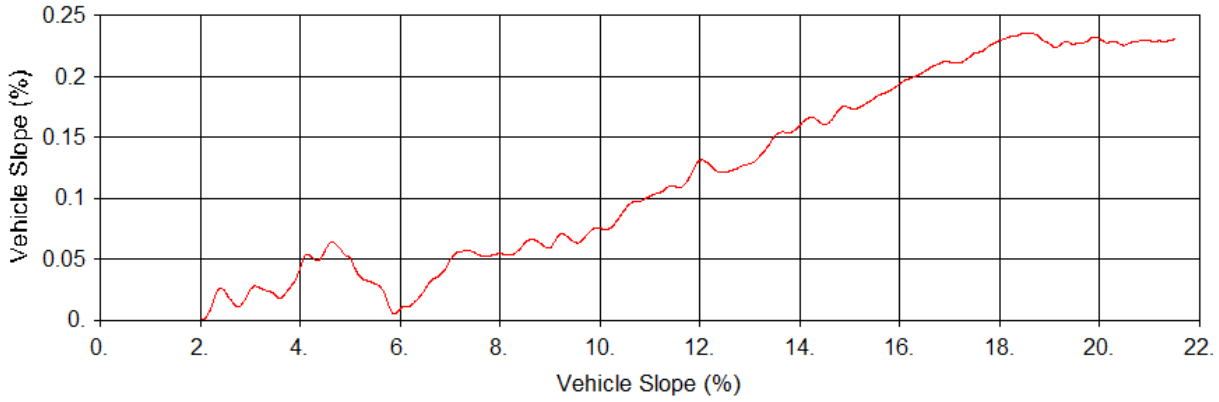

Figure 43: Vehicle slope as a function of time during the sand grade climb. The maximum slope reached is about 23%.

9. EVENTS 9-12: HALF-ROUNDS 4-18 INCH

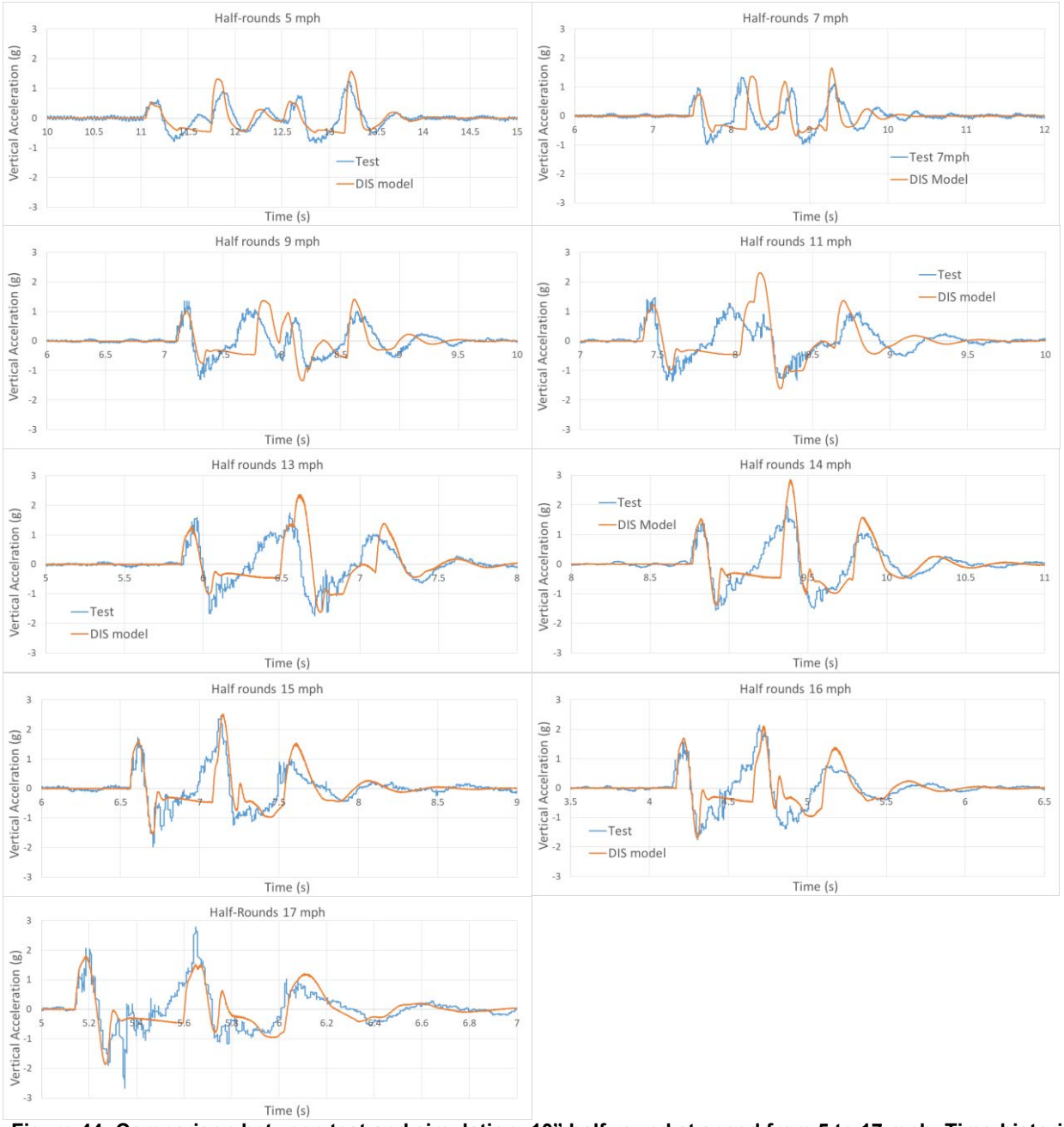

Figure 44: Comparison between test and simulation: 10” half-round at speed from 5 to 17 mph: Time-histories of vertical acceleration at the driven seat.

A comparison between the DIS model simulation results and the test for the vehicle going aincreasing speeds over the 10” half-round bumps is shown in Figure 44. A summary of the DIS simulation results of the maximum

driver seat base acceleration for the FED vehicle going over 4”, 8”, 10” and 12” half-rounds is shown in Figure 45.

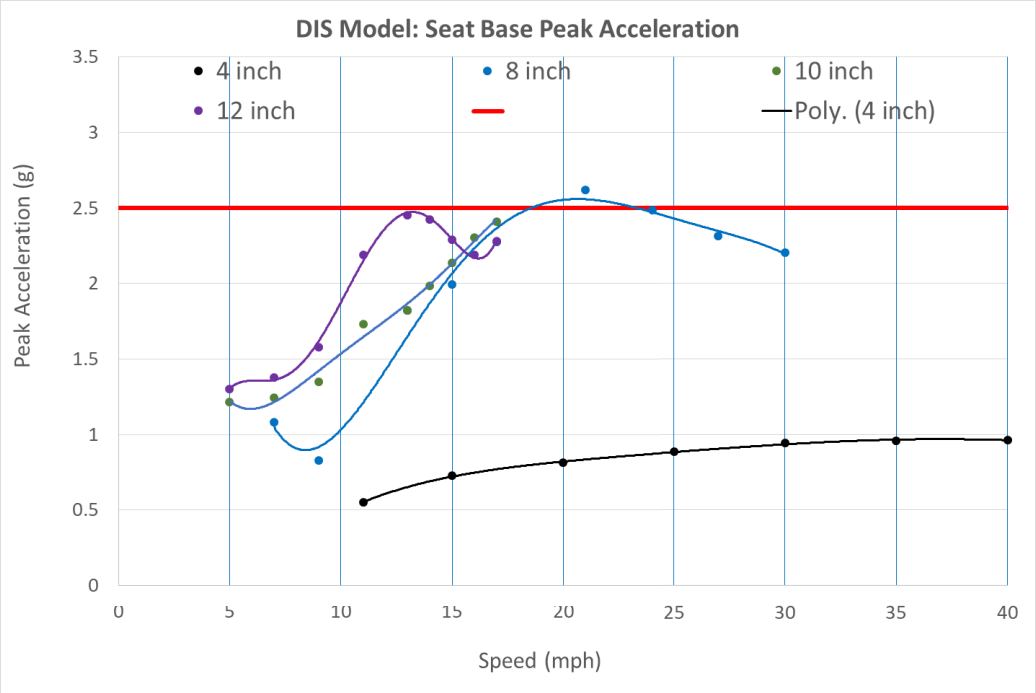

Figure 45: Driver seats base vertical acceleration versus vehicle speeds predicted using DIS for the vehicle going at increasing speeds over the 4”, 8”, 10”, and 12” half-round bumps.

A comparison between the driver/passenger seats vertical acceleration vehicle speeds predicted using DIS model simulation results and the KRC experiments for the vehicle going at increasing speeds over the 4”, 8”, 10”, and 12” half-round bumps is shown in Figure 46.

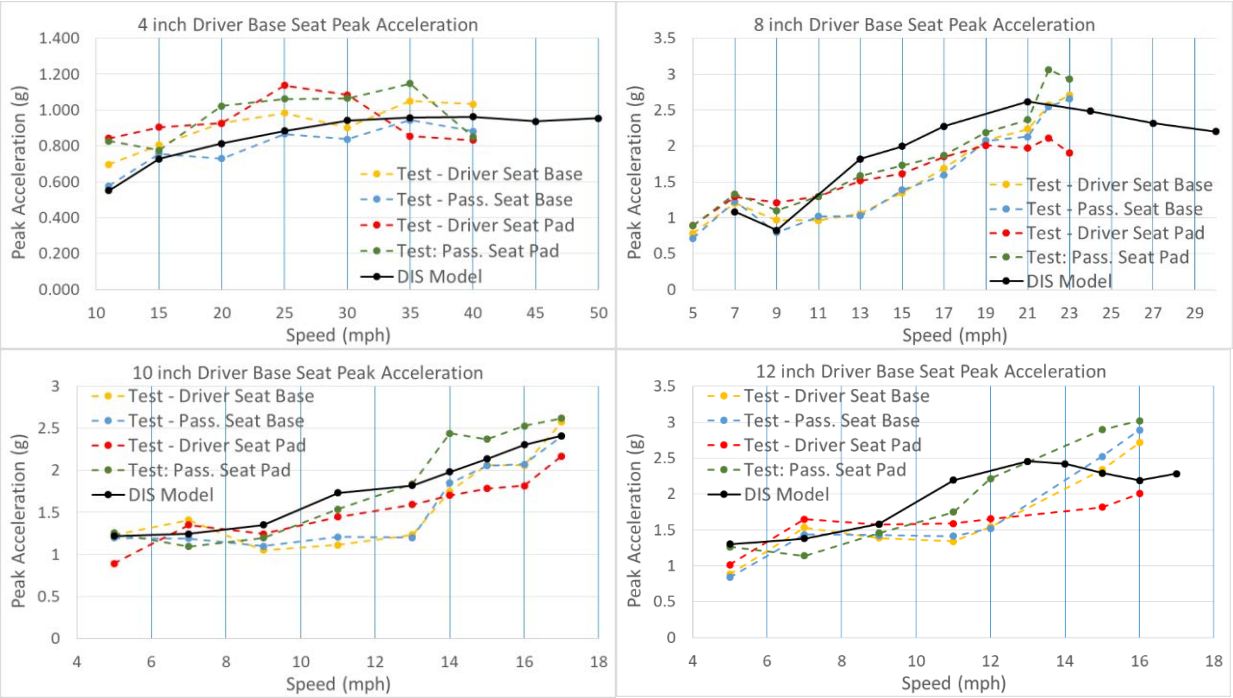

Figure 46: Driver/passenger seats vertical acceleration vehicle speeds predicted using DIS model simulation results and the KRC experiments for the vehicle going at increasing speeds over the 4", 8", 10", and 12" half-round bumps.

A comparison between the 2.5 g driver/passenger seats vertical acceleration vehicle speeds predicted using DIS model simulation results and the KRC experiments for the FED vehicle going over the 4", 8", 10", and 12" half-round bumps is shown in the table below.

Table 7: Summary of 2.5 g driver/passenger seats vertical acceleration vehicle speeds predicted using DIS model simulation results and the KRC experiments for the vehicle going at increasing speeds over the 4", 8", 10", and 12" half-round bumps.

	DIS Model	Test: Driver Seat Base (mph)	Test: Passenger Seat Base (mph)	Test: Driver Seat Pad (mph)	Test: Passenger Seat Pad (mph)
4 inch	No limit	No limit	No limit	No limit	No limit
8 inch	21	21	22.5	No limit	21
10 inch	17	16.5	17.5	No limit	16
12 inch	13	15	14.9	No limit	13.5

10. EVENT 13-14: VERTICAL STEPS

We performed simulations of the vehicle going over 12”, 18”, and 24” vertical steps at a slow speed of about 0.5 m/s. The results are:

- 12” step is a go.
- There is slight interference on the bottom of the front bumper for the 18” step. Therefore, the 18” is a no go.
- There is major interference on the front bumper for the 24” step. Therefore the 24” step is a no go.

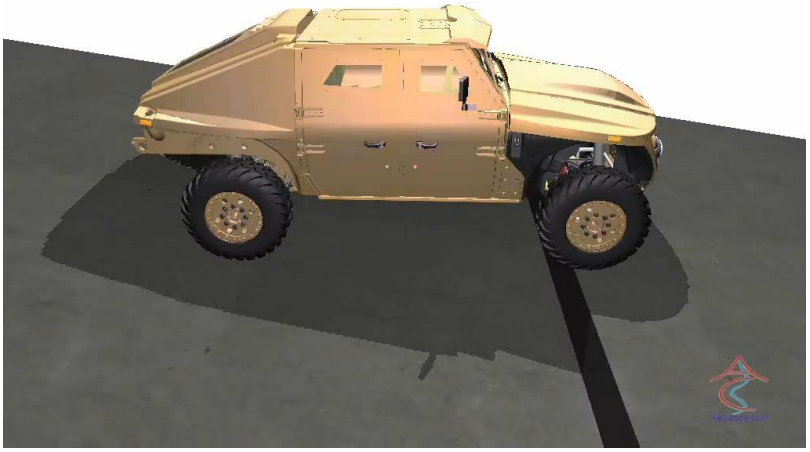

Figure 47: Snapshots of the vehicle going over 18” vertical step.

11. EVENT 15: V-DITCH

We performed a simulation of the vehicle going over the given V-ditch at about 0.5 m/s. The vehicle can cross the V-ditch with no interference.

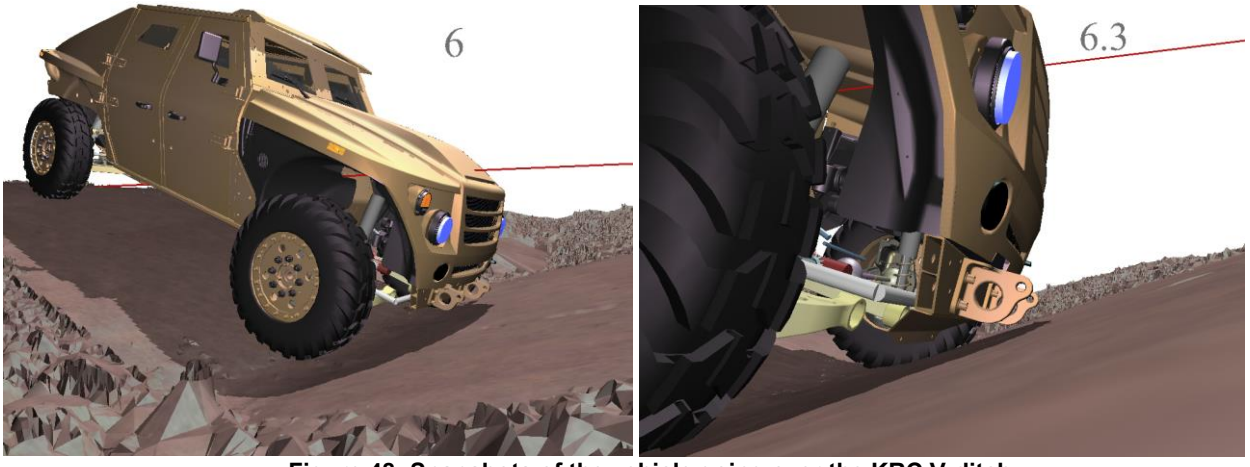

Figure 48: Snapshots of the vehicle going over the KRC V-ditch.

12. EVENTS 16-18: DRAW-BAR PULL ON SOFT SOIL

We tuned the soil material properties for FGS-Dry, CGS-Dry, and FGS-Wet using the provided shear cell lab tests and the cone penetrometer in-situ tests (see Table 6). Based on those test the following material properties are used:

- Fine Grain Soil Dry (FGS-Dry)
  - Cone index range = 75 to 90 psi; Cohesion = 3.4 kPa, Average friction angle = 38^o
- Coarse Grain Soil Dry (CGS-Dry)
  - Cone index range = 45 to 55 psi; Cohesion = 4.15 kPa, Average friction angle = 22^o
- Fine Grain Soil Wet (FGS-Wet)
  - Cone index range = 20 to 25 psi; Cohesion = 3.4 kPa, Friction angle range = 11^o - 13^o.

Then, the tuned soil model was then used in the drawbar pull simulation (Figure 49) on the three soil types. The DIS model simulation and corresponding test results of the drawbar pull force versus slip are shown in Figure 50, Figure 51, and Figure 52.

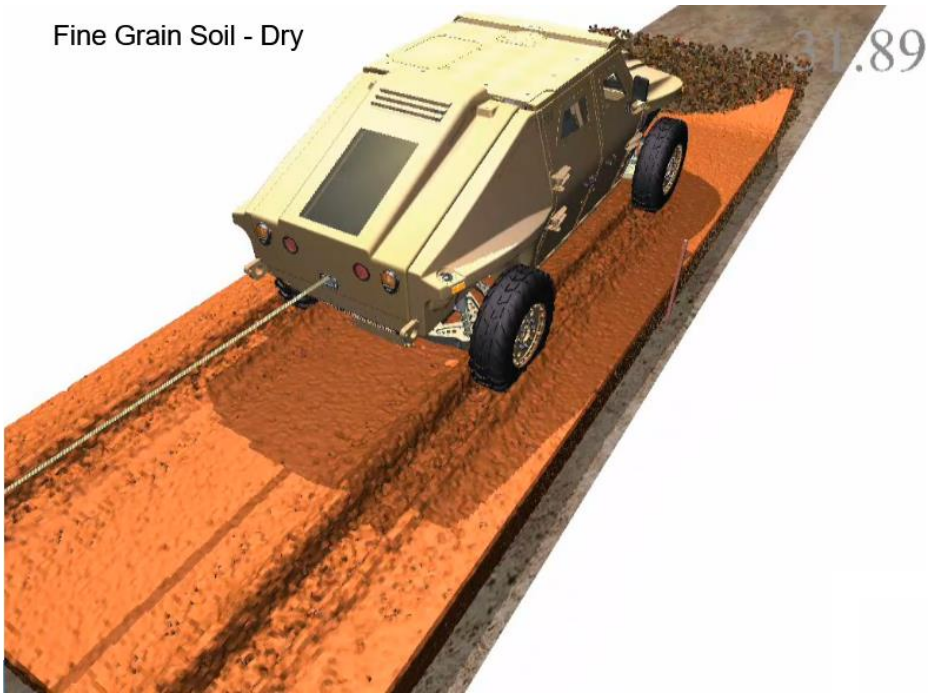

Figure 49: Snapshot during of the drawbar pull simulation on FGS-Dry.

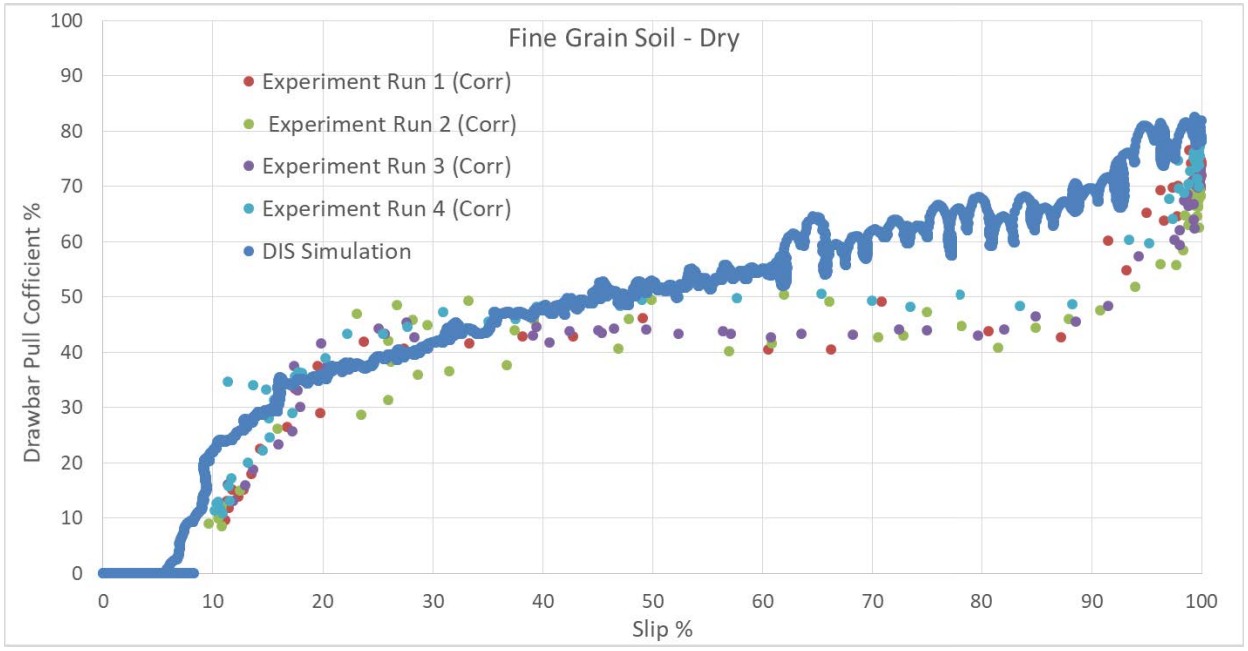

Figure 50: Test (inertia corrected) drawbar pull coefficient versus wheel slip results (top) and DIS model results (bottom) for FGS-Dry.

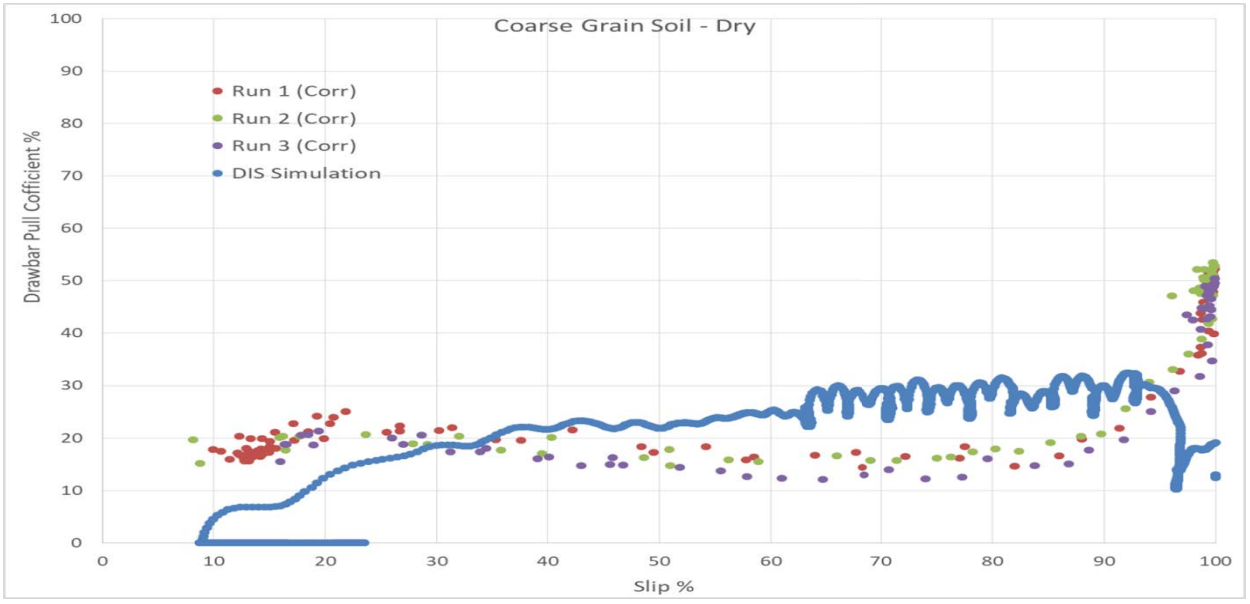

Figure 51: Test (inertia corrected) drawbar pull coefficient versus wheel slip results (top) and DIS model results (bottom) for CGS-Dry.

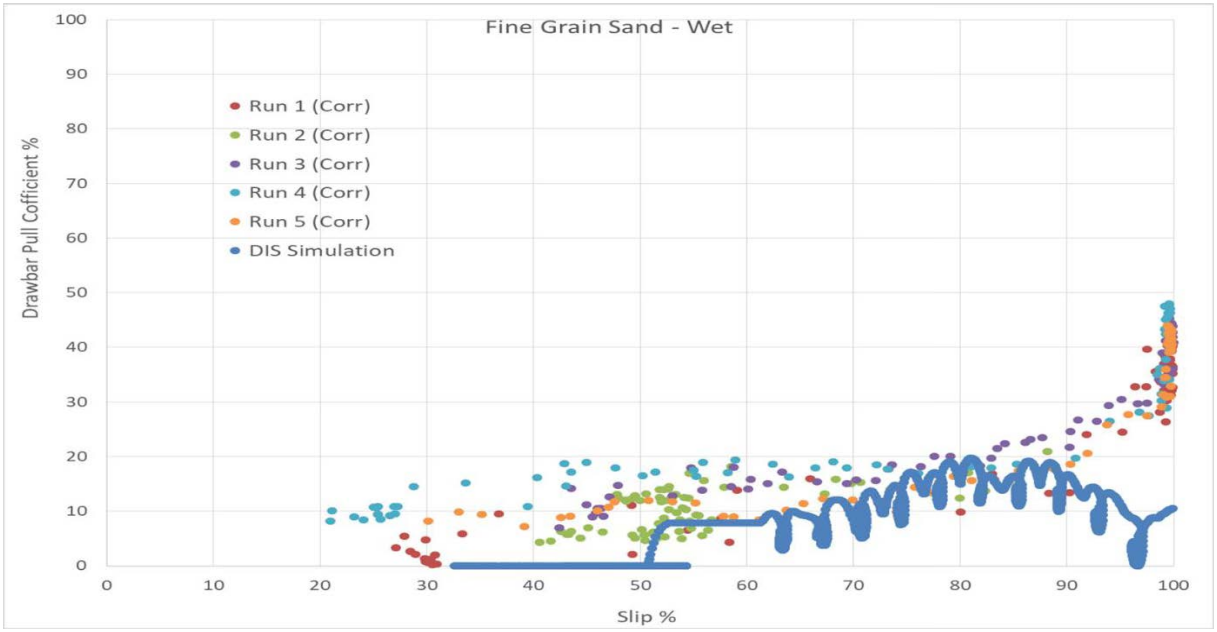

Figure 52: Test (inertia corrected) drawbar pull coefficient versus wheel slip results (top) and DIS model results (bottom) for FGS-Wet.

Notes:

- Drawbar pull physical test was conducted under unsteady state conditions (vehicle was decelerating). So it was not straight forward to extract the drawbar pull versus slip curve from the raw experimental data. The drawbar pull force had to be corrected for inertial forces which probably introduced errors into the drawbar pull force.
- The full tire radius should be used to calculate slip rather than a loaded tire radius. Otherwise the drawbar-pull versus slip curve shows positive drawbar-pull at zero slip which is not physically possible since this means that the soil is propelling the vehicle forward while the tires are not producing traction forces. In the actual drawbar-pull test, the tires have to have some slip to overcome the soil resistance before starting to generate a drawbar-pull. The physical justification for using the full tire radius rather than a loaded tire radius is that the tire has a steel belt under the tread which keeps the tire circumference length constant independent of the normal load and tire air pressure.

13. EVENTS 20-22: ASYMMETRIC RMS 1 TO 3 INCH COURSES

DIS simulations were performed of the FED vehicle going at speeds from 5 to 20 mph on 1.0” – 1.5” and 1.5” – 2.0” asymmetric RMS test courses (Figure 53). From each simulation the absorbed vibration power at the driver seat base is extracted and plotted versus vehicle speed. This is then compared with the test results of absorbed vibration power versus vehicle speed at the driver and passenger seats base on pad. The results are shown in Figure 54 to Figure 57.

Figure 53: Snapshots from the vehicle simulation over the 1.0” – 1.5” asymmetric RMS test course.

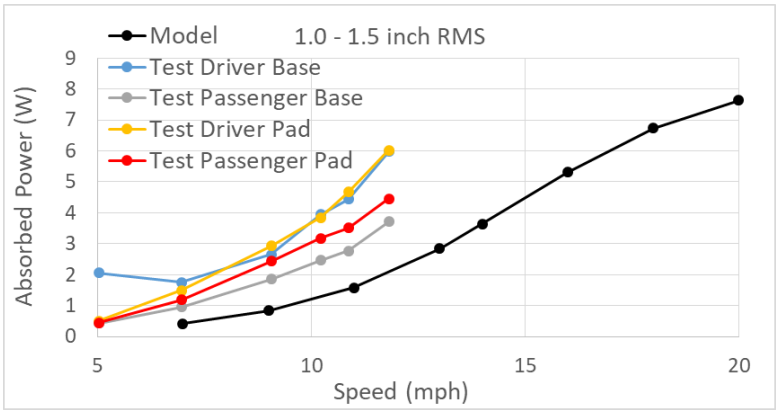

Figure 54: Comparison between absorbed vibration power versus vehicle speed for the 1.0” – 1.5” asymmetric RMS test course.

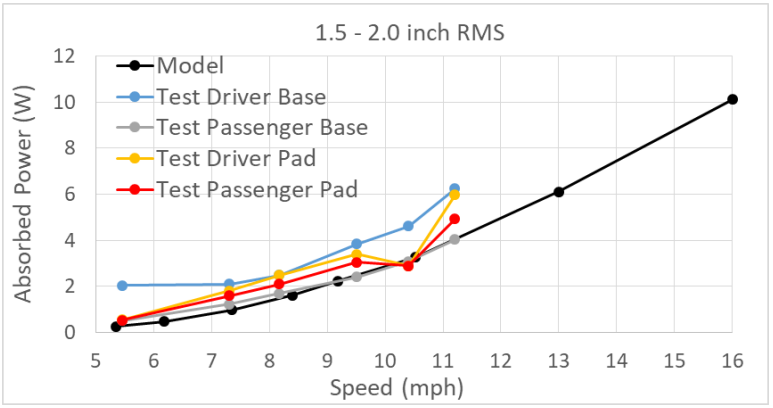

Figure 55: Comparison between absorbed vibration power versus vehicle speed for the 1.5” – 2.0” asymmetric RMS test course.

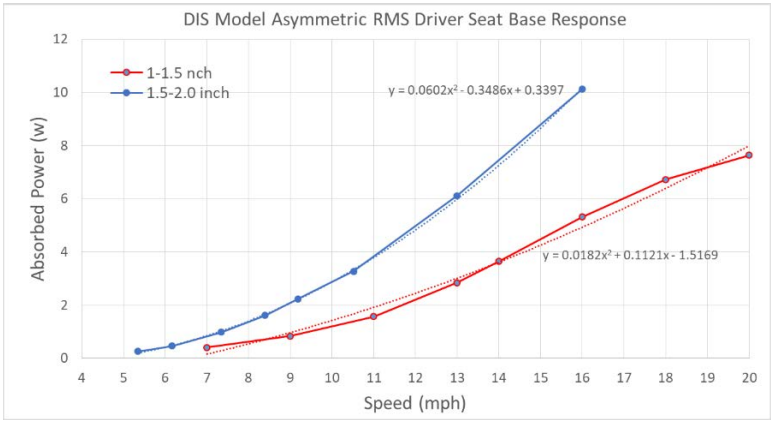

Figure 56: DIS model vibration power versus vehicle speed for the 1.0” – 1.5” and 1.5” – 2.0” and asymmetric RMS test courses.

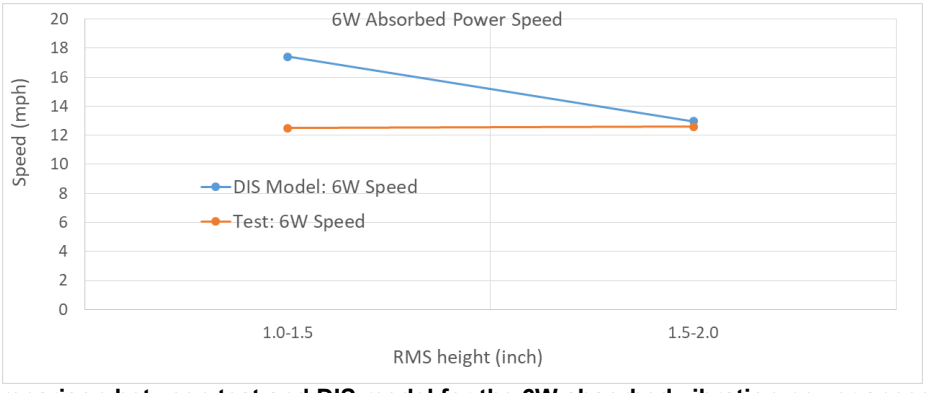

Figure 57: Comparison between test and DIS model for the 6W absorbed vibration power speed versus RMS amplitude for the asymmetric RMS test courses.

14. EVENTS 27-31: SYMMETRIC RMS 1 TO 5 INCH COURSES

DIS simulations were performed of the FED vehicle going at speeds from 4 to 16 mph on 1.0”, 1.5”, 2.0”, 3.0” and 4.0” symmetric RMS test courses. From each simulation the absorbed vibration power at the driver seat base is extracted and plotted versus vehicle speed. This is then compared with the test results of absorbed vibration power versus vehicle speed at the driver and passenger seats base on pad. The results are shown in Figure 58 to Figure 65.

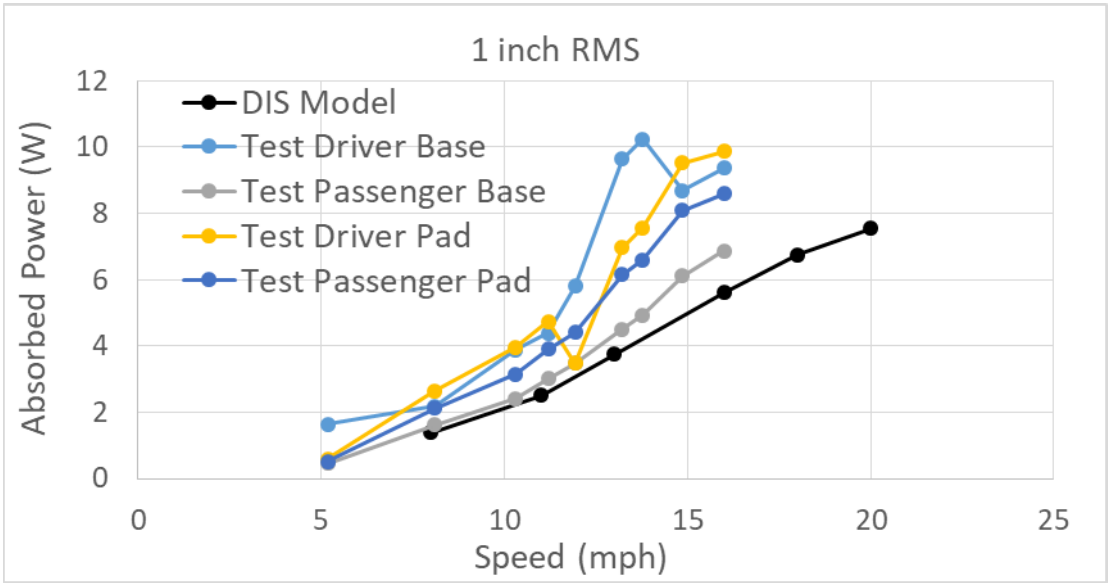

Figure 58: Comparison between DIS model and test for the 1.0" symmetric RMS course: Absorbed vibration power at the driver seat base versus vehicle speed. The solid black line is the DIS model simulation results.

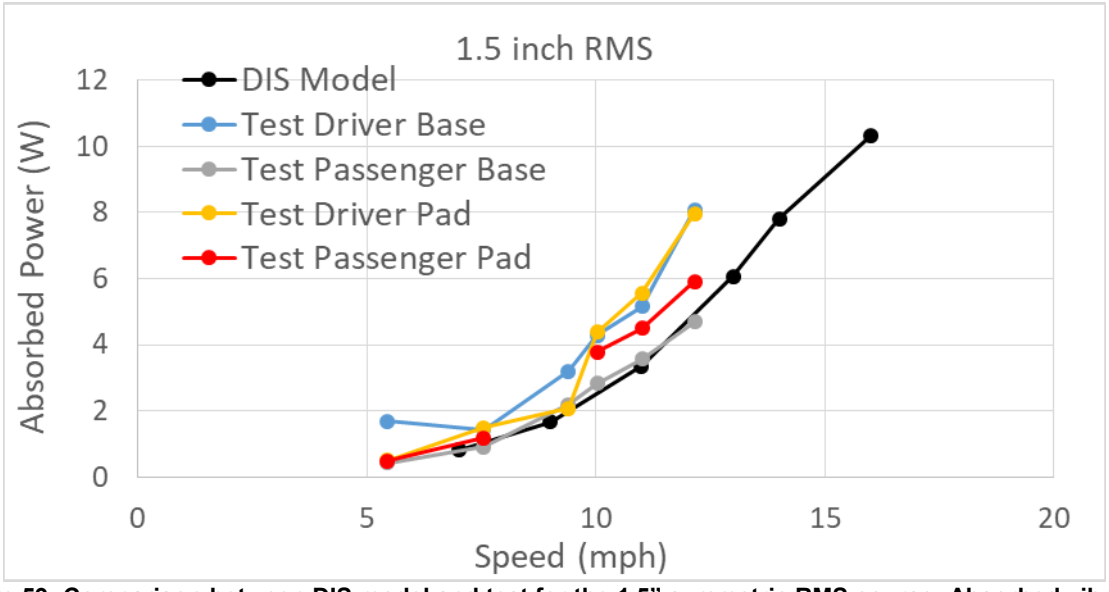

Figure 59: Comparison between DIS model and test for the 1.5" symmetric RMS course: Absorbed vibration power at the driver seat base versus vehicle speed. The solid black line is the DIS model simulation results.

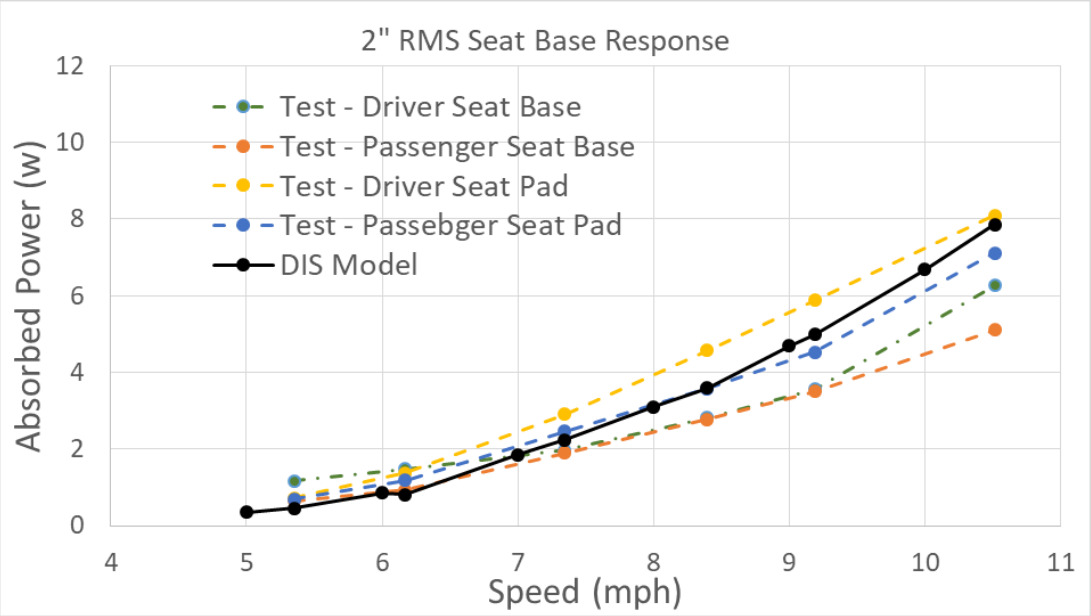

Figure 60: Comparison between DIS model and test for the 2.0" symmetric RMS course: Absorbed vibration power at the driver seat base versus vehicle speed. The solid black line is the DIS model simulation results.

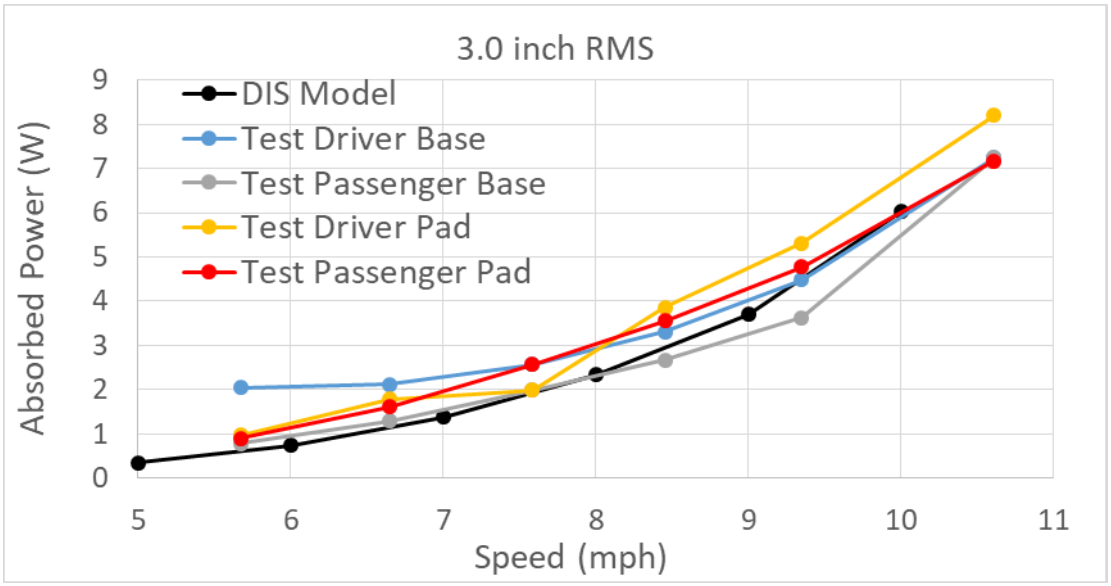

Figure 61: Comparison between DIS model and test for the 3.0" symmetric RMS course: Absorbed vibration power at the driver seat base versus vehicle speed. The solid black line is the DIS model simulation results.

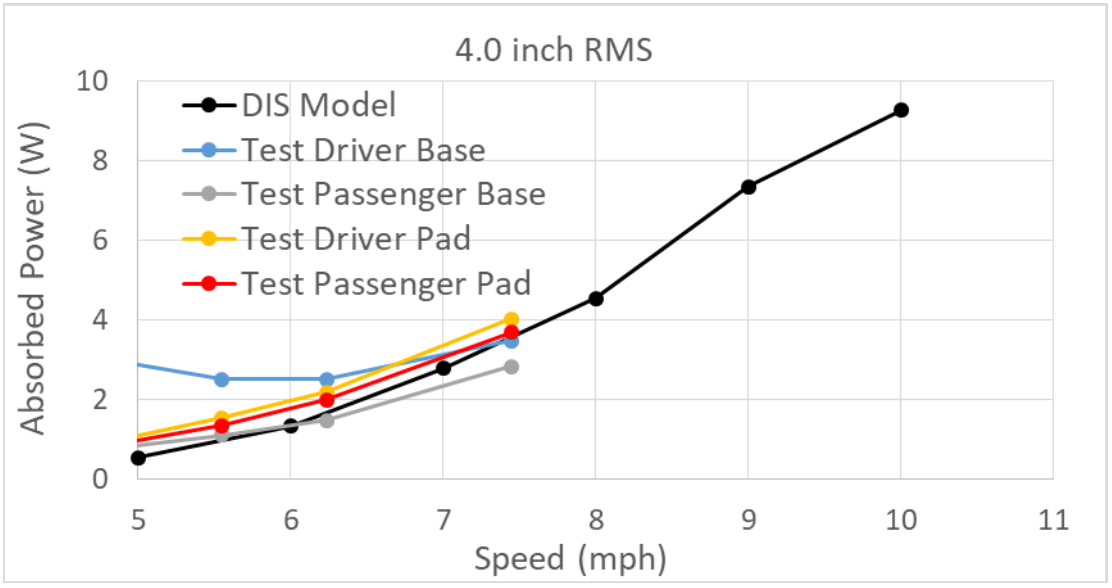

Figure 62: Comparison between DIS model and test for the 4.0” symmetric RMS course: Absorbed vibration power at the driver seat base versus vehicle speed. The solid black line is the DIS model simulation results.

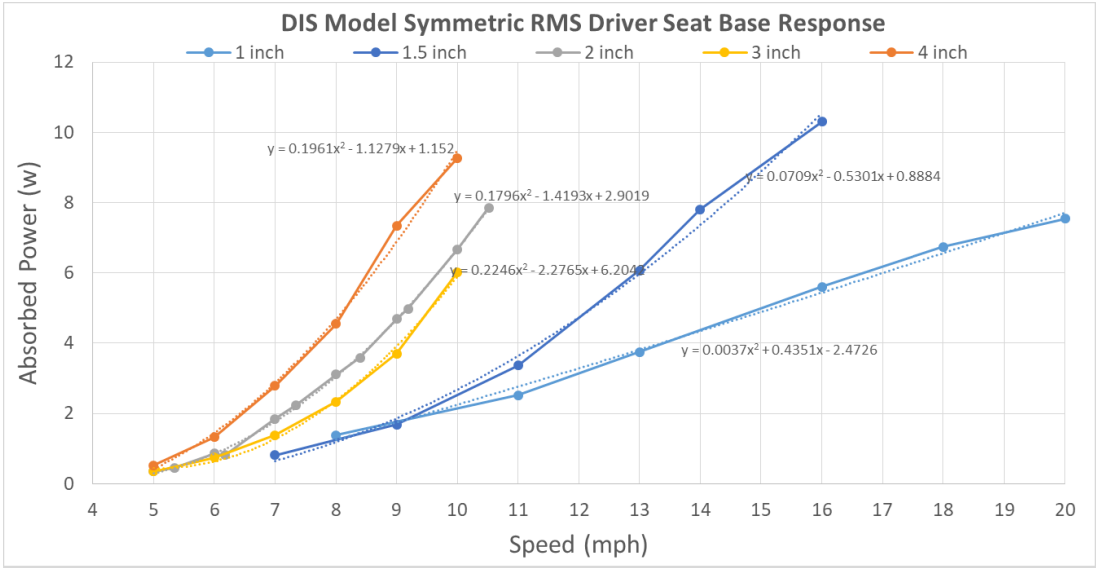

Figure 63: DIS model absorbed vibration power at the driver seat base versus vehicle speed for the 1.0”, 1.5”, 2.0”, 3.0”, and 4.0” symmetric RMS courses.

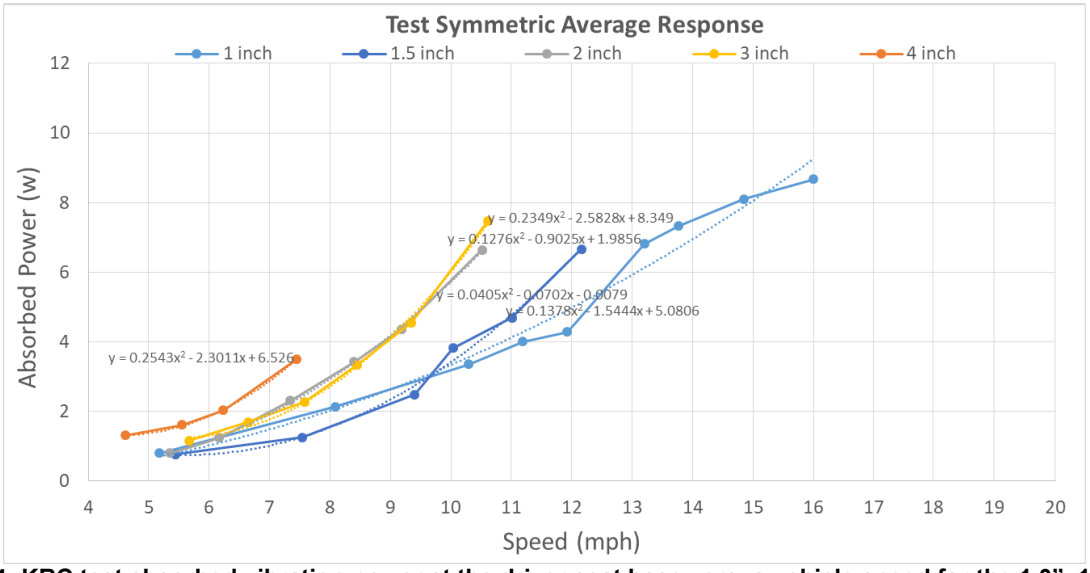

Figure 64: KRC test absorbed vibration power at the driver seat base versus vehicle speed for the 1.0", 1.5", 2.0", 3.0", and 4.0" symmetric RMS courses.

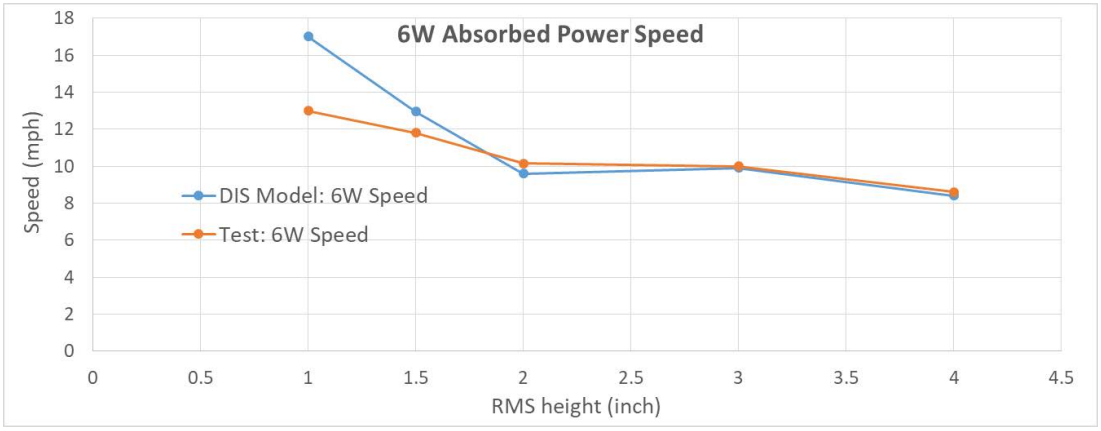

Figure 65: Comparison between test and DIS model for the 6W absorbed vibration power speed versus RMS amplitude for the symmetric RMS test courses.

15. EVENT 32: MOBILITY TRAVERSE

DIS includes the capability to model both hard and soft soil long arbitrary topology and arbitrary length terrains. This capability was used to model vehicle going over the soft soil and hard terrain mobility traverse segments. Complex topography includes:

1. Sloped terrains: positive and negative long slopes and side slopes.
2. Roughness which can be modeled using wave length versus amplitude.
3. Discrete ditches and bumps specified by depth, width, and spacing distribution.
4. Turns.
5. Variable soil/terrain conditions along the terrain.

Hard terrains long arbitrary topology are represented using polygonal surfaces (consisting of triangles and/or quadrilateral faces) of the following types:

- A 2D digitized surface (Figure 66).
- A 1D distance versus height list (Figure 53). This surface was used to model RMS courses. Left and right track surfaces can be different.

A master/slave contact model is used where contact is detected between discrete points on a master contact surface (such as tire or track) and a polygonal slave contact surface [5-9] (the terrain). A general fast binary-tree hierarchical bounding box/sphere contact search algorithm allows DIS to quickly find the contact penetration between points on a master contact point and the contact polygon on the slave contact surface [8, 9]. The penalty technique including both normal stiffness and damping is used for imposing the normal contact constraint [5-9] between the master and slave contact surfaces. The penalty stiffness and damping are set to the resultant stiffness and damping of the running gear (tire/track segment) and the terrain. Contact friction is modeled using an accurate and efficient asperity-based friction model [4, 6]. In addition, the coefficient of friction and road compliance between the running gear and the road can be set as a function of the distance along the vehicle steering path.

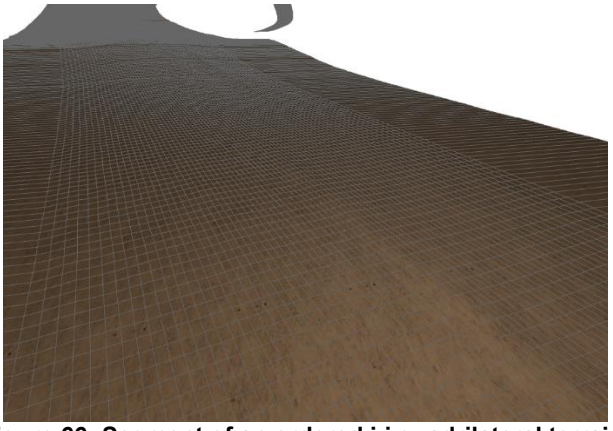

Figure 66: Segment of an ordered i-j quadrilateral terrain.

DIS also includes the capability of modeling soft soil complex topography terrains of arbitrary length using a moving soil patch technique [10]. Using this technique particles which are far behind the vehicle are continuously eliminated and then reemitted as new particles in front of the vehicle. The terrain is defined using an *i-j* ordered quadrilateral grid along with an emitter surface, a leveling surface, and a sink surface (Figure 67). The simulation starts by filling a rectangular range, say from i_1 to i_2 and j_1 to j_2, where the i index is along the length of the soil patch and j is along the width, on the *i-j* terrain surface with DEM particles up to a desired depth. Side wall surface at $j = j_1$ and $j = j_2$ along with the sink and emitter surfaces keep the particles inside the soil box. Then, the initial particles are compressed and leveled from the top using the terrain surface such that the same terrain topography is impressed on the soft soil. Next, the sink, emitter, and leveling surfaces are enabled and moved along with the center of the vehicle. When a particle touches the sink surface behind the vehicle it is immediately disabled and then reemitted as a new particle from a random point on the emitter surface in front of the vehicle. The leveling surface levels and compresses the DEM particles that are emitted from the emitter surface. This effectively moves the soil patch along with the vehicle on the terrain. Since the sink, emitter and leveling surfaced all follow the underlying terrain's *i-j* surface, the topography of the soft soil

patch follows the topography of the terrain's *i-j* surface. Figure 68 shows snapshots of typical vehicle simulations on complex topography terrains with terrain roughness, turns, and variable long slopes.

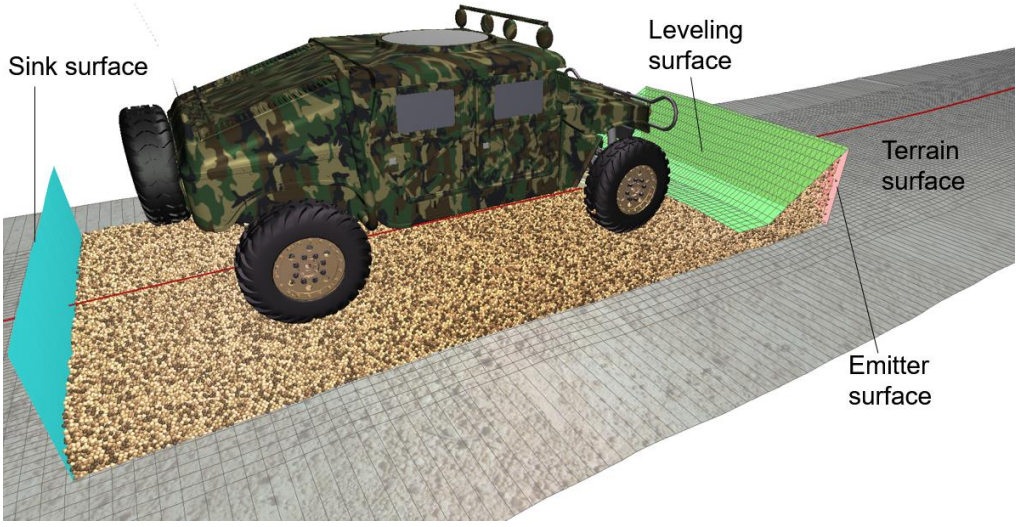

Figure 67: Moving DEM complex topography terrain patch modeled using an *i-j* ordered quadrilateral grid representing the terrain's surface, an emitter surface, a leveling surface, and a sink surface.

Figure 68: Snapshots of the moving DEM complex topography terrain patch in typical vehicle mobility simulations: 90° turn (left) and going down a slope (right) on rough soft soil terrains.

The moving soil patch technique ensures that the number of DEM particles remains constant and relatively small for long vehicle travel distances, and that the simulation can complete in a reasonable amount of time. To reach its maximum speed of 60 mph from rest and run a few seconds at steady-state, the vehicle needs about a

400 m long terrain patch. If the patch width is 3.5 meters, consolidated soil depth is 0.4 meters, and consolidated particle diameter is 26.5 mm, then the required number of particles is about 67,000 particles per meter of terrain. So for a 400 m long terrain patch about 27 million particles are needed. At current simulation computational speeds, a 40 sec simulation with 27 million particles will take about 4.5 months to complete on five 32 core HPC nodes. However, for typical DIS vehicle mobility simulations, the moving terrain patch is about 9 m to 11 m long and the number of particles is about 600k to 1M, a 40 sec vehicle simulation takes about 2.5 to 5 days on five 32 core HPC nodes.

The following tasks were performed to create the mobility traverse simulations:

- The traverse surface which was provided as a set of TIN files was loaded into the IVRESS software (Figure 69).
- A capability to convert the traverse TINs to an ordered *i-j* quadrilateral mesh for DIS's complex terrain topography moving soil patch was developed (Figure 70).
- The complex terrain topography was tested on a typical traverse segment (Figure 71).
- The variable sand grade was used as test for the traverse segments (Figure 72). The maximum slope achieved in the run was 13.37%.
- The vehicle steering paths data for the 14 traverse segments was cleaned (Figure 73).
- The soil type along the 14 traverse segments was extracted from the Map11 terrain file.
- Initial vehicle speed as a function of distance along each traverse segment was specified for the 14 traverse segments.

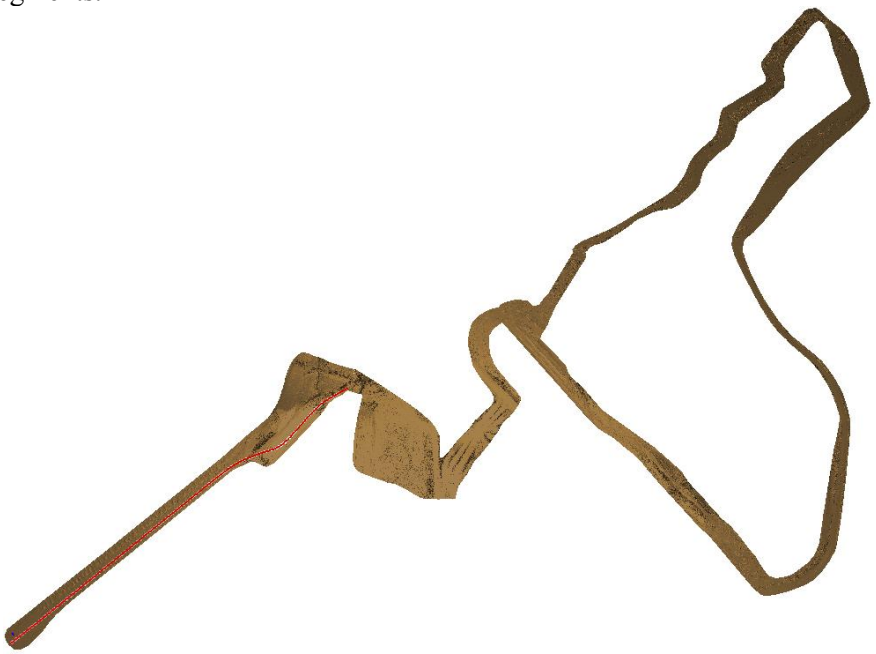

Figure 69: Traverse triangular network (TIN) surface.

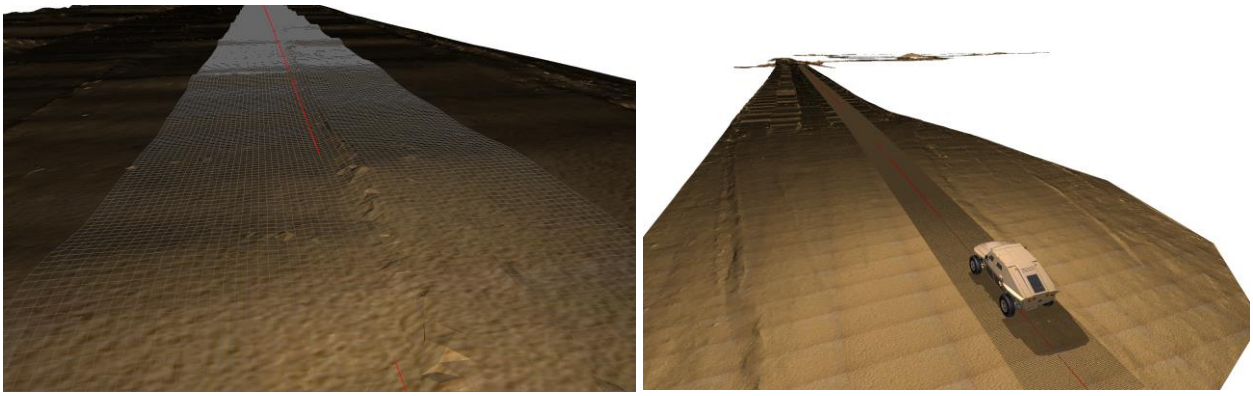

Figure 70: Conversion of the traverse triangular network surface into an ordered i-j mesh.

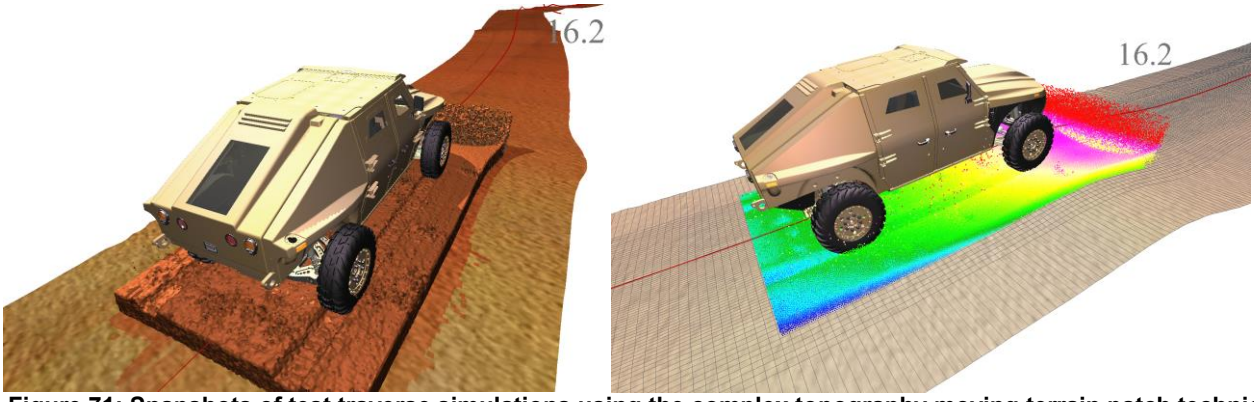

Figure 71: Snapshots of test traverse simulations using the complex topography moving terrain patch technique.

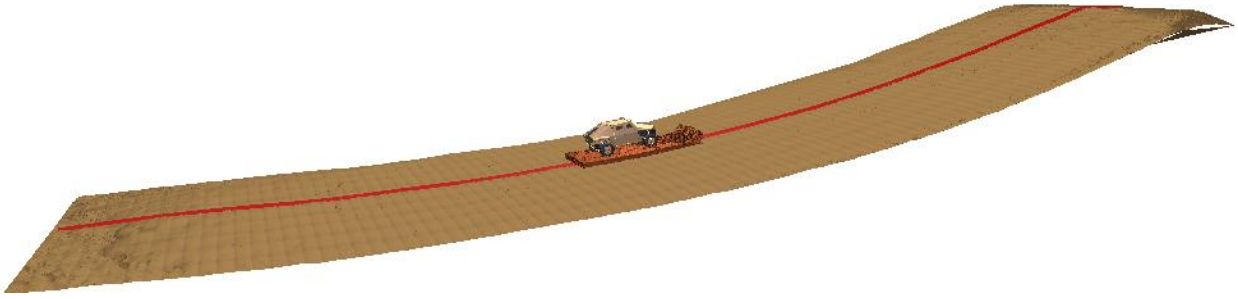

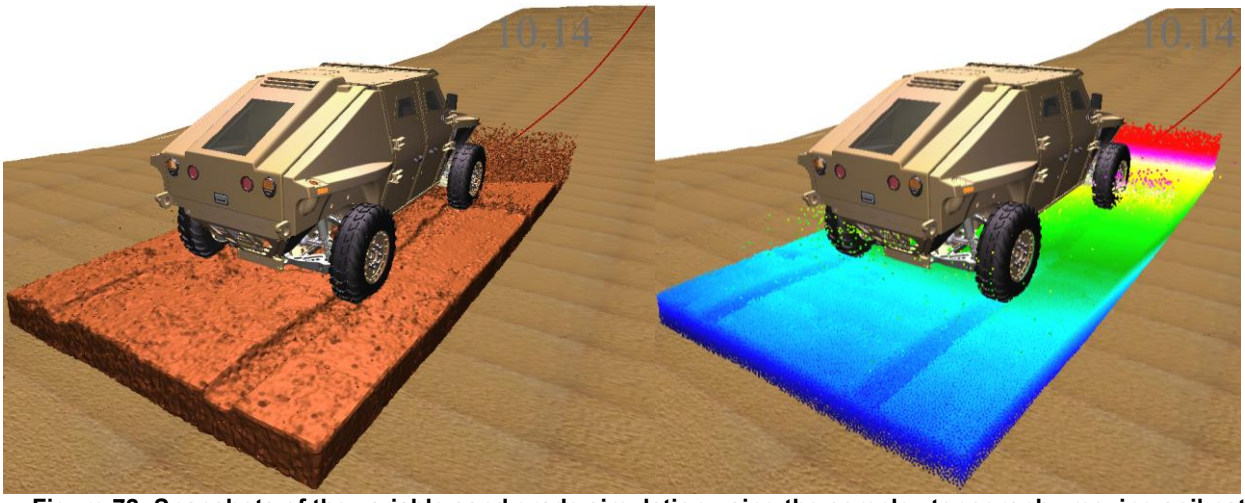

Figure 72: Snapshots of the variable sand grade simulation using the complex topography moving soil patch technique.

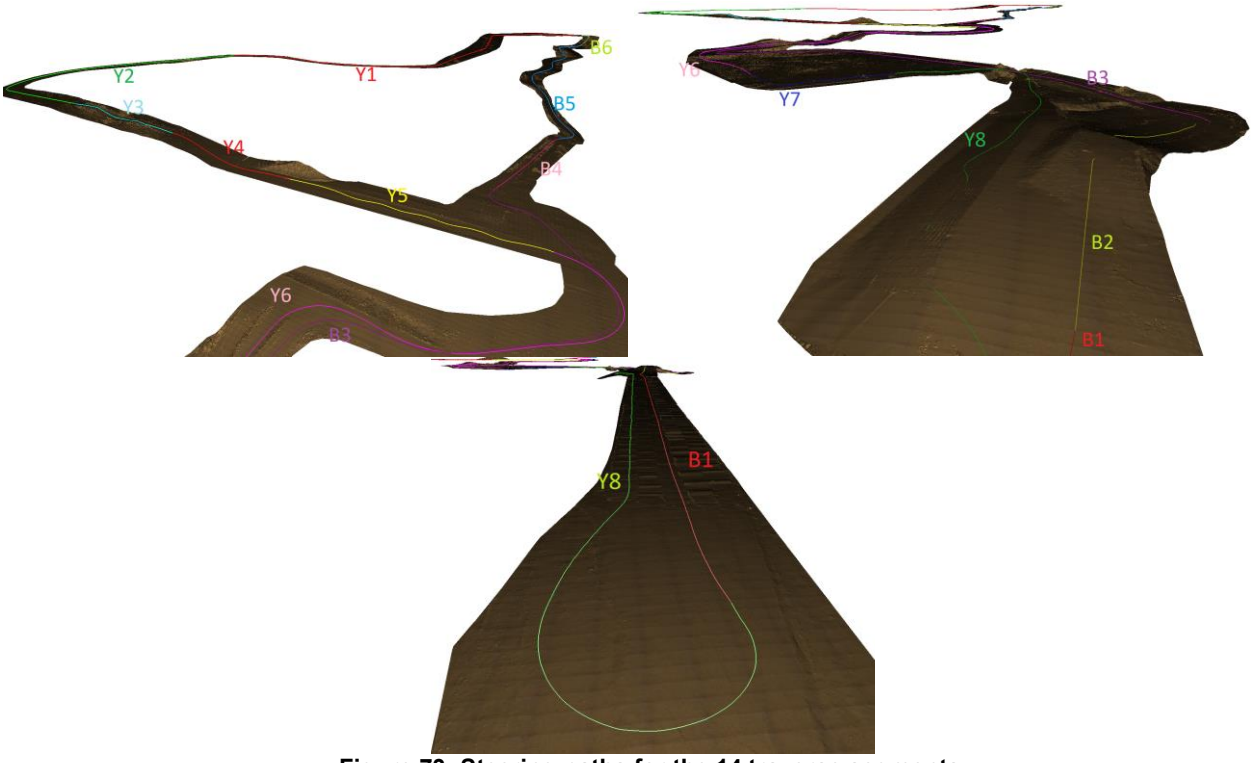

Figure 73: Steering paths for the 14 traverse segments.

Multiple simulations were performed for the assigned traverse segments with increasing speed in order to find the maximum speed as a function of time each traverse segment. The following results were obtained for the assigned mobility traverse segments:

- DEM soft soil segments:

- **Y5**: Sinusoidal thru Coarse Grain Soil Pit. Figure 74 shows snapshots of the Y5 traverse segment simulation. Figure 75 shows comparison between the DIS model and test vehicle speeds for the Y5 traverse segment.
- **Y7**: 90º in Fine Grain Wet Soil pit. Figure 76 shows snapshots of the Y7 traverse segment simulation. Figure 77 shows comparison between the DIS model and test vehicle speeds for the Y7 traverse segment.
- **B2**: Down Sand Grade with short length of gravel pad. Figure 78 shows snapshots of the B2 traverse segment simulation. Figure 79 shows comparison between the DIS model and test vehicle speeds for the B2 traverse segment.
- **Up sand grade**. Figure 42 shows snapshots of the FED vehicle going over the variable 2NS variable sand grade. Figure 43 the vehicle slope as a function of time during the climb. The vehicle can climb up to 15% to 23% depending on the value of the soil internal friction angle which ranges from 22º to 25º.

- Hard terrain segments:
  - Y1: Transition to Panic Stop - Secondary Road, Sinusoidal of Packed Trail, and Packed Trail (Figure 80).
  - Y2: Transition from Max Acceleration - Secondary Road & Packed Trail (Figure 81).
  - Y3: Wadi (Figure 82).
  - Y4: Transition - Packed Trail (Figure 83).
  - Y6: Transition - Secondary Road and Packed Trail (Figure 84).
  - Y8: Side Slope & RMS 2.0 (Figure 85).

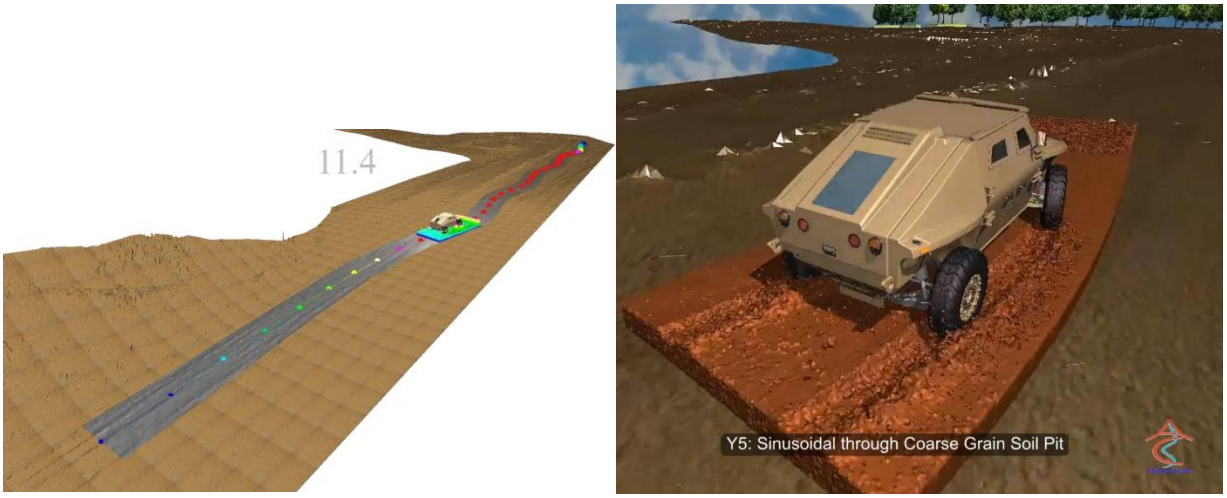

Figure 74: Snapshots of the FED vehicle crossing the Y5 (Sinusoidal thru Coarse Grain Soil Pit) segment.

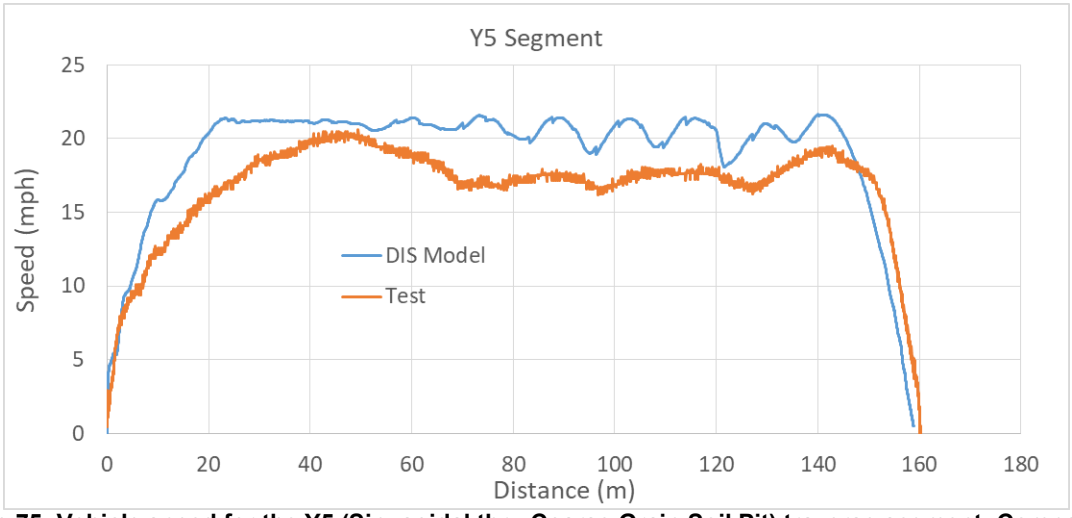

Figure 75: Vehicle speed for the Y5 (Sinusoidal thru Coarse Grain Soil Pit) traverse segment: Comparison between test and DIS model results.

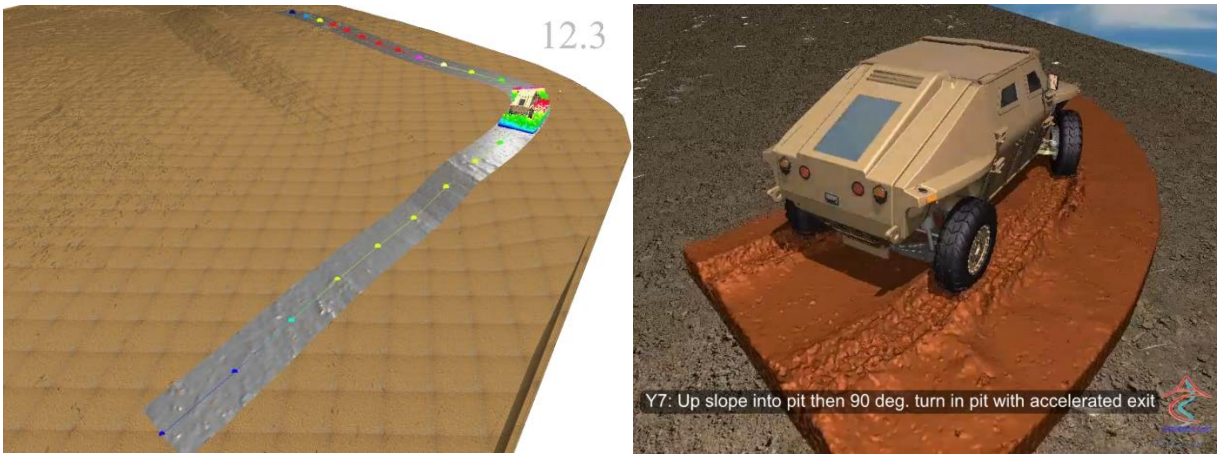

Figure 76: Snapshots of the FED vehicle crossing the Y7 (90º turn in Fine Grain Wet Soil Pit) segment.

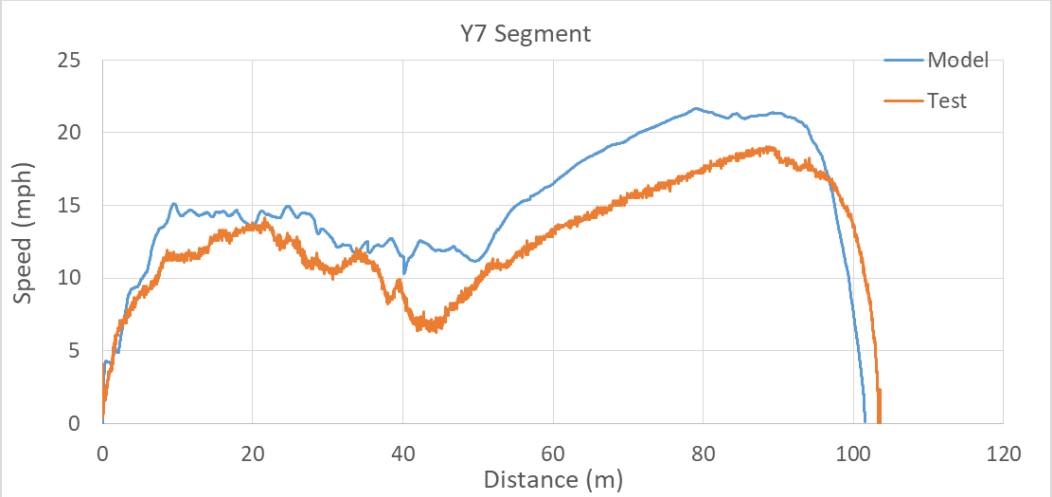

Figure 77: Vehicle speed for the Y7 (90° turn in Fine Grain Wet Soil Pit) traverse segment: Comparison between test and DIS model results.

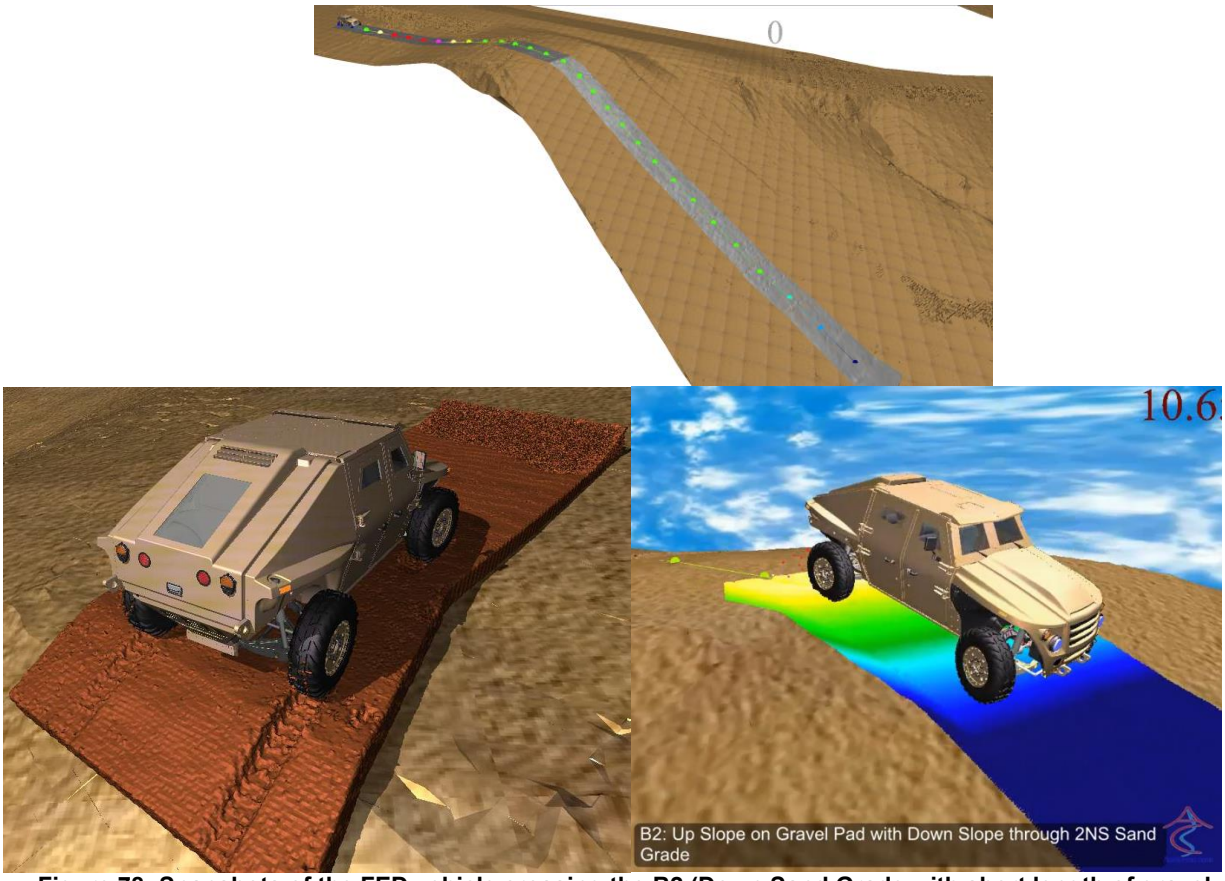

Figure 78: Snapshots of the FED vehicle crossing the B2 (Down Sand Grade with short length of gravel pad) segment.

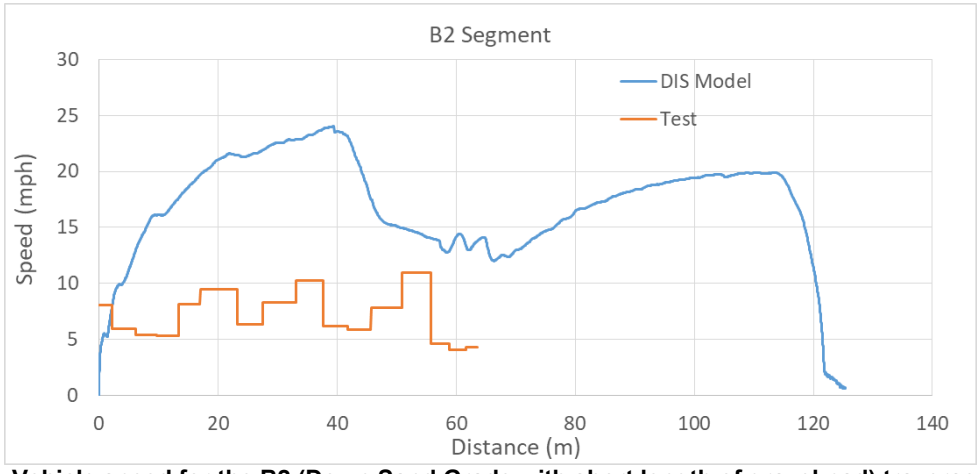

Figure 79: Vehicle speed for the B2 (Down Sand Grade with short length of gravel pad) traverse segment: Comparison between test and DIS model results.

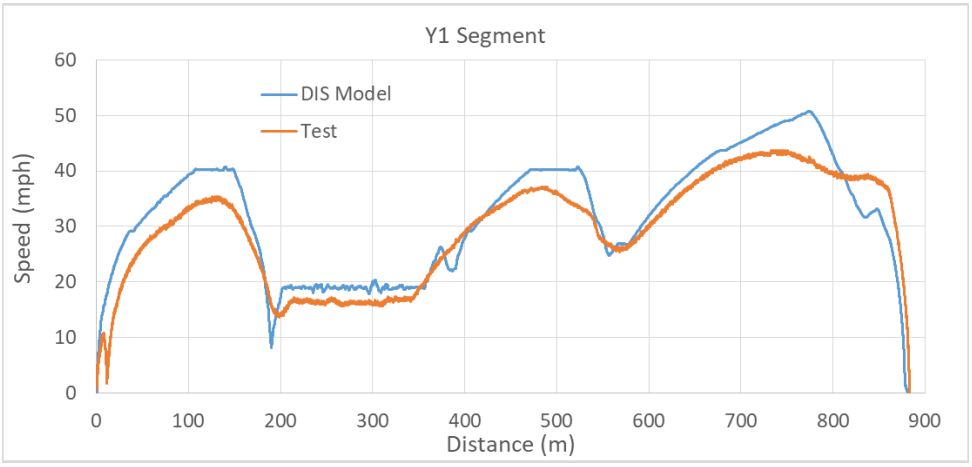

Figure 80: Vehicle speed for the Y1 (Transition to Panic Stop - Secondary Road, Sinusoidal of Packed Trail, and Packed Trail) traverse segment: Comparison between test and DIS model results.

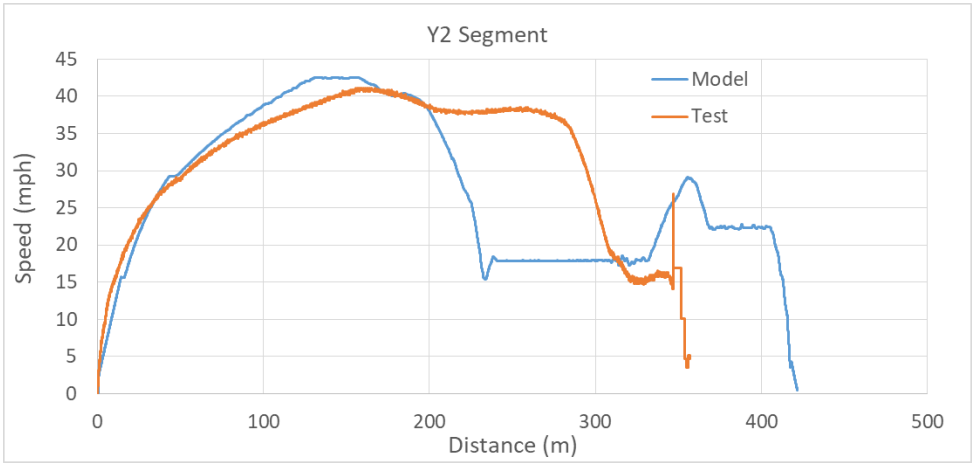

Figure 81: Vehicle speed for the Y2 (Transition from Max Acceleration - Secondary Road & Packed Trail) traverse segment: Comparison between test and DIS model results.

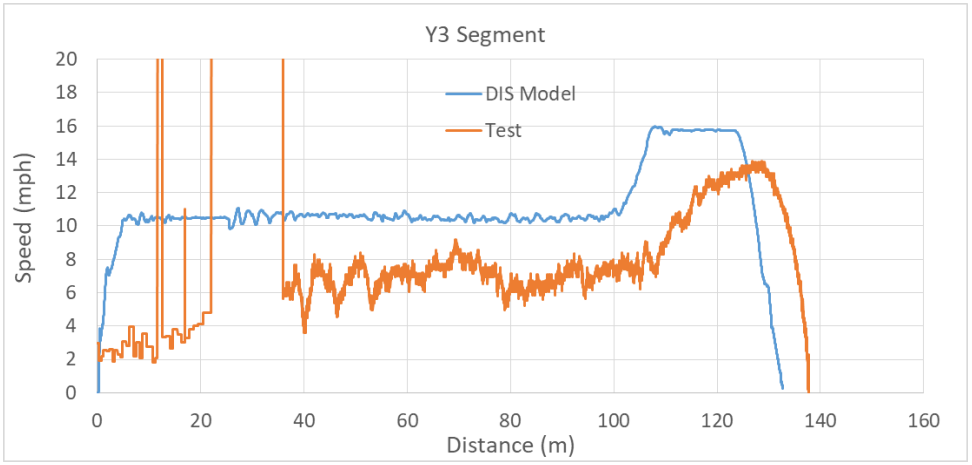

Figure 82: Vehicle speed for the Y3 (Wadi) traverse segment: Comparison between test and DIS model results.

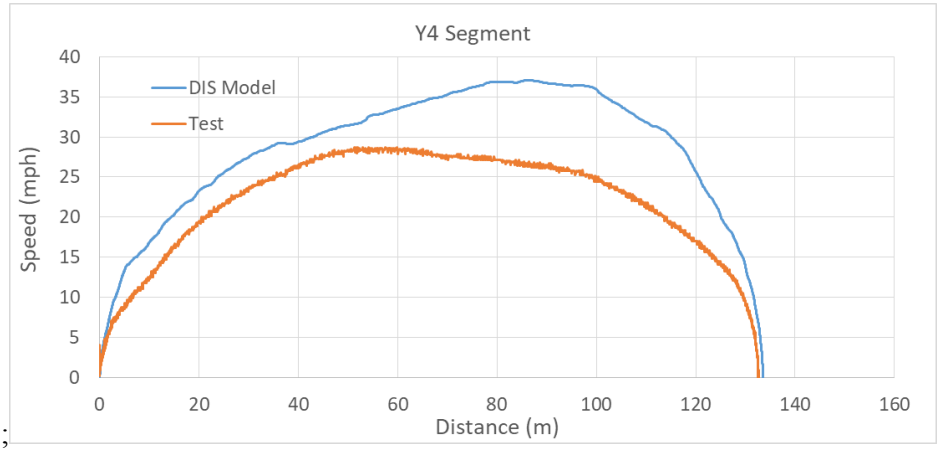

;

Figure 83: Vehicle speed for the Y4 (Transition - Packed Trail) traverse segment: Comparison between test and DIS model results.

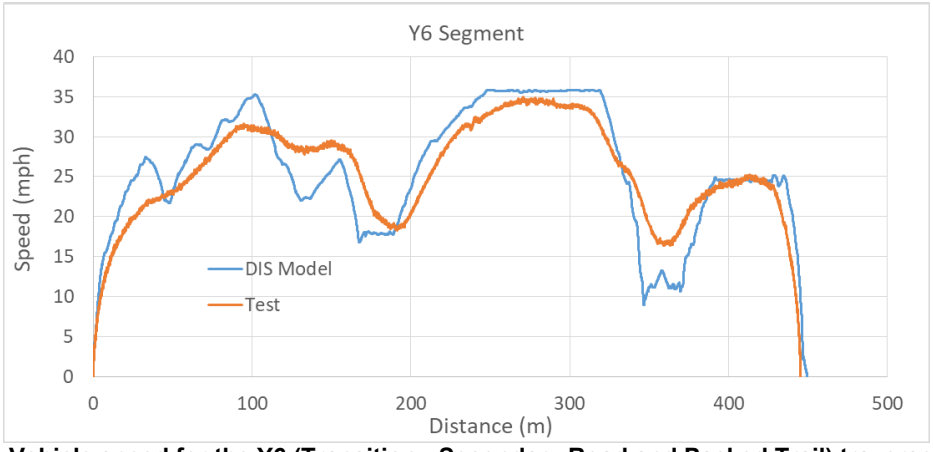

Figure 84: Vehicle speed for the Y6 (Transition - Secondary Road and Packed Trail) traverse segment: Comparison between test and DIS model results.

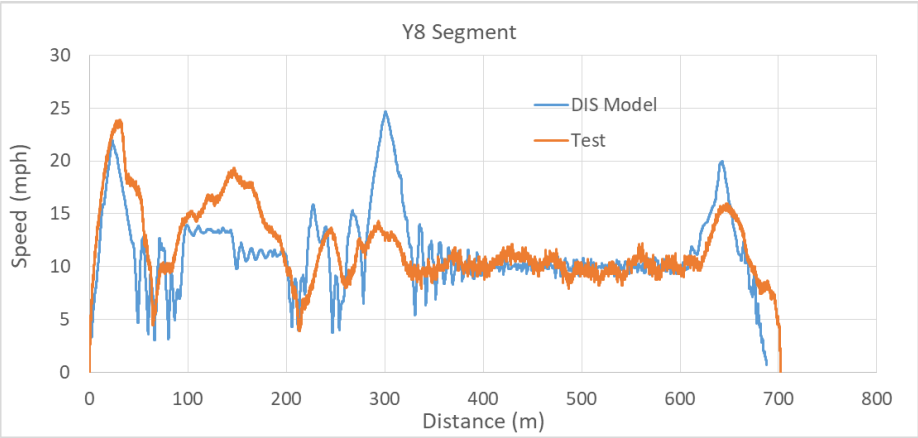

Figure 85: Vehicle speed for the Y8 (Side Slope & RMS 2.0) traverse segment: Comparison between test and DIS model results.

16. GO-NOGO AND MOBILITY MAPS

The KRC soils were divided into two types A and B, where A are relatively weak soils and B are relatively strong soils. The ranges of cohesion, friction angles, and bulk density of the soils are given below:

- A soils:
  - Cohesion: 0 to 4 kPa
  - Friction angle: 15.5^o to 44.5^o
  - Bulk density: 1290 to 1930 kg/m^3
- B soils:
  - Cohesion: 6.25 to 20.75 kPa
  - Friction angle: 24^o to 50^o
  - Bulk density: 1550 to 2020 kg/m^3

The minimum slope of the KRC terrain is 0 degrees and the maximum slope is about 40 degrees. Note that more than 99% of the terrain has a slope of less than 16.7% degrees (30% grade). Therefore, most of the simulations are performed in the lower slope range. The DOE variables are:

1. Soil cohesion
2. Soil friction angle
3. Soil bulk density
4. Terrain long slope.

Four sets of DOE runs were performed:

- Set #1: of 60 DOE points (Table 8).
- Set #2: of 60 DOE points.
- Set #3: of 50 DOE points.
- Set #4: of 40 DOE points.

The deterministic go-nogo and speed-made-good mobility maps are shown in Figure 86 and Figure 87, respectively. The non-deterministic UQ go-nogo and speed-made-good mobility maps are shown in Figure 88 and Figure 89, respectively.

Table 8: Speed-made-good results of mobility map DOE set #1.

#	SoilType	Phi_Degrees	C_kPa	BulkDensity_kgm3	Slope_Degrees	Speed (m/s)
1	A_Soils	15.5	1.2666667	1620.45	26.5	0.000
2	A_Soils	16.5	3	1927.05	29.5	0.000
3	A_Soils	17.5	1.6666667	1313.85	7.5	5.766
4	A_Soils	18.5	1.5333333	1686.15	2.5	9.408
5	A_Soils	19.5	2.3333333	1642.35	12.5	5.753
6	A_Soils	20.5	3.2666667	1795.65	22.5	1.849
7	A_Soils	21.5	3.8	1335.75	16.5	6.230
8	A_Soils	22.5	0.33333333	1423.35	9.5	4.952
9	A_Soils	23.5	1.8	1905.15	13.5	6.662
10	A_Soils	24.5	0.73333333	1357.65	21.5	1.597
11	A_Soils	25.5	0.46666667	1817.55	18.5	2.430
12	A_Soils	26.5	3.9333333	1598.55	4.5	14.412
13	A_Soils	27.5	2.6	1467.15	24.5	1.871
14	A_Soils	29.5	0.2	1554.75	15.5	5.297
15	A_Soils	30	2	1609.5	15	8.522
16	A_Soils	30.5	2.8666667	1839.45	28.5	0.000
17	A_Soils	31.5	3.6666667	1532.85	19.5	7.497
18	A_Soils	32.5	1	1708.05	1.5	15.071
19	A_Soils	33.5	1.1333333	1664.25	27.5	0.000
20	A_Soils	34.5	0.6	1861.35	17.5	7.206
21	A_Soils	35.5	1.4	1291.95	25.5	1.513
22	A_Soils	36.5	3.4	1773.75	10.5	14.083
23	A_Soils	37.5	3.1333333	1729.95	0.5	16.154
24	A_Soils	38.5	1.9333333	1883.25	14.5	11.073
25	A_Soils	39.5	3.5333333	1379.55	3.5	15.754
26	A_Soils	40.5	2.7333333	1401.45	11.5	14.112
27	A_Soils	41.5	2.0666667	1751.85	8.5	14.911
28	A_Soils	42.5	0.86666667	1445.25	5.5	15.226
29	A_Soils	43.5	0.066666667	1510.95	20.5	7.074
30	A_Soils	44.5	2.4666667	1576.65	23.5	7.544
31	B_Soils	24.433333	10.75	1795.8333	26.5	6.542
32	B_Soils	25.3	17.25	2015.1667	29.5	1.003
33	B_Soils	26.166667	12.25	1576.5	7.5	15.183
34	B_Soils	27.033333	11.75	1842.8333	2.5	15.988
35	B_Soils	27.9	14.75	1811.5	12.5	14.469
36	B_Soils	28.766667	18.25	1921.1667	22.5	9.986
37	B_Soils	29.633333	20.25	1592.1667	16.5	12.442
38	B_Soils	30.5	7.25	1654.8333	9.5	14.630
39	B_Soils	31.366667	12.75	1999.5	13.5	14.067
40	B_Soils	32.233333	8.75	1607.8333	21.5	8.970
41	B_Soils	33.1	7.75	1936.8333	18.5	10.232
42	B_Soils	33.966667	20.75	1780.1667	4.5	16.178
43	B_Soils	34.833333	15.75	1686.1667	24.5	9.003
44	B_Soils	36.566667	6.75	1748.8333	15.5	11.386
45	B_Soils	37	13.5	1788	15	13.725
46	B_Soils	37.433333	16.75	1952.5	28.5	7.975
47	B_Soils	38.3	19.75	1733.1667	19.5	11.791
48	B_Soils	39.166667	9.75	1858.5	1.5	16.460
49	B_Soils	40.033333	10.25	1827.1667	27.5	7.616
50	B_Soils	40.9	8.25	1968.1667	17.5	11.578
51	B_Soils	41.766667	11.25	1560.8333	25.5	8.253
52	B_Soils	42.633333	18.75	1905.5	10.5	15.326
53	B_Soils	43.5	17.75	1874.1667	0.5	16.769
54	B_Soils	44.366667	13.25	1983.8333	14.5	14.384
55	B_Soils	45.233333	19.25	1623.5	3.5	16.357
56	B_Soils	46.1	16.25	1639.1667	11.5	15.033
57	B_Soils	46.966667	13.75	1889.8333	8.5	15.540
58	B_Soils	47.833333	9.25	1670.5	5.5	15.803
59	B_Soils	48.7	6.25	1717.5	20.5	10.822
60	B_Soils	49.566667	15.25	1764.5	23.5	9.995

Figure 86: Deterministic go-nogo map.

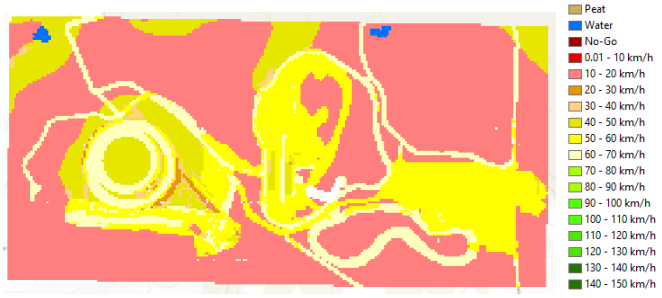

Figure 87: Deterministic speed-made-good mobility map.

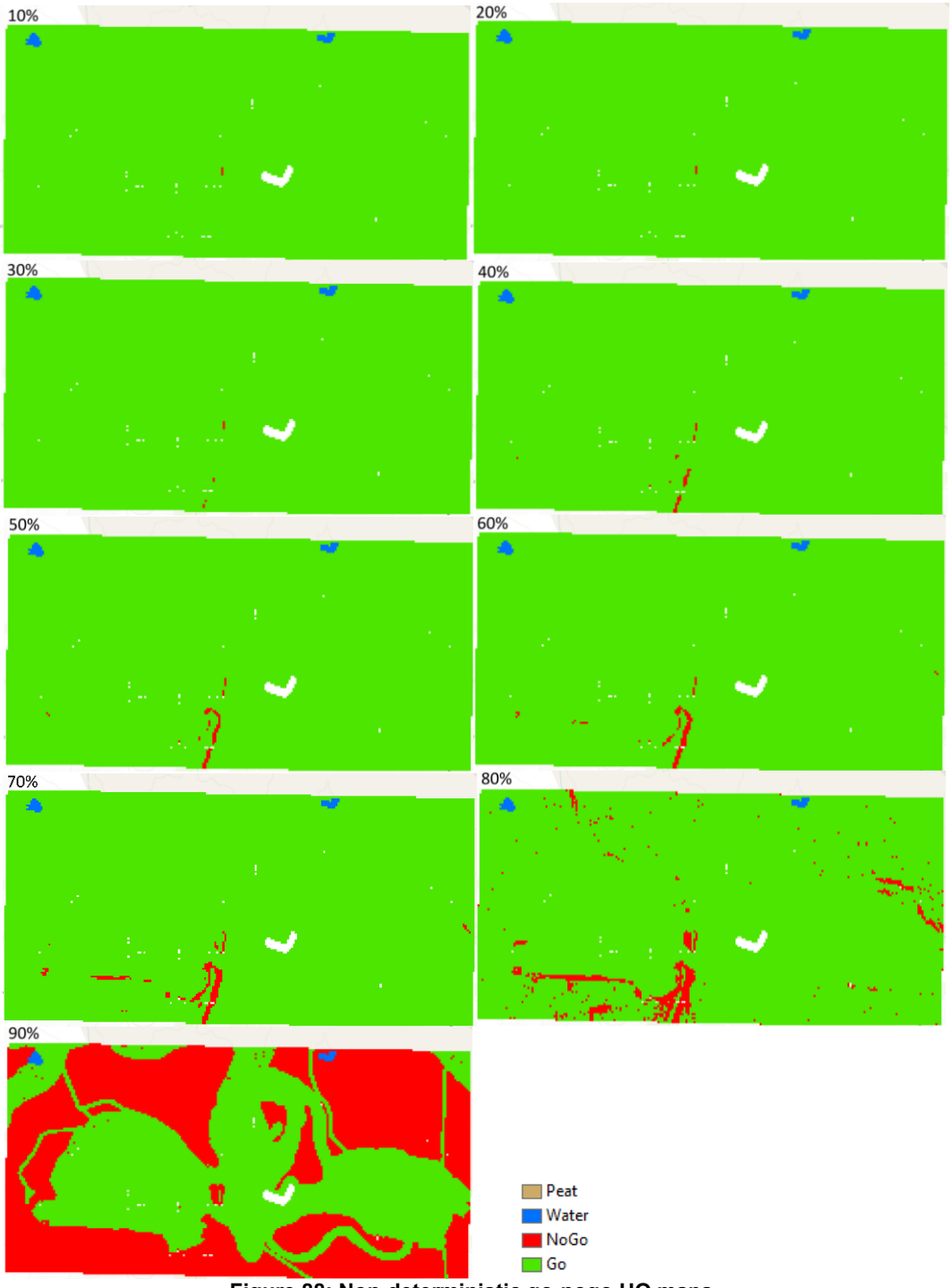

Figure 88: Non-deterministic go-nogo UQ maps.

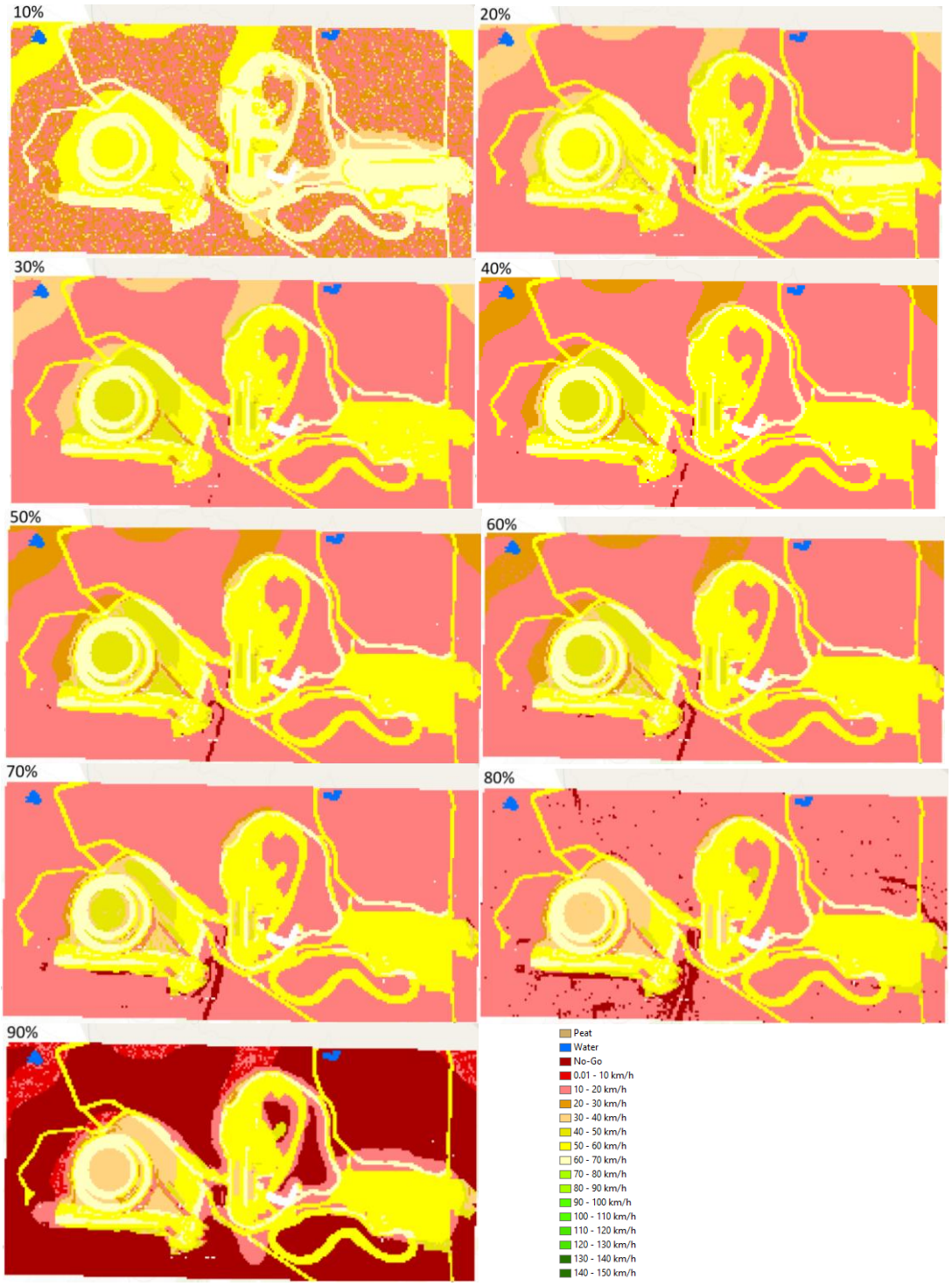

Figure 89: Non-deterministic speed-made-good mobility UQ maps.

4. CONCLUSIONS, GAPS, AND PATH FORWARD

The following new capabilities were developed during the CDT:

1. Soil model calibration procedure based on CI and shear cell data.
2. Complex topography moving soil patch for modeling the soft soil traverse segments.

The following CDT issues need further work:

1. Shear cell, tri-axial, and bevameter tests with the soil under a normal load result in soil internal friction angle which is much higher than the soil friction angle measured using a CI or the drawbar pull tests. Thus we need to investigate the effects of confinement on soil mechanical response.
2. Drawbar-pull test should be performed under steady-state conditions.
3. Drawbar-pull force should be zero for up to a certain value of positive slip because slip is needed to overcome the soil/terrain motion resistance. Thus, we need to modify the standard algorithm to calculate tire slip including the tire radius for slip calculations.

Finally, the following tasks are needed in order to develop an operational NG-NRMM vehicle mobility tool that can be replace NRMM:

- Validate and calibrate DEM complex terramechanics soil models for all soil types. This will include developing a database of calibrated DEM soil models to include: 20 USCS soil types, 7 moistures, and 3-5 temperatures.
- Investigate/develop a soil classification system designed for vehicle mobility applications.
- Validate and calibrate of finite Element tire – soil models.
- Develop, calibrate & validate models for:
    - Multi-layer terrains.
    - Water covered soft soil terrains.
    - Heterogeneous terrain.
    - Vegetation (Figure 90 and Figure 91).
    - Urban obstacles.
- Perform fundamental research of micro-scale soil models which model individual soil particles along with the inter-particle forces including: elastic, friction, and capillary liquid bridging forces.
- Develop terramechanics experiments to measure soil damping, viscosity, and dilation.
- Add visibility (due to terrain topography and obstacles) as a mobility parameter.
- Develop a stochastic mobility expert system to generate vehicle mobility maps, while considering all terrain parameters, for manned and unmanned (autonomous and semi-autonomous) vehicles.

Figure 90: Coupled vegetation – vehicle simulation. Vegetation blades are modeled using thin beam elements.

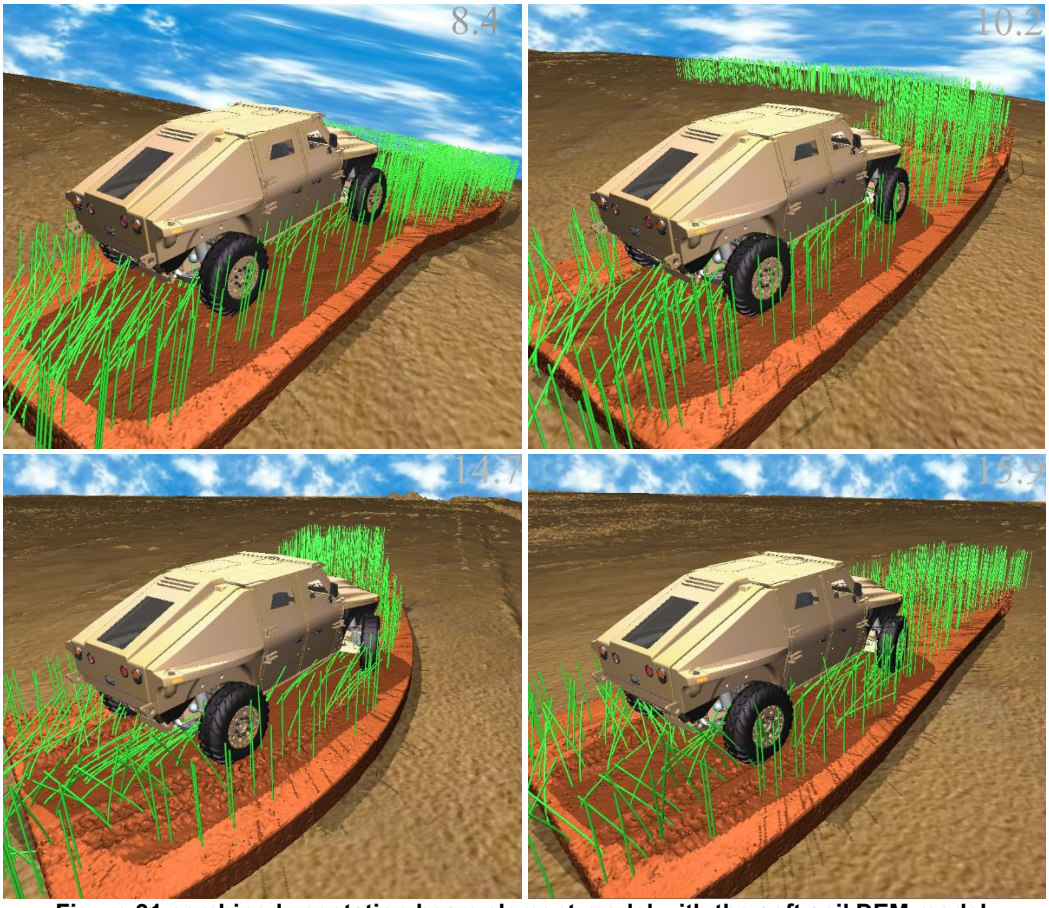

Figure 91 combined vegetation beam element model with the soft soil DEM model.

APPENDIX A: FED-ALPHA MODEL SPREADSHEETS

Vehicle Frame

Vehicle1	**Comment:**	FED-Alpha Vehicle Frame Data							
Parameter Description	**Symbol**	**Value1**	**Value2**	**Value3**	**Units**				
Enable vehicle	*Enabled*	Yes							
Vehicle global position (ground point at center of front axle)	*GlobalPos*	1	0	0.13					
CG position (X, Y, Z) relative to center of front axle	*CG*	-1.6	0	0.44	m				
Mass of frame/body	*M*	4164			kg				
Inertia of frame/body around (length, width, height) directions	*I*	3300	12302	13803	kg.m^2				
Off-diagonal Inertia of frame/body around (Ixy, Ixz, Iyz)	*Ioff*	0	0	0	kg.m^2				
Frame icon file name	*File*	..\VRML\FED_Vehicle.wrl							
Frame icon translation (*X*, *Y*, *Z*)	*Trans*	1.264	0	-0.708					
Frame icon scale (*X*, *Y*, *Z*)	*Scale*	1	1						
Euler Angles	*Angles*	90	0	(					
Initial icon visibility	*IconVisible*	Yes							
Front Axle	*FrontAxle*	Axle1							
Back Axle 1	*BackAxle1*	Axle2							
Back Axle 2	*BackAxle2*	None							
Steering	*Steering*	PitmanArm1							
Motor	*Motor*	ICengine1							
Vehicle Steering and Speed	*SteerAndSpeed*	SteeringAndSpeed1							
Air density	Ro_{Air}	1.225							
Vehicle frontal area	$Area_{Front}$	3.8							
Vehicle side area	$Area_{Side}$	4.2			m^2				
Vehicle top area	$Area_{Top}$	4.86			m^2	5694.3	0.656142		
Characteristic lift length	L_{Lift}	2			m	1.447368	4396.149	16403.54	18371.96
Aerodynamic frontal drag coefficient	$C_{DragFront}$	0.6				4.861111			
Aerodynamic side drag coefficient	$C_{DragSide}$	1							
Aerodynamic top drag coefficient	$C_{DragTop}$	1				0.81624			
Aerodynamic lift coefficient	C_{Lift}	0							
Aerodynamic lift moment coefficient	$C_{MomLift}$	0							
Wind velocity	v_{wind}	0	0	0	m/s				
Slave contact geometry file	*SlaveContFile*	..\VRML\VehicleContactSurface.wrl							
Slave contact geometry translation (*X*, *Y*, *Z*)	*TransSlave*	1.264	0	-0.7085	m				
Slave contact geometry scale (*X*, *Y*, *Z*)	*ScaleSlave*	1	1	1					
Slave contact geometry Euler Angles	*AnglesSlave*	90	0	0	degree				
Initial slave contact surface visibility	*SlaveVisible*	No							
Master contact geometry file	*MasterContFile*								
Master contact geometry translation (*X*, *Y*, *Z*)	*TransMaster*	0	0	0	m				
Master contact geometry scale (*X*, *Y*, *Z*)	*ScaleMaster*	0	0	0					
Master contact geometry Euler Angles	*AnglesMaster*	0	0	0	degree				
Initial master contact surface visibility	*MasterVisible*	No							
Bounding box size (*X*, *Y*, *Z*)	*BoundBoxSize*	0	0	0	m				
Bounding box center (*X*, *Y*, *Z*)	*BoundBoxCenter*	0	0	0	m				
Bounding box rotation euler angles	*BoundBoxAngles*	0	0	0	degree				
Enable shared memory parallel processing for vehicle	*parallel*	Yes							

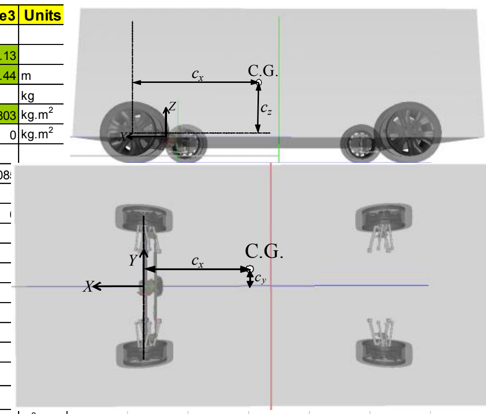

Engine & Gear Box

ICengine1

This a comment....

Parameter Description	Symbol	Value1	Units
Proportional Gain	*propGain*	10	
Derivative Gain	*derGain*	0	
Enable Traction control	*traction*	no	
Max. allowable wheel slip	*maxSlip*	200	%
Zero torque slip	*noTorqueSlip*	400	%
Maximum forward gear	*maxForeGear*	6	
Maximum backward gear	*maxBackGear*	1	
Drive shaft mass	*driveMass*	40	kg
Rotating drive inertia	*driveInertia*	20	kg.m^2
Additional gear ratio	*gearRatio2*	1	
Additional gear losses	*gearLoss2*	0	

#	Full Throttle Torque-Speed Ang.Vel.(RPM)	Full Throttle Torque-Speed Torque (N.m)	Engine Brake Torque-Speed Ang.Vel.(RPM)	Engine Brake Torque-Speed Torque (N.m)
1	0	370	0	-185
2	700	400	700	-200
3	800	416.6950612	800	-208.3475306
4	900	458.3192975	900	-229.1596487
5	1000	551.2685618	1000	-275.6342809
6	1100	640.7633944	1100	-320.3816972
7	1200	724.5875491	1200	-362.2937745
8	1300	758.0528184	1300	-379.0264092
9	1400	793.2492416	1400	-396.6246208
10	1500	794.0891567	1500	-397.0445784
11	1600	789.4936568	1600	-394.7468284
12	1700	787.3347752	1700	-393.6673876
13	1800	768.7168608	1800	-384.3584304
14	1900	752.058972	1900	-376.029486
15	2000	716.8774418	2000	-358.4387209
16	2100	686.4513864	2100	-343.2256932
17	2200	674.6845266	2200	-337.3422633
18	2300	636.3604335	2300	-318.1802167
19	2400	550	2400	-275
20	2500	350	2500	-175
21	2525	320	2525	-160
22	2700	0	2700	0
36				

Gear #	Forward Gears Gear Ratios	Gear Losses %	Min Shift RPM	Max Shift RPM	Shift time (s)
1	3.74	25	0	2400	0.3
2	2.003	32	1000	2400	0.3
3	1.343	43	1000	2400	0.3
4	1	50	1000	2400	0.3
5	0.773	55	1000	2350	0.3
6	0.634	57	1000	2300	0.3

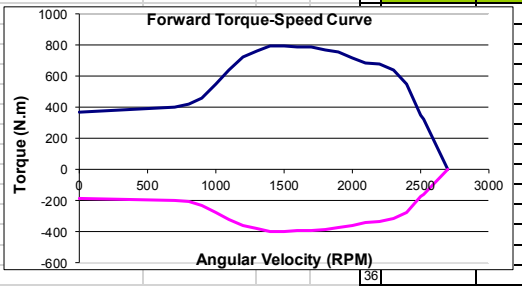

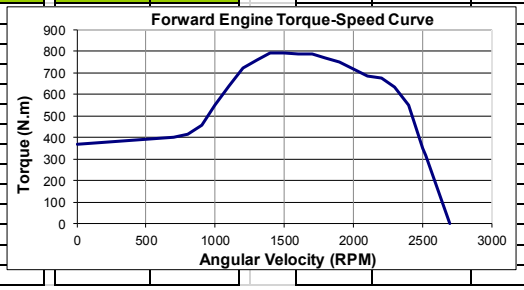

Steering System

SteeringPitmanArm1	Comment:				
Parameter Description	**Symbol**	**Value1**	**Value2**	**Value3**	**Units**
Enabled	*enabled*	Yes			
Hard points reference frame origin	*origin*	*Axle Center*			
Ttie rod inner point p_1	p_1	-0.223702	0.381	0.105228	m
Tie rod outer point p_2	p_2	-0.2	0.818897	0.066082	m
Pitman arm rearward point p_3	p_3	-0.41026	0.381	0.209605	m
Pitman arm foreward point p_4	p_4	-0.291973	0.381	0.166557	m
Idler arm rearward point p_5	p_5	-0.41026	-0.381	0.209605	m
Idler arm foreward point p_6	p_6	-0.291973	-0.381	0.166557	m
Tie rod connection	*tieRodConn*	Arm			
Pitman arm mass	m_{pitman}	4			Kg
Pitman arm inertia	i_{pitman}	0.002	0.04	0.04	Kg.m^2
Idler arm mass	m_{idler}	4			Kg
Idler arm inertia	i_{idler}	0.002	0.04	0.04	Kg.m^2
Center link mass	m_{center}	6			Kg
Center link inertia	i_{center}	0.006	0.08	0.08	Kg.m^2
Tie rod mass	m_{tierod}	1			Kg
Tie rod inertia	i_{tierod}	0.002	0.04	0.04	Kg.m^2
Steering gear ratio	*gearRatio*	1			
Steering column stiffness	*steerStiff*	88888.8889			N.m/rad
Steering column damping	*steerDamp*	0			N.(m.s)/rad
Steering column inertia	*steerInertia*	0.0493			Kg.m^2
Steering column stop stiffness	*steerStopStiff*	222222.222			N.m/rad
Steering column stop damping	*steerStopDamp*	8			N.(m.s)/rad
Steering positon gain	*steerPosGain*	0.2			
Steering heading direction gain	*steerDirGain*	0.25			
Maximum steering wheel torque	*maxTorque*	6000			N.m
Speed controller gain (wheel Torque/RPM)	*speedGain*	0.8			
Look ahead time	*timeAhead*	1			sec
Steering averaging time	*steerAveTime*	0.1			sec
Min steering distance	*steerDistance*	5			m
Minimum steering wheel angle	*minSteerAngle*	-28			degree
Maximum steering wheel angle	*maxSteerAngle*	28			degree

Tie Rod Connection: Center link

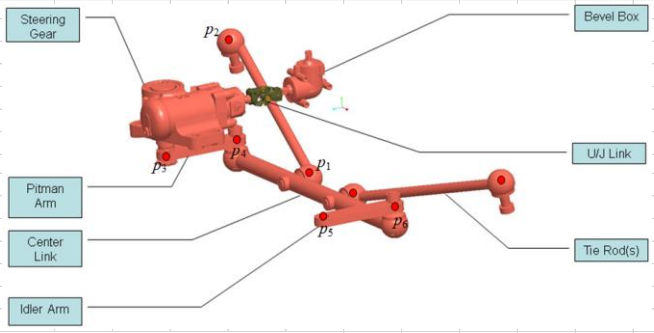

Tie Rod Connection: Arm (Pitman and Idler arms)

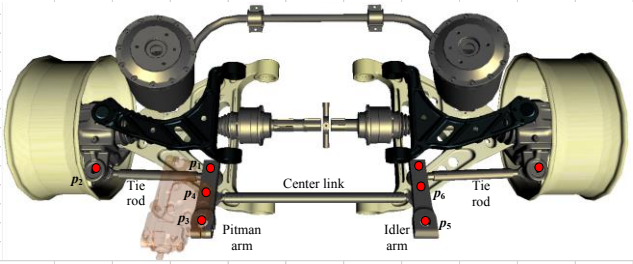

Front Axle

Axle1	Comment:	Front axle	
Parameter Description	**Symbol**	**Value1**	**Units**
Axle Propulsion	*prop Axle*	on	
Distance to front axle	*l*	0	m
Axle width (distance between wheels)	*w*	1.9785	
Axle height above ground	*h*	0.415	
See figure	a_{w1}	0.25	m
See figure	a_{w2}	0.575877	m
Mass of axle	m_{Axle}	120	kg
Rotational inerita	j_{Axle}	5	kg.m^2
Size of differential	*diffSize Axle*	0.26	m
Differential Model	*diffModel*	Analytical	
Mass of differential	m_{Diff}	30	kg
Final Differential drive ratio	*ratio*	4.88	
Tire	*tire*	TireLumped1	
Suspension	*suspension*	SuspDWB1	
Brake	*brake*	Brake1	
Brake multiplier	*brakeMult*	1	
Axle Joints	*jointType*	CV-joint	
Lock Differential	*lock*	no	
Antiroll bar	*antiRoll*	AntiRollBar1	

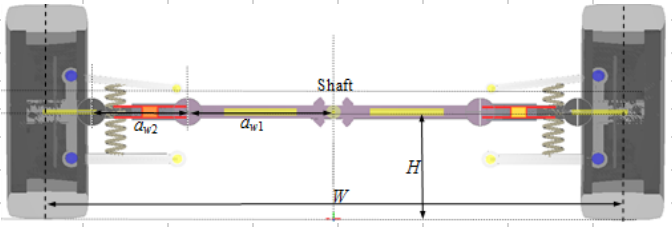

0.825877

0.825877

Rear Axle

Axle2	Comment:	Rear axle	
Parameter Description	**Symbol**	**Value1**	**Units**
Axle Propulsion	$prop_{Axle}$	on	
Distance to front axle	l	3.302	m
Axle width (distance between wheels)	w	1.9785	
Axle height above ground	h	0.415	
See figure	a_{w1}	0.25	m
See figure	a_{w2}	0.575877	m
Mass of axle	m_{Axle}	120	kg
Rotational inerita	j_{Axle}	5	$kg.m^2$
Size of differential	$diffSize_{Axle}$	0.26	m
Differential Model	$diffModel$	Analytical	
Mass of differential	m_{Diff}	30	kg
Final Differential drive ratio	$ratio$	4.88	
Tire	$tire$	TireLumped1	
Suspension	$suspension$	SuspDWB2	
Brake	$brake$	Brake1	
Brake multiplier	$brakeMult$	0.8	
Axle Joints	$jointType$	CV-joint	
Lock Differential	$lock$	no	
Antiroll bar	$antiRoll$	None	

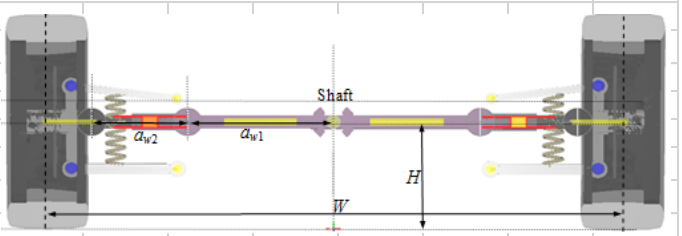

Transfer Case

TransferCase1	Comment:		
Parameter Description	**Symbol**	**Value1**	**Units**
Vehicle	*vehicle*	Vehicle1	
Driver	*driver*	Vehicle1	
First Axle	*axle1*	Axle1	
Second Axle	*axle2*	Axle2	
Lock	*lock*	Yes	

Brake

Brake1

Wheel max braking torque-speed

#	Wheel RPM	Torque (N.m)
1	0	12000
2	125	12000
3	250	8000
4	375	8000
5	500	8000
6	625	8000
7	750	8000
8	875	8000
9	1000	8000
10	1125	8000
11	1250	8000
12	1375	8000
13	1500	8000
14	1625	8000
15	1750	8000
16	1875	8000
17	2000	8000
18		

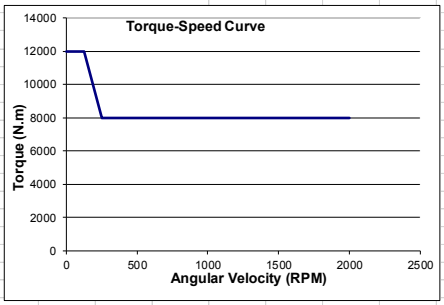

Tire

TireLumped1	Comment:																				
Parameter Description	**Symbol**	**Value1**	**Value2**	**Value3**	**Units**																
Wheel mass	m_{Wheel}	102.62			kg															13.184	
Wheel rotational inertia	j_{Wheel}	13			$kg.m^2$																
Wheel radial inertia	i_{Wheel}	10			$kg.m^2$																
Wheel icon file name	$file_{Wheel}$	..\VRML\FEDwheel.wrl																			
Wheel icon translation (length, width, height)	$trans_{Wheel}$	0	0	0	m																
Wheel icon scale (radius, width)	$scale_{Wheel}$	1	1																		
Wheel icon Euler angles	$angles_{Wheel}$	0	0	0	degree																
Tire surface file name	$file_{Tire}$	..\VRML\FED_Tire2.wrl																			
Tire surface translation (length, width, height)	$trans_{Tire}$	0	0	0	m																
Tire surface scale (radius, width)	$scale_{Tire}$	1	1																		
Tire euler angles	$angles_{Tire}$	0	0	0	degree																
Tire Model Type	*tireModel*	Std_TireCorrPatch																			
Standard tire Wheel width	$width_{Wheel}$	0.24			m																
Standard tire Middle of tire width	$width_{MidTire}$	0.3			m																
Tire outer width for display & area calculations	$width_{OutTire}$	0.25			m																
Tire outer width for contact calculations	$width_{Contact}$	0.2			m																
Tire width divisions	*widthDivs*	1																			
Standard tire Wheel radius	$radius_{Wheel}$	0.285			m																
Standard tire Middle of tire radius	$radius_{MidTire}$	0.4			m																
Outer tire radius	$radius_{OutTire}$	0.5055			m																
Tire contact tolerance	tol_{Tire}	0.25			m																
Tire coefficient of friction	mu_{Tire}	0.8																			
Tire friction spring stiffness per unit area	$fricSpring_{Tire}$	1.00E+09			$N/m/m^2$																
Tire velocity stiffness per unit area	$velStiff_{Tire}$	1.00E+07			$N/(m/sec)/m^2$																
Tire normal stiffness per unit area	$norStiff_{Tire}$	0.00E+00			$N/m/m^2$																
Tire normal force per unit area	$norForce_{Tire}$	Graph3			N/m^2																
Tire normal damping per unit area	$norDamp_{Tire}$	0			$N/(m/sec)/m^2$																
Time additional damping per unit area vs penetration	$addDamp_{Tire}$	Graph13			$N/(m/sec)/m^2$																
Tire separation damping factor	$sepDamp_{Tire}$	1																			
Normal averaging	*normalAve*	0																			
Pneumatic trail as a function of normal force	*pneumaticTrail*	Zero			m																
Rolling radius (with loaded vehicle)	$radius_{Tire}$	0.5055			m																
Tire nominal width	$width_{Tire}$	0.24			m																
Number of tires	num_{Tire}	1																			
Center distance between tires	$centerDist_{Tire}$	0.3			m																
Number of circumference divisions	$circDivs_{Tire}$	128																			
Use Pacejka magic formula	*magicFormula*	Pacejka89																			
Pacejka lateral force parameters	*pacejkaLateral*	1.0012	-0.6774	1017.452	5707.292	62.6561	0	0.008	0.9419	0.1124	-0.0026	-0.1197	-17.2366	9.9733	-10.7445						
Pacejka lateral force scale	*pacejkaLateralScale*	1																			
Pacejka aligning moment parameters	*pacejkaAlignTorque*	1.8392	-0.2289	-11.239	-0.0298	-6.6725	0	0	0.0035	-0.282	2	0.3595	0.0157	0.0011	0.2298	0.0194	-0.764	-2.275	40.78		
Pacejka aligning moment parameters	*pacejkaAlignTorqueScale*	1																			

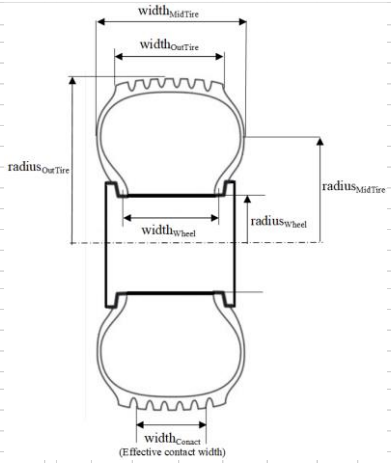

Notes:
The tire contact surface for pavement is defined by the following parameters:
- $radius_{OutTire}$
- $width_{OutTire}$
- $width_{Contact}$
- $width_{Contact}$

The tire contact surface for soft DEM soil is defined by $file_{Tire}$ surface.

If $file_{Tire}$ is defined then it is used to initially display the tire.

Front Suspension System

SuspDWB1	Comment:	Front suspension system			
Parameter Description	**Symbol**	**Value1**	**Value2**	**Value3**	**Units**
Hard points reference frame origin	*origin*	*Axle Center*			
Upper control arm inner front point P_1 (X, Y, Z)	p_1	0.139748	0.29579	0.2872	m
Upper control arm inner rear point P_2 (X, Y, Z)	p_2	-0.176137	0.29579	0.2872	m
Lower control arm inner front point P_3 (X, Y, Z)	p_3	0.279309	0.21821	-0.10418	m
Lower control arm inner rear point P_4 (X, Y, Z)	p_4	-0.305945	0.21821	-0.07315	m
Upper knuckle outer point P_5 (X, Y, Z)	p_5	-0.00922569	0.77536	0.24432	m
Lower knuckle outer point P_6 (X, Y, Z)	p_6	0.00566887	0.8582	-0.16226	m
Lower suspension strut lower point P_7 (X, Y, Z)	p_7	0.118962	0.65018	-0.1002	m
Upper suspension strut upper point P_8 (X, Y, Z)	p_8	0.118963	0.49338	0.57659	m
Lower Suspension Strut P_7 is connected to:	*strutConn*	*Lower control arm*			
Strut Data	*strut*	*Spring1*			
Mass of upper control arm	m_U	8.49			kg
Mass of lower control arm	m_L	31.55			kg
Mass of knuckle	m_K	58.44			kg
Mass of strut lower part	m_{SL}	15			kg
Mass of strut upper part	m_{SU}	16			kg
Moment of inertia of upper control arm	i_U	0.3	0.3	0.3	$kg.m^2$
Moment of inertia of lower control arm	i_L	1	1	1	$kg.m^2$
Moment of inertia of knuckle	i_K	1	1	1	$kg.m^2$
Moment of inertia of strut lower part	i_{SL}	0.03	0.6	0.6	$kg.m^2$
Moment of inertia of strut upper part	i_{SU}	0.03	0.6	0.6	$kg.m^2$
Upper right control arm icon	$file_{UR}$	../VRML/FrontUCAR.wrl			
Upper right control arm icon translation (X, Y, Z)	$trans_{UR}$	0	0	0	m
Upper left control arm icon	$file_{UL}$	../VRML/FrontUCAL.wrl			
Upper left control arm icon translation (X, Y, Z)	$trans_{UL}$	0	0	0	m
Upper control arm icon scale (X, Y, Z)	$scale_U$	1	1	1	
Lower right control arm icon	$file_{LR}$	../VRML/FrontLCAR.wrl			
Lower right control arm icon translation (X, Y, Z	$trans_{LR}$	0	0	0	m
Lower left control arm icon	$file_{LL}$	../VRML/FrontLCAL.wrl			
Lower left control arm icon translation (X, Y, Z)	$trans_{LL}$	0	0	0	m
Lower control arm icon scale (X, Y, Z)	$scale_L$	1	1	1	
Knuckle right icon	$file_{KR}$	../VRML/FrontKnuckleR.wrl			
Knuckle right icon translation (X, Y, Z)	$trans_{KR}$	0	0	0	m
Knuckle left icon	$file_{KL}$	../VRML/FrontKnuckleL.wrl			
Knuckle left icon translation (X, Y, Z)	$trans_{KL}$	0	0	0	m
Knuckle icon scale (X, Y, Z)	$scale_K$	1	1	1	
Enable contact with Upper control arm	$contact_U$	No			
Enable contact with Lower control arm	$contact_L$	Yes			
Enable contact with Knuckle	$contact_K$	No			
Automatically set joint stiffnees and damping	*autoStiff*	SpecifyStiff			
Radial Bushing Stiffness for P_1	$stiffRad_1$	90000000			N/m
Radial Bushing Stiffness for P_2	$stiffRad_2$	90000000			N/m
Radial Bushing Stiffness for P_3	$stiffRad_3$	90000000			N/m
Radial Bushing Stiffness for P_4	$stiffRad_4$	90000000			N/m
Radial Bushing Stiffness for P_5	$stiffRad_5$	90000000			N/m
Radial Bushing Stiffness for P_6	$stiffRad_6$	90000000			N/m
Radial Bushing Damping for P_1	$dampRad_1$	90000			N/(m/sec)
Radial Bushing Damping for P_2	$dampRad_2$	90000			N/(m/sec)
Radial Bushing Damping for P_3	$dampRad_3$	90000			N/(m/sec)
Radial Bushing Damping for P_4	$dampRad_4$	90000			N/(m/sec)
Radial Bushing Damping for P_5	$dampRad_5$	90000			N/(m/sec)
Radial Bushing Damping for P_6	$dampRad_6$	90000			N/(m/sec)
Axial Bushing Stiffness for P_1	$stiffAxial_1$	25000000			N/m
Axial Bushing Stiffness for P_2	$stiffAxial_2$	25000000			N/m
Axial Bushing Stiffness for P_3	$stiffAxial_3$	25000000			N/m
Axial Bushing Stiffness for P_4	$stiffAxial_4$	25000000			N/m
Axial Bushing Stiffness for P_5	$stiffAxial_5$	25000000			N/m
Axial Bushing Stiffness for P_6	$stiffAxial_6$	25000000			N/m
Axial Bushing Damping for P_1	$dampAxial_1$	25000			N/(m/sec)
Axial Bushing Damping for P_2	$dampAxial_2$	25000			N/(m/sec)
Axial Bushing Damping for P_3	$dampAxial_3$	25000			N/(m/sec)
Axial Bushing Damping for P_4	$dampAxial_4$	25000			N/(m/sec)
Axial Bushing Damping for P_5	$dampAxial_5$	25000			N/(m/sec)
Axial Bushing Damping for P_6	$dampAxial_6$	25000			N/(m/sec)
Joint Length for P_1	le_1	0.04			m
Joint Length for P_2	le_2	0.04			m
Joint Length for P_3	le_3	0.04			m
Joint Length for P_4	le_4	0.04			m
Joint Length for P_5	le_5	0.25			m
Joint Length for P_6	le_6	0.25			m

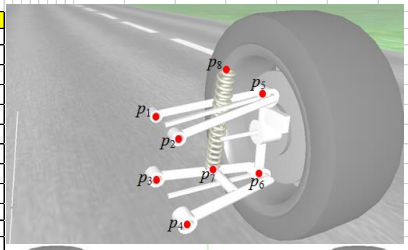

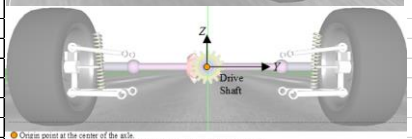

Origin point at the center of the axle.
X-axis is along the length of the vehicle and pointing to the front of the vehicle.

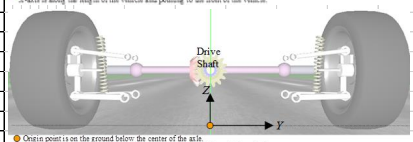

Origin point is on the ground below the center of the axle.
X-axis is along the length of the vehicle and pointing to the front of the vehicle.

Rear Suspension System

SuspDWB2	Comment:	Rear suspension system			
Parameter Description	**Symbol**	**Value1**	**Value2**	**Value3**	**Units**
Hard points reference frame origin	*origin*	*Axle Center*			
Upper control arm inner front point P_1 (X, Y, Z)	p_{1}	0.17492	0.29578	0.2872	m
Upper control arm inner rear point P_2 (X, Y, Z)	p_{2}	-0.13808	0.29578	0.2872	m
Lower control arm inner front point P_3 (X, Y, Z)	p_{3}	0.30332	0.22033	-0.06878	m
Lower control arm inner rear point P_4 (X, Y, Z)	p_{4}	-0.28089	0.21821	-0.10276	m
Upper knuckle outer point P_5 (X, Y, Z)	p_{5}	0.00689	0.77536	0.24432	m
Lower knuckle outer point P_6 (X, Y, Z)	p_{6}	-0.00647	0.86112	-0.1625	m
Lower suspension strut lower point P_7 (X, Y, Z)	p_{7}	-0.11853	0.64782	-0.09971	m
Upper suspension strut upper point P_8 (X, Y, Z)	p_{8}	-0.11853	0.49154	0.57484	m
Lower Suspension Strut P_7 is connected to:	*strutConn*	*Lower control arm*			
Strut Data	*strut*	*Spring2*			
Mass of upper control arm	m_{U}	8.49			kg
Mass of lower control arm	m_{L}	31.55			kg
Mass of knuckle	m_{K}	58.44			kg
Mass of strut lower part	m_{SL}	15			kg
Mass of strut upper part	m_{SU}	16			kg
Moment of inertia of upper control arm	i_{U}	0.3	0.3	0.3	$kg.m^2$
Moment of inertia of lower control arm	i_{L}	1	1	1	$kg.m^2$
Moment of inertia of knuckle	i_{K}	1	1	1	$kg.m^2$
Moment of strut lower part	i_{SL}	0.03	0.6	0.6	$kg.m^2$
Moment of strut upper part	i_{SU}	0.03	0.6	0.6	$kg.m^2$
Upper right control arm icon	$file_{UR}$	../VRML/BackUCAR.wrl			
Upper right control arm icon translation (X, Y, Z)	$trans_{UR}$	0	0	0	m
Upper left control arm icon	$file_{UL}$	../VRML/BackUCAL.wrl			
Upper left control arm icon translation (X, Y, Z)	$trans_{UL}$	0	0	0	m
Upper control arm icon scale (X, Y, Z)	$scale_{U}$	1	1	1	
Lower right control arm icon	$file_{LR}$	../VRML/BackLCAR.wrl			
Lower right control arm icon translation (X, Y, Z)	$trans_{LR}$	0	0	0	m
Lower left control arm icon	$file_{LL}$	../VRML/BackLCAL.wrl			
Lower left control arm icon translation (X, Y, Z)	$trans_{LL}$	0	0	0	m
Lower control arm icon scale (X, Y, Z)	$scale_{L}$	1	1	1	
Knuckle right icon	$file_{KR}$	../VRML/BackKnuckleR.wrl			
Knuckle right icon translation (X, Y, Z)	$trans_{KR}$	0	0	0	m
Knuckle left icon	$file_{KL}$	../VRML/BackKnuckleL.wrl			
Knuckle left icon translation (X, Y, Z)	$trans_{KL}$	0	0	0	m
Knuckle icon scale (X, Y, Z)	$scale_{K}$	1	1	1	
Enable contact with Upper control arm	$contact_{U}$	No			
Enable contact with Lower control arm	$contact_{L}$	Yes			
Enable contact with Knuckle	$contact_{K}$	No			
Automatically set joint stiffnees and damping	*autoStiff*	SpecifyStiff			
Radial Bushing Stiffness for P_1	$stiffRad_{1}$	90000000			N/m
Radial Bushing Stiffness for P_2	$stiffRad_{2}$	90000000			N/m
Radial Bushing Stiffness for P_3	$stiffRad_{3}$	90000000			N/m
Radial Bushing Stiffness for P_4	$stiffRad_{4}$	90000000			N/m
Radial Bushing Stiffness for P_5	$stiffRad_{5}$	90000000			N/m
Radial Bushing Stiffness for P_6	$stiffRad_{6}$	90000000			N/m
Radial Bushing Damping for P_1	$dampRad_{1}$	90000			N/(m/sec)
Radial Bushing Damping for P_2	$dampRad_{2}$	90000			N/(m/sec)
Radial Bushing Damping for P_3	$dampRad_{3}$	90000			N/(m/sec)
Radial Bushing Damping for P_4	$dampRad_{4}$	90000			N/(m/sec)
Radial Bushing Damping for P_5	$dampRad_{5}$	90000			N/(m/sec)
Radial Bushing Damping for P_6	$dampRad_{6}$	90000			N/(m/sec)
Axial Bushing Stiffness for P_1	$stiffAxial_{1}$	25000000			N/m
Axial Bushing Stiffness for P_2	$stiffAxial_{2}$	25000000			N/m
Axial Bushing Stiffness for P_3	$stiffAxial_{3}$	25000000			N/m
Axial Bushing Stiffness for P_4	$stiffAxial_{4}$	25000000			N/m
Axial Bushing Stiffness for P_5	$stiffAxial_{5}$	25000000			N/m
Axial Bushing Stiffness for P_6	$stiffAxial_{6}$	25000000			N/m
Axial Bushing Damping for P_1	$dampAxial_{1}$	25000			N/(m/sec)
Axial Bushing Damping for P_2	$dampAxial_{2}$	25000			N/(m/sec)
Axial Bushing Damping for P_3	$dampAxial_{3}$	25000			N/(m/sec)
Axial Bushing Damping for P_4	$dampAxial_{4}$	25000			N/(m/sec)
Axial Bushing Damping for P_5	$dampAxial_{5}$	25000			N/(m/sec)
Axial Bushing Damping for P_6	$dampAxial_{6}$	25000			N/(m/sec)
Joint Length for P_1	le_{1}	0.04			m
Joint Length for P_2	le_{2}	0.04			m
Joint Length for P_3	le_{3}	0.04			m
Joint Length for P_4	le_{4}	0.04			m
Joint Length for P_5	le_{5}	0.25			m
Joint Length for P_6	le_{6}	0.25			m

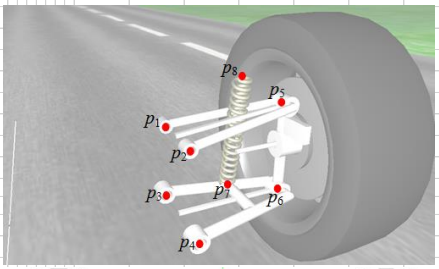

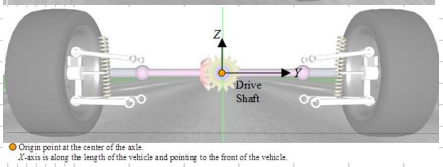

Origin point at the center of the axle.
X-axis is along the length of the vehicle and pointing to the front of the vehicle.

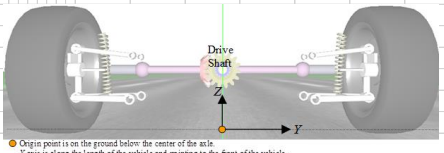

Origin point is on the ground below the center of the axle.
X-axis is along the length of the vehicle and pointing to the front of the vehicle.

Antiroll bar

AntiRollBar1	Comment:				
Parameter Description	**Symbol**	**Value1**	**Value2**	**Value3**	**Units**
Enabled	*enabled*	Yes			
Hard points reference frame origin	*origin*	*Axle Center*			
Center link (tie rod inner) point p_1	p_1	0.227144	0.584429	-0.16569	m
Steering knuckle (tie rod outer) point p_2	p_2	0.227145	0.584429	0.004793	m
Pitman arm rearward point p_3	p_3	0.493326	0.265005	-0.00878	m
Connection	*endLinkConn*	LowerArm			
Anti Roll Bar mass	m_{Bar}	15			Kg
Pitman arm inertia	i_{Bar}	0.1	3	3	Kg.m^2
End link mass	m_{Link}	2.62			Kg
Idler arm inertia	i_{Link}	0.001	0.0262	0.0262	Kg.m^2
Anti Roll Bar torsional stiffness	*barStiff*	8900			N.m/rad
Anti Roll Bar torsional damping	*barDamp*	20			N.(m/s)/rad

Bar radius 0.019135

Front Strut

Spring1	Comment:	Front Strut		
Force-Deflection (Stiffness)		**Force-Velocity (Damping)**		
Deflection (m)	**Force (N)**	**Velocity (m/s)**	**Force (N)**	
-0.11	-90000	-4	-50000	
-0.085	-31373.71297	-0.33	-10500	
-0.08	-30013.7711	-0.13	-6500	
-0.075	-28706.977	0	0	
-0.07	-27451.70415	0.13	8000	
-0.065	-26246.32604	0.33	11500	
-0.06	-25089.21617	4	60000	
-0.055	-23978.74802			
-0.05	-22913.29509			
-0.045	-21891.23086			
-0.04	-20910.92883			
-0.035	-19970.76248			
-0.03	-19069.10531			
-0.025	-18204.3308			
-0.02	-17374.81245			
-0.015	-16578.92375			
-0.01	-15815.03819			
-0.005	-15081.52925			
0	-14376.77044			
0.005	-13699.13523			
0.01	-13046.99712			
0.015	-12418.7296			
0.02	-11812.70616			
0.025	-11227.3003			
0.03	-10660.88549			
0.035	-10111.83524			
0.04	-9578.523025			
0.045	-9059.322345			
0.05	-8552.606687			
0.055	-8056.749543			
0.06	-7570.124403			
0.065	-7091.104757			
0.07	-6618.064095			
0.075	-6149.375908			
0.08	-5683.413686			
0.085	-5218.550921			
0.09	-4753.161101			
0.11	30000			

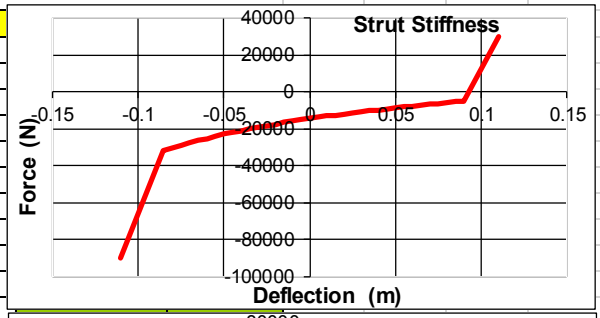

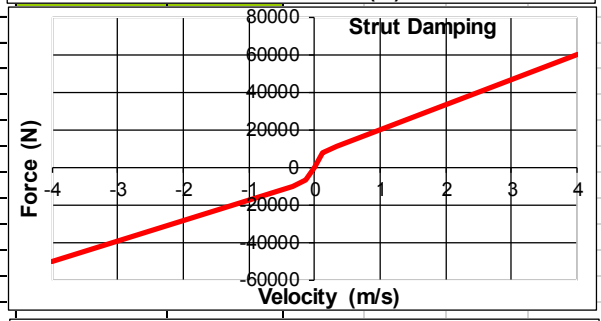

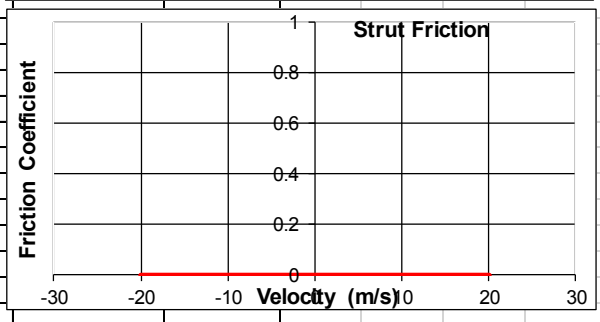

Rear Strut

Spring2 | **Comment:** | Rear strut

Force-Deflection (Stiffness)		Force-Velocity (Damping)	
Deflection (m)	Force (N)	Velocity (m/s)	Force (N)
-0.165	-90000	-4	-50000
-0.14	-43240.6618	-0.33	-10500
-0.135	-41485.95618	-0.13	-6500
-0.13	-39809.62254	0	0
-0.125	-38208.80005	0.13	8000
-0.12	-36680.62786	0.33	11500
-0.115	-35222.24512	4	60000
-0.11	-33830.791		
-0.105	-32503.40465		
-0.1	-31237.22523		
-0.095	-30029.39189		
-0.09	-28877.04379		
-0.085	-27777.3201		
-0.08	-26727.35995		
-0.075	-25724.30253		
-0.07	-24765.28697		
-0.065	-23847.45243		
-0.06	-22967.93808		
-0.055	-22123.88307		
-0.05	-21312.42656		
-0.045	-20530.7077		
-0.04	-19775.86565		
-0.035	-19045.03957		
-0.03	-18335.36861		
-0.025	-17643.99194		
-0.02	-16968.0487		
-0.015	-16304.67806		
-0.01	-15651.01917		
-0.005	-15004.21119		
0	-14361.39328		
0.005	-13719.70459		
0.01	-13076.28428		
0.015	-12428.27151		
0.02	-11772.80543		
0.025	-11107.0252		
0.03	-10428.06998		
0.035	-9733.078923		
0.045	30000		

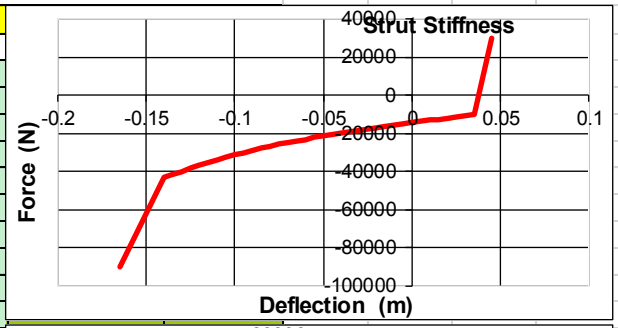

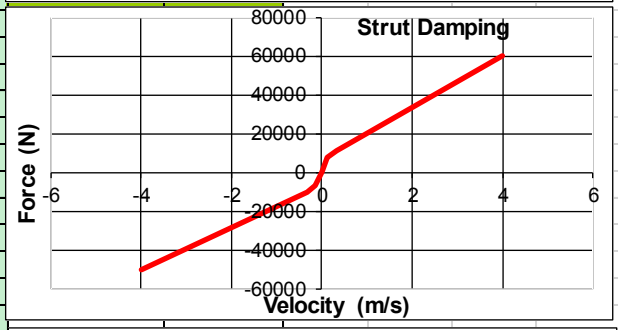

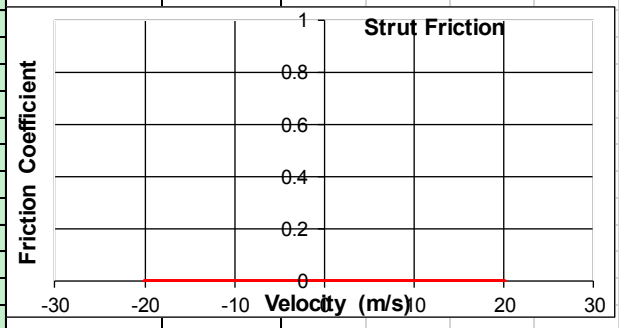

REFERENCES

1. Wasfy, T., *Thrust Area 3: DIS/GroundVehicle: Complex Terramechanics Prototype*, in *AVT-248 Next-Generation NATO Reference Mobility Model (NRMM) Development*, J. Dasch and P. Jayakumar, Editors. 2019, North Atlantic Treaty Organiation (NATO) Research and Technology Organiation.
2. Wasfy, T.M., P. Jayakumar, D. Mechergui, and S. Sanikommu, *Prediciton of Vehicle Mobility on Large –Scale Soft-Soil Terrain Maps using Physics-Based Simulation.* To appear in the International Journal of Vehicle Performance, 2017.
3. Wasfy, T.M., Wasfy, H.M. and Peters, J.M., *High-Fidelity Multibody Dynamics Vehicle Model Coupled with a Cohesive Soil Discrete Element Model for predicting Vehicle Mobility*, in *11th International Conference on Multibody Systems, Nonlinear Dynamics, and Control*. 2015, ASME: Boston, MA.
4. Wasfy, T.M., *Asperity spring friction model with application to belt-drives*, in *19th Biennial Conference on Mechanical Vibration and Noise*. 2003, ASME International: Chicago, IL.
5. Wasfy, T.M., Yildiz, C., Wasfy, H.M., and Peters, J.M., *Effect of Flat Belt Thickness on Steady-State Belt Stresses and Slip.* ASME Journal of Computational and Nonlinear Dynamics, 2016. **11**(5).
6. Wasfy, T.M.a.L., M.J., *Modeling the dynamic frictional contact of tires using an explicit finite element code*, in *5th International Conference on Multibody Systems, Nonlinear Dynamics, and Control*. 2005, ASME: Long Beach, CA.
7. Leamy, M.J., Wasfy, T.M., *Transient and steady-state dynamic finite element modeling of belt-drives.* ASME Journal of Dynamics Systems, Measurement, and Control, 2002. **124**(4): p. 575-581.
8. Wasfy, T.M. and J. O'Kins, *Finite Element Modeling of the Dynamic Response of Tracked Vehicles*, in *International Design Engineering Technical Conferences, 7th International Conference on Multibody Systems, Nonlinear Dynamics, and Control*. 2009, ASME: San Diego, CA.
9. Yildiz, C. and T.M. Wasfy, *Time-accurate multibody dynamics model for toroidal traction drives*, in *2011 International Design Engineering Technical Conferences & Computers and Information in Engineering Conference (IDETC/CIE 2011), 8th International Conference on Multibody Systems, Nonlinear Dynamics, and Control*. 2011, ASME: Washington, DC.
10. Wasfy, T.M., P. Jayakumar, D. Mechergui, and S. Sanikommu, *Prediction of Vehicle Mobility on Large-Scale Soft-Soil Terrain Maps Using Physics-Based Simulation*, in *GVSETS 2016, 2016 NDIA Ground Vehicle Systems Engineering and Technology Symposium, Modeling & Simulation, Testing and Validation (MSTV) Technical Session*. 2016: Novi, MI.